

# **IIT BOMBAY STUDENT SATELLITE**

## **Proposal and Requirements Capture Report**

By

**IIT Bombay Student Satellite Team**

Edited by

**System Engineer Saptarshi Bandyopadhyay**



**Department of Aerospace Engineering,  
Indian Institute of Technology, Bombay**

**April, 2008**

## Preface

The IIT Bombay Student Satellite is an initiative of the students of the Indian Institute of Technology, Bombay to make a satellite all by themselves. With this goal in mind, over forty students from various departments have been working on this project over eight months till date.

In this report, the team has documented the work done by all the groups towards making the satellite. Part A describes the mission of the satellite and the essential features to make the mission a reality. Part B describes each subsystem of the satellite to maximum detail available to till date.

After the initial analysis of the students, reviews of the different subsystems have been carried out by the professors of the institute. The review comments have also been added in the end as a separate chapter.

The IIT Bombay Student Satellite project is a dream of the students of the institute. We hope to see the satellite in orbit by the end of this decade.

## Table of Contents

Introduction.....	15
Part A – Planning of the Satellite Mission.....	16
Chapter 1: Total Electron Count: Mission Overview .....	16
1.1: Introduction .....	16
1.1.1: Total Electron Count .....	17
1.1.2: Faraday rotation of Polarized Radio Waves by TEC .....	18
1.2 Mission Objectives .....	20
1.2.1: Equatorial Ionisation Anomaly .....	20
1.2.2: Variation of TEC .....	22
1.2.2.1: Day to Day Variation of TEC .....	22
1.2.2.2: Day Night Variation of TEC.....	22
1.2.2.3: Variation of TEC in Equatorial Regions.....	23
1.2.2.4: Climatic Variation of TEC.....	23
1.3: Mission Elements .....	25
1.3.1: Transmitted Data.....	25
1.3.2: Antenna used on Satellite .....	26
1.3.3: Location and Features of the Ground Station .....	26
1.4: Requirements from other Subsystems.....	27
1.5: A Social Goal .....	27
1.5.1: Frequency of transmission.....	27
1.5.2: Monopole antenna for receiving data.....	28
1.5.3: Low noise amplifiers .....	28
1.5.4: FSK Demodulators.....	29
Chapter 2: Thermal Imaging: Mission Overview.....	30
2.1: Introduction .....	30
2.1.1: Choice of Device.....	30
2.1.2: Working Principle .....	31
2.1.3: Noise Levels .....	33
2.2: Mission Objectives .....	33
2.2.1: Choice of Bands .....	34

2.2.2: Choice of Swath.....	35
2.2.3: Expected Values of Heat Flux .....	36
2.3: Mission Elements .....	36
2.3.1: Choice of Thermopile .....	36
2.3.2: Associated Circuits .....	37
2.3.3: Collimators .....	39
2.3.4: Filters .....	40
2.4: Post Processing of Data.....	41
2.4.1 Method of Deconvolution.....	41
2.4.2: Method of Polynomial Interpolation .....	43
2.5: Requirements from other Subsystems.....	44
Chapter 3: Orbit Selection Criteria.....	45
3.1: Orbit Planning .....	45
3.1.1: Calculation of Orbital elements .....	45
3.1.2: Time Period .....	47
3.1.3: Communication Time.....	47
3.1.3.1: Angle from zenith.....	48
3.1.3.2: Footprint .....	48
3.1.3.3: Ground Track .....	49
3.1.3.4: Revisit time .....	49
3.1.3.5: Satellite passes over ground station.....	49
3.1.4: Orbit Simulation Software.....	50
3.2: Orbit Determination .....	51
3.2.1: Need for Orbit Determination.....	51
3.2.2: Methods of Orbit Determination.....	51
3.2.2.1: Orbit Propagation .....	51
3.2.3: Global Positioning System (GPS).....	52
3.2.3.1: Introduction.....	52
3.2.3.2: Calculation of position from these data .....	52
3.2.3.3: Reference frames used to describe the motion of a satellite .....	53
3.2.3.4: Measurement of position by GPS receiver .....	54
3.2.3.4.1: Distance measurement .....	54

3.2.3.4.2: Errors .....	54
3.2.3.5: Potential Uses in satellite programme .....	56
3.2.3.6: GPS Sensors.....	59
3.2.3.6.1: The SGR series .....	60
3.2.3.6.1.1: SGR-05 GPS Receiver .....	60
3.2.3.6.1.2: SGR-10 GPS Receiver .....	62
3.2.3.6.1.3: SGR-20 GPS Receiver .....	64
3.2.3.6.2: UBLOX.....	67
Part B – Making of the Satellite: Subsystems .....	69
Chapter 4: Communication .....	69
4.1 Introduction .....	69
4.2.1 Transmitting frequency 434 MHz.....	70
4.2.2 Transmitting frequency 868 MHz.....	70
4.2.3 Transmitting frequency: - 902 MHz.....	70
4.3 Modulation .....	71
4.3.1 ASK.....	71
4.3.2 PSK .....	71
4.3.3 GMSK .....	72
4.3.4 FSK .....	72
4.4 Antenna .....	73
4.4.1 Antenna fundamentals .....	73
4.4.1.1 Resonant frequency .....	73
4.4.1.2 Gain .....	73
4.4.1.3 Radiation pattern .....	74
4.4.1.4 Impedance .....	74
4.4.1.5 Bandwidth.....	74
4.4.1.6 Polarization .....	74
4.4.2 Types of Antennae .....	75
4.4.2.1 The microstrip patch.....	75
4.4.2.1.1 Introduction to patch.....	75
4.4.2.1.2 Important Correlations .....	75
4.4.2.1.2.1 Length and width .....	75

4.4.2.1.2.2 Bandwidth.....	76
4.4.2.1.2.3 Input Impedance.....	76
4.4.2.1.2.4 Mass of patch.....	76
4.4.2.1.2.5 Voltage Standing Wave Ratio (VSWR) .....	77
4.4.2.1.3 Specifications of the Patch Antenna .....	77
4.4.2.1.3.1 Downlink frequency: 434 MHz .....	77
4.4.3.1.3.2 Downlink frequency 868 MHz .....	78
4.5 Link budget analysis .....	78
4.5.1 Satellite.....	78
4.5.2 Transmitting Frequency: 434 MHz .....	79
4.5.2.1 Downlink Path.....	79
4.5.2.2 Ground Station .....	79
4.5.2.3 Eb/No method .....	79
4.5.2.4 SNR Method .....	79
4.5.3 Transmitting Frequency: 868 MHz .....	80
4.5.3.1 Downlink Path.....	80
4.5.3.2 Ground Station .....	80
4.5.3.3 Eb/No method .....	80
4.5.3.4 SNR Method .....	80
Chapter 5: Attitude and Orbit Control System.....	81
5.1 Introduction .....	81
5.2 Sensors .....	82
5.2.1 Reference sensors.....	82
5.2.1.1 Star Sensor .....	82
5.2.1.2. Sun Sensor .....	83
5.2.1.3 Horizon Sensor.....	83
5.2.1.4 Magnetometer .....	83
5.2.2 Inertial sensors .....	84
5.2.2.1 Gyroscopes.....	84
5.2.3 Sensors chosen for our use .....	85
5.2.3.1 Magnetometer .....	85
5.2.3.1.1 Introduction .....	85

5.2.3.1.2 Reference frames .....	85
5.2.3.1.3 Earth's Magnetic Field.....	86
5.2.3.1.4 Analytic Models .....	88
5.2.3.1.5 International Geomagnetic Reference Field (IGRF).....	89
5.2.3.1.6 Orbit estimator.....	90
5.2.3.1.7 Attitude determination from magnetometer readings .....	91
5.2.3.1.8 Types of magnetometers .....	92
5.2.3.1.8.1 Vector Magnetometers .....	92
5.2.3.1.8.2 Vector Gaussmeters .....	93
5.2.3.1.8.3 Scalar Magnetometers .....	93
5.2.3.1.8.4 Comparison between various types of magnetometers .....	94
5.2.3.1.9 Problem with 3 axis magnetometer and the need for an additional sensor .....	94
5.2.3.1.10 Magnetometer Comparison .....	94
5.2.3.2 Sun Sensor .....	109
5.2.3.2.1 Sun sensor types .....	109
5.2.3.2.1.1 Analog Sun sensors .....	109
5.2.3.2.1.2 Sun Presence detector.....	112
5.2.3.2.1.3 Digital Sun sensors.....	112
5.2.3.2.2 Our options .....	114
5.2.3.2.3 Solar Cells as Sun sensors .....	114
5.2.3.2.4 Manufacturing/ purchasing 2-axis Sun sensors .....	116
5.3 Kalman Filter.....	117
5.4 Actuators .....	117
5.4.1 Active Actuators .....	117
5.4.1.1 Thrusters .....	117
5.4.2 Passive Actuators .....	118
5.4.2.1 Passive Permanent Magnet .....	118
5.4.2.2 Magnetorquers .....	118
5.4.2.3 Gravity Gradient Boom .....	119
5.4.2.4 Spin Stabilization .....	120
5.4.3 Actuators chosen for our use .....	120
5.4.3.1.1 Hardware Design .....	120

5.4.3.1.2 Calculations of torque parameters .....	122
5.4.3.1.2.1 Magnetic moment .....	123
5.4.3.1.2.2 Weight .....	123
5.4.3.1.2.3 Voltage .....	123
5.4.3.1.2.4 Torque .....	124
5.4.3.1.3 Calculations for maximum torque req.....	124
5.4.3.1.4 Specifications .....	125
5.4.3.2 Gravity Gradient Boom .....	126
5.4.3.2.1 GGB Design .....	126
5.4.3.2.2 Various Concepts for GGB .....	127
5.4.3.2.2.1 Original Design.....	127
5.4.3.2.2.2 Heritage Methods.....	128
5.4.3.2.2.2.1 Storable Tubular Extendible Member .....	128
5.4.3.2.2.2.2 Very Long Deployable Booms.....	129
5.5 Controller .....	130
5.5.1 Control law .....	131
5.5.2 Other important issues.....	133
Chapter 6: On Board Computer .....	134
6.1 Hardware .....	134
6.1.1 Microcontroller .....	134
6.1.1.1 AT91M40800 Core .....	138
6.1.1.2 Radiation Hardening.....	140
6.1.1.3 ECOS Support.....	140
6.1.1.4 Low Power .....	141
6.1.1.5 Computing Power and Speed .....	141
6.1.1.6 Memory .....	142
6.1.1.7 Availability .....	143
6.1.2 SRAM chips .....	145
6.1.3 FLASH chips .....	147
6.1.4 ADC .....	147
6.1.5 Location of Hardware Components and the Main Board .....	148
6.2 Software .....	149

6.2.1 Need for an operating system .....	149
6.2.1.1 List of Interfaces connected to the Onboard computer.....	149
6.2.1.2 List of Computational Tasks for the Onboard Computer .....	149
6.2.1.3 Other factors.....	150
6.2.1.3.1 Reliability of Software .....	151
6.2.1.3.2 Time Constraint .....	151
6.2.2 Operating Systems .....	151
6.2.2.1 Process management .....	151
6.2.2.1.1 Cooperative operating system .....	151
6.2.2.1.2 Pre-emptive operating systems .....	151
6.2.2.2 Memory management .....	152
6.2.2.3 Interrupt handling.....	152
6.2.3 Selection of Operating System.....	152
6.2.3.1 Must have multi threading support.....	152
6.2.3.2 Must have low memory and computational requirements .....	152
6.2.3.3 Must be compatible with our architecture .....	152
6.2.3.4 Pre-emptive .....	153
6.2.3.5 Very little porting should be required.....	153
6.2.3.6 Free Software .....	153
6.2.3.7 Documentation .....	153
6.2.3.8 Experience .....	153
6.2.4 Comparison of various Operating Systems .....	153
6.2.4.1 eCos vs. SALVO .....	154
6.2.4.2 SALVO.....	154
6.2.5 Implementation of eCos .....	155
6.2.5.1 Pre-requisites for eCos (Windows based installation).....	155
6.2.5.2 Step by step procedure to install eCos .....	155
6.2.5.2.1 Installing the cygwin bash shell.....	155
6.2.5.2.2 Downloading the ecos source files .....	156
6.2.5.2.3 Modifying the default installation for compatibility.....	156
6.2.5.2.4 The After Effects of this modified install.....	156
6.3 Data.....	157

6.3.1 Size of Data .....	157
6.3.2 Error Detection and Correction.....	158
6.3.2.1 Parity Checksum .....	159
6.3.2.2 Hamming Codes.....	159
6.3.2.3 Cyclic Redundancy Check (CRC).....	159
6.3.2.5 Reed Mueller and LDPC codes .....	160
6.3.2.6 Conclusion .....	160
6.3.2.7 Implementation .....	160
6.3.3 Data Compression.....	161
6.3.3.1 Data compression by fourier transforms.....	161
6.3.3.2 Data compression by using statistical information.....	162
6.3.3.3 Data compression by advanced techniques using AVL trees .....	162
6.3.3.3 Data compression by saving only the differences .....	163
6.3.4 Baseband Data Handling .....	163
6.3.4.1 Amplification .....	163
6.3.4.2 Analog to Digital Converter.....	163
Chapter 7: Power System.....	164
7.1 Introduction .....	164
7.2 Solar array .....	164
7.3 Estimation of solar power incident on the satellite .....	165
7.3.1 Reference Frame .....	165
7.3.2 Position of the satellite .....	166
7.3.3 Power incident at a point of time .....	167
7.3.4 Calculation of the eclipsed region.....	168
7.3.5 Final calculation.....	169
7.3.6 Estimating the power output of the solar panels .....	171
7.4 Maximum power point tracking and battery charge regulation.....	172
7.4.1 Description of P&O algorithm.....	173
7.4.2 The analog method for MPPT .....	175
7.4.3 Battery charging algorithm.....	175
7.5 Battery and battery protection .....	176

7.6 Voltage regulator .....	177
7.7 Power Distribution Switches .....	179
7.8 Power systems microcontroller .....	179
7.9 Rough power budget .....	179
Chapter 8: Mechanical and Thermal Configuration .....	181
8.1: Introduction .....	181
8.2: Structural Aspects of the Satellite.....	181
8.2.1: Introduction .....	181
8.2.2 Shape of the Satellite.....	182
8.2.2.1: Factors affecting choice of shape for the satellite .....	182
8.2.2.2: Shapes considered for satellite .....	182
8.2.2.2.1: Satellite with cubical shape .....	182
8.2.2.2.2: Satellite with spherical shape .....	183
8.2.2.2.3: Satellite with dodecahedral shape.....	183
8.2.2.2.4: Satellite with other Platonic solid as shape .....	183
8.2.2.2.5: Satellite with cuboidal shape.....	183
8.2.3: Method of Fabrication .....	184
8.2.3.1: Side panels .....	184
8.2.3.2: Fastening of body panels .....	184
8.2.3.3: Weight reduction methods .....	184
8.2.4: Material for Satellite Body .....	185
8.2.4.1: Aluminium honeycomb .....	185
8.2.4.2: CFRP Sheets .....	185
8.2.4.3: Anodized aluminium .....	185
8.2.5: Conclusion.....	186
8.3: Satellite Subsystems .....	186
8.3.1: Payload .....	186
8.3.1.1: Mechanical Considerations for Thermopiles .....	186
8.3.1.1.1: Introduction .....	186
8.3.1.1.2: Specifications of Thermopile Array.....	186
8.3.1.1.2.1: Thermopile specifications .....	186
8.3.1.1.3: Preliminary Calculations .....	187

8.3.1.1.3.1: Field of view of each thermopile .....	187
8.3.1.1.3.2: Relative orientation of thermopiles .....	187
8.3.1.1.4: Method of Collimation.....	188
8.3.1.1.5: Arrangement of Thermopile-Collimator Array .....	188
8.3.1.1.5.1: Parabolic base .....	188
8.3.1.1.5.2 Alternating arrangement .....	189
8.3.1.1.5.3 Collimators with variable lengths .....	189
8.3.1.1.5.4 Flat base Cut-and-shift arrangement .....	190
8.3.1.1.6 Specifics of Affixation .....	190
8.3.1.1.7 Other Significant Details .....	190
8.3.1.1.7.1 Lengths of each collimator .....	190
8.3.1.1.7.2 Material for base .....	191
8.3.1.1.7.3 Placement of thermopile array on satellite body.....	191
8.3.1.2 Thermal Environment Control and Maintenance for thermopiles.....	191
8.3.1.2.1 Introduction .....	191
8.3.1.2.2 Heat Sensory Details of Thermopile Arrays .....	191
8.3.1.2.3 Thermal Environment Requisites for Thermopile Array .....	191
8.3.1.2.4 Qualitative Description of Design for Thermal Control of Associated Onboard Components .....	192
8.3.1.2.4.1 Assumed filter characteristics .....	193
8.3.1.2.4.2 Design for passive thermal control system .....	193
8.3.1.2.4.3 Design for active thermal control system .....	194
8.3.1.2.5 Conclusion.....	195
8.3.1.3 Specifics of Monopole Antennae .....	195
8.3.2 Controls .....	195
8.3.2.1 Considerations Regarding Moments of Inertia .....	195
8.3.2.2 Magnetorquers .....	196
8.3.2.3 Sun Sensors .....	196
8.3.2.4 Specifics of Placement of Other Components.....	196
8.3.3 Onboard Computer.....	196
8.3.4 Power Systems .....	197
8.3.4.1 Mounting of Battery .....	197

8.3.4.1.1 Issues to be considered.....	197
8.3.4.1.2 Data Required from Other Teams.....	197
8.3.4.1.3 Structural Issues.....	197
8.3.4.1.4 Electrical Insulation .....	198
8.3.4.1.5 Inertial Constraints.....	198
8.3.4.1.6 Thermal Issues .....	198
8.3.4.2 Solar Panels.....	198
8.3.4.3 Power Distribution and Controller Circuits .....	198
8.3.5 Communication.....	199
8.3.5.1 Deployment of Monopole Antennae .....	199
8.3.5.1.1 Various Deployment Mechanisms.....	199
8.3.5.1.1.1. Antenna deployment using nylon wire.....	199
8.3.5.1.1.2 Keeping antenna along one edge .....	199
8.3.5.1.1.3. Using spool .....	199
8.3.5.1.1.4. Placement on deployed surface.....	199
8.3.5.2 Deployment of Patch Antenna .....	200
8.3.5.2.1 Necessity of deployment .....	200
8.3.5.2.2 Description of mechanism.....	200
8.3.5.2.3 Alternative mechanism .....	201
8.3.5.2.4 Patch antenna control.....	202
8.3.5.3 Communication Circuits .....	202
8.4 Satellite Subsystem Layout .....	203
8.4.1 Mounting of Circuit Boards .....	203
8.4.1.1 Introduction.....	203
8.4.1.2 Flexural Vibrations of Simply Supported Rectangular Plates.....	203
8.4.1.3 Placement of PCBs.....	204
8.4.1.4 Layout of PCBs on Satellite Faces .....	204
8.4.1.5 Conclusion .....	205
8.4.2 Selection of Fasteners.....	205
8.4.2.1 Things to consider .....	205
8.4.2.2 Types of attachment .....	206
8.4.2.3 Comparison of attachment options .....	206

8.4.2.4 Mechanical Fasteners .....	207
8.4.2.5 Welding .....	208
8.4.2.6 Adhesive Bonding .....	208
8.4.2.7 Choice of Fasteners for Various Applications .....	209
8.5 Handling and Transportation .....	210
8.5.1 Handling and Storage .....	210
8.5.1.1 Issues to be addressed .....	210
8.5.1.2 Contamination .....	210
8.5.1.3 Shock & vibration .....	210
8.5.1.4 Electrostatic discharge .....	210
8.5.1.5 Ambient Conditions .....	211
8.5.1.6 Temperature constraints .....	211
8.5.1.7 Storage Environment .....	211
8.5.1.8 Adhesives .....	211
8.5.2 Packaging .....	211
8.5.3 Transportation .....	212
8.6 Thermal Requirements .....	212
8.6.1 Thermal Control Elements .....	212
8.6.1.1 Coatings .....	212
8.6.1.2 Other materials .....	212
8.6.2 Thermally Sensitive Points .....	213
8.6.2.1 Battery Box .....	213
8.6.2.2 Surfaces .....	213
8.6.2.3 Internal Circuits that will generate heat .....	213
8.7 Specifics of Satellite Design and Layout .....	213
8.7.1 Allocation of Resources .....	213
8.7.1.1. Payload .....	213
8.7.1.2. Controls .....	213
8.7.1.3. Onboard Computer .....	214
8.7.1.4. Power Systems .....	214
8.7.1.5. Communication .....	214
8.7.1.6 Total Allocation .....	215

8.7.2 List of Mechanics .....	215
8.7.3 List of thermals .....	215
8.7.4 Satellite in Orbit .....	215
Chapter 9: Review meetings .....	217
9.1 System Engineer's Review.....	217
9.2 Structures and Thermals Review .....	219
9.3 Controls Review .....	220
9.4 Power System Review .....	221
9.5 Timeline and Budget Review .....	222

## **Introduction**

The IITB Student Satellite is an initiative of the students of the institute under the guidance of the Department of Aerospace to build a micro satellite. The main objective of the micro satellite is to bring the technology of satellite building into the institute. The proposed missions of the satellite include:

1. Thermally imaging earth from about 670km altitude and finding the carbon dioxide content of the atmosphere, with resolution about 50kmX50km. This will help in further studies in the greenhouse gas emission and its effects.
2. Measure the Total Electron Count of the ionosphere with the use of polarized electromagnetic waves. There are also proposals to study the Electron Ionization Anomaly close to the magnetic equator because of the extremely favorable location of India.
3. Transmit a part of the data from the heat flux sensors at a very low bit rate from space and make it available to all with the correct receiver on Earth. This will enable students from universities all over India and the world to receive this data and analyze it. We believe that this will foster the enthusiasm to build many more student satellites in the country and all over the world.

The current proposed dimensions of the satellite are 200mmX300mmX300mm. The maximum weight of the flight model will be less than 10kgs. The plan is to use the faces of the satellite's structure for power generation in orbit by harnessing solar energy. The control algorithm for the satellite in orbit will be designed by the students themselves and then tested using hardware in loop simulations. The satellite will be equipped with microprocessors and operating system for data handling, storage and communication purposes. A separate ground station will be setup within the IITB campus for communication with the satellite when in orbit.

The satellite will have a minimum lifetime of over 3 months in space, but it will be designed for over 1 year orbit life. The proposed launch date using ISRO's PSLV rocket is 1<sup>st</sup> quarter of 2009. The flight model will be ready by December 2008. The knowledge gained from the satellite project will be the first step towards more advanced projects.

## **Part A – Planning of the Satellite Mission**

### **Chapter 1: Total Electron Count: Mission Overview**

One simple characteristic of our ionosphere is the total electron count along a column. The value of the total electron count gives us an insight into various characteristics of the ionosphere. The satellite will be using two beacons transmitting linearly polarised waves at 150MHz and 433MHz. The difference in the rotation of the angle of polarisation of these two linearly polarised waves, as they pass through the ionosphere gives the value of the total electron count. The values of TEC obtained at our ground station in Mumbai and at other locations set up by ISRO to support the payload of Youthsat will enable us to analyze the latitudinal dependence of TEC.

TEC provides an overall description of the ionosphere and has many practical applications like satellite navigation, time delay and range error corrections for single frequency Global Positioning System (GPS) satellite signal receivers. In recent years, with the increasing demand on the transionospheric communication systems used in the navigation of space vehicles, such as satellites, aircraft, as well as surface transportation systems, the measurement of the true value of the Total Electron Content (TEC) of the ionosphere has become important for making appropriate range corrections, as well as in accounting for errors introduced in the range delays owing to the effects of space weather related events, such as geomagnetic storms and scintillations due to ionospheric irregularities. The numerous TV channel broadcasts happening these days need an estimate of TEC values for uninterrupted and clear transmission.

The correlation between solar activity and ionisation in earth's ionosphere can also be studied by comparing TEC values with solar activity data from other sources. Also, by measuring the TEC values at different latitudes, the latitudinal variation of the total electron count can be studied. This can further be used to analyse the equatorial ionisation anomaly.

#### **1.1: Introduction**

Ionosphere is a region of the earth's atmosphere where ionization caused by incoming solar radiation affects the transmission of radio waves. It extends from a height of 70 kilometers (43 miles) to 400 kilometers (250 miles) above the surface. Solar radiation, acting on the different compositions of the atmosphere with height, generates layers of ionization. The

ionosphere has four layers: D, E, F1 and F2. The density of the ionosphere varies with solar activity and earth's latitude. During night time, D vanishes completely, E also vanishes and F1, F2 combine to form a single layer. The layers of the ionosphere are shown in Fig 1.1.

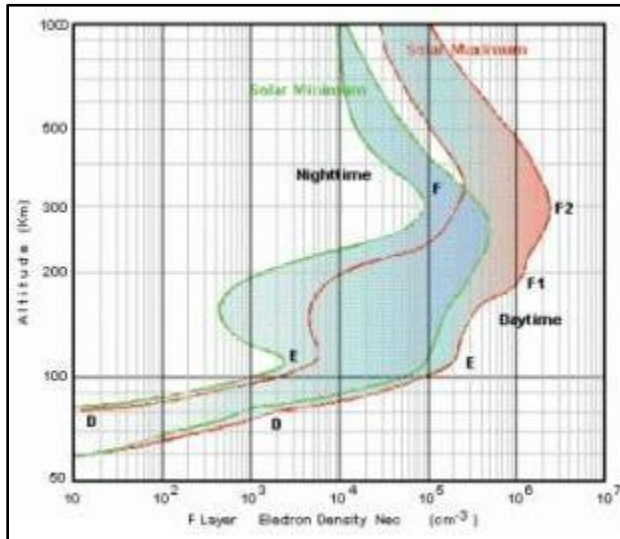


Figure 1. 1 Layers of the Ionosphere

As the electron density of F region is greater than that of D and E, the ground based observations rely solely on F layer for their ionospheric measurements. And hence their wave reflection method can't be used to measure the total electron count of the ionosphere to a high degree of accuracy as they can't really predict the electron count of that part of atmosphere which is above the F layer. This is where one realizes the importance of a satellite in the field of ionospheric measurements. The Faraday rotation method will give us the total count of all the electrons lying in the path starting from the transmitting antenna to the receiving antenna.

#### 1.1.1: Total Electron Count

TEC refers to the Total Electron Count of the atmosphere i.e. the total number of electrons in a cylinder of unit cross section area ( $1 \text{ m}^2$ ) extending from the transmitter to the receiving antenna on the earth's surface.

The slant total electron content (STEC) is a measure of the total number of electrons per  $\text{m}^2$  along the line of sight from the transmitter on a satellite to the receiver on ground.

Electromagnetic waves propagating through the ionosphere are scattered due to irregularities in plasma density which is manifested in the form of amplitude, frequency and

phase variations. These variations can be used to infer important properties about the plasma density irregularities.

With this experiment, we will first measure the Slant TEC as the satellite passes over us and will be later converting it to Vertical TEC, so that it can be of some practical use.

### 1.1.2: Faraday rotation of Polarized Radio Waves by TEC

As any EM wave passes through the ionosphere, it interacts with the ions present in it. So, if we transmit a linearly polarized radio wave through the ionosphere, it will rotate and its angle of polarization will change. A linearly polarized plane transverse electromagnetic wave can be considered as composed of two contra-rotating circularly polarized plane transverse electromagnetic waves. Since the two wave modes supported by uniform anisotropic plasma for propagation along the direction of a static magnetic field correspond to a left-hand circular mode and a right-hand circular mode, a linearly polarized incident wave can be used to simultaneously study the interaction of these wave modes with anisotropic plasma. At high-electron densities the right-hand circularly polarized component is completely attenuated and the variation of the transmitted signal is entirely due to the left-hand circularly polarized component. Alternatively at low electron densities the plasma is transparent to the left-hand mode and the variation in transmitted signal is due to the right-hand mode. So as this wave moves through the ionosphere, the field due to ions presenting the ionosphere affect the speeds of motions of these circularly polarized lights, and hence we begin to observe a net rotation in one direction . This angle through which it has rotated while traveling through ionosphere, basically gives us the Total Electron Count (TEC) in a uniform column of unit cross section extending along the direction of propagation of radio wave. This principle is called Faraday rotation.

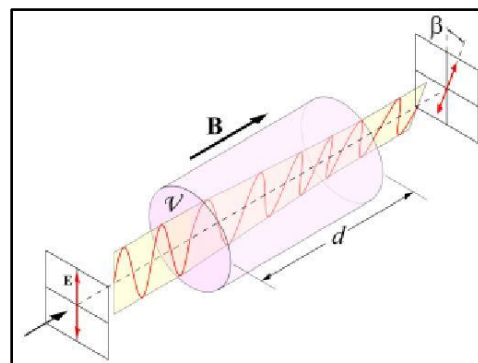


Figure 1. 2 Linearly polarized light passing through the Ionosphere

In the prototype shown in Fig 1.2,  $\beta$  is the angle through which the ray has rotated while travelling through the ionosphere. What we intend to do in this mission is that to measure  $\beta$  and hence infer the STEC over a place. Once we have STEC data over a place, we will convert it to VTEC and hence will get the TEC of ionosphere over our ground station.

The method is based upon the fact that the plane of polarization of a linearly polarized wave during its passage through the ionosphere is rotated by an amount  $\beta$  which is directly proportional to the TEC in the path of ray and is inversely proportional to the square of the frequency of the EM wave, as is evident from formula given below

$$\varphi = 4.72 \times 10^4 f^{-2} B \cos \theta \sec \delta \int_{H_1}^{H_2} N dh \text{ (radians)}$$

where  $\varphi$  (or  $\beta$ ) is the angle through which the ray has rotated,

$f$  is the frequency of the transmitted wave in Hz,

$B$  is the Earth's magnetic field in gauss at ionospheric levels,

$\theta$  is the angle between the direction of propagation and the Earth's field,

$\delta$  is the zenith angle of the path,

$N$  is the electron density per centimeter cube and

$dh$  is an element of height in centimeter.

The limits of integration correspond to the region in which the ionization is large enough to make an appreciable contribution to the rotation. By putting typical values for above variables,

$B_{\text{net}} = 34656 \text{nT} = 3.4656 \text{Gauss}$  (  $1 \text{T} = 10,000 \text{ Gauss}$  ),

$f = 433 \text{MHz}$ ,

$\delta = 45^\circ$ ,

Integral  $Ndh$  as 25 TECU i.e.  $25 \times 10^{16}$  electrons per  $\text{m}^2$ ,

We get the angle of rotation to be about 20 degrees. This rotation angle can be measured by our ground station. Peak value of electron concentration's vertical profile is denoted by  $N_{\text{max}}$  (obtained from Ground based observations) and hence the height of the atmosphere can be estimated as Integral  $Ndh / N_{\text{max}}$

A rough estimate of the TEC values can be seen from this graph in Figure 1.3 adapted from a report on TEC measurement by Sudha Ravindran, Smitha V Thampi, C V. Devasia, Tarun K Pant, P Sreelatha, G. Manju and R Sridharan of Space Physics Laboratory, Vikram Sarabhai Space Centre, Trivandrum, INDIA.

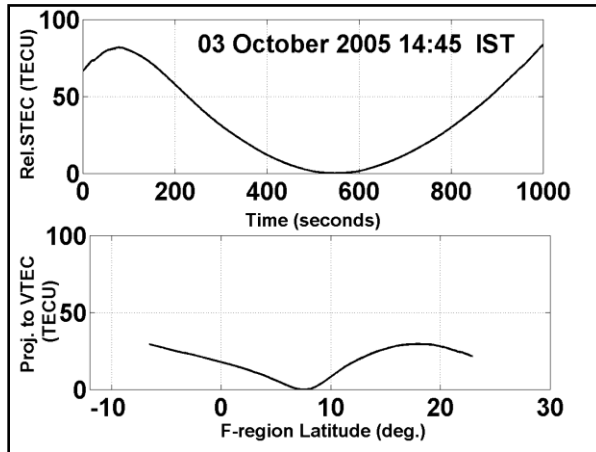


Figure 1: 1 The Observed Relative slant TEC and its projection onto the vertical plane

## 1.2 Mission Objectives

We will require two beacons onboard the satellite, which will be transmitting at different frequencies and hence by noting the difference in the polarization angle of these two waves we will get the TEC. Since we will also get the attitude information of the satellite, even a single beacon will do the job. But having two beacons increases accuracy of our readings and we don't need to aim for very large attitude stabilization.

For carrying out the analysis we will require the value of magnetic field over our ground station, angle between wave's propagation and earth's magnetic field, and zenith angle of the path. As value of Earth's magnetic field and its direction are known to satisfactory level, we will substitute the value of polarization angle and get the TEC along the path of propagation of wave.

We will use the TEC values obtained at the different ground stations to study the Equatorial Ionisation Anomaly (EIA).

### 1.2.1: Equatorial Ionisation Anomaly

The Equatorial Ionization Anomaly (EIA) is characterized by a depression in ionization densities (or trough) at the geomagnetic equator and two peaks (crests) on either side of the equator at

about  $15^{\circ}$  magnetic latitudes. This Fig 1.3 shows a schematic diagram of Equatorial ionization Anomaly.

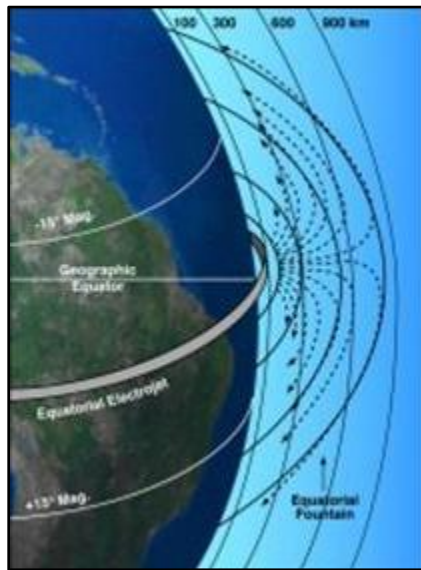


Figure 1. 3 Schematic diagram of Equatorial Ionization Anomaly

There have been many explanations given for EIA. It is suggested that the trough exists because plasma produced by photo ionization at great heights over the magnetic equator diffuses downwards and outwards to the north and south leaving depletion at the equator.

Another explanation is that the mutually perpendicular east-west electric field and north-south geomagnetic field give rise to an upward electrodynamic ( $E \times B$ ) drift of plasma during the daytime. As the plasma is lifted to greater heights, it diffuses downward along geomagnetic field lines towards higher latitudes under the influence of gravity and pressure gradients and produces the anomaly.

The anomaly crests in both hemispheres occur at lower altitudes and become weaker with height. The ratio of the electron density at the crest to the electron density at the trough is a measure of the intensity of the anomaly. The crest-to-trough ratio is maximum near the height of the F2 region peak and decreases both downward and upward. The EIA is also asymmetric about the geomagnetic equator caused by field aligned plasma flow due to factors like neutral winds.

#### 1.2.1.1 Advantages of Studying EIA from India

An interesting feature in the geographic location of India is that the magnetic equator passes through the bottom-side tip of the country and the northern crest of the equatorial

ionization anomaly lies in the middle of the country, providing a unique opportunity for making studies on the latitudinal variation equatorial ionization anomaly (EIA) which occurs at 5 – 25 geographical latitude. So as Mumbai falls in this region, we can easily get good data on EIA with this experiment.

In India, a coordinated TEC measurement campaign was undertaken in 1975 using the ATS-6 geostationary satellite. In recent times, a joint coordinated programme under the project named GAGAN (Geo And GPS Augmented Navigation), the Indian version of Wide Area Augmentation System (WAAS), to monitor TEC at eighteen locations across India using GPS satellites was launched in 2003 by the Indian Space Research Organisation (ISRO) and Airport Authority of India.

### 1.2.2: Variation of TEC

The TEC values over a region are seen to vary over an appreciable range due to a large number of reasons. Some of the reasons have been studied here.

#### 1.2.2.1: Day to Day Variation of TEC

The randomness in the day-to-day variation in TEC may be attributed to the changes in the activity of the Sun itself and to the associated changes in the intensity of the incoming radiations, and the zenith angle at which they fall on the Earth's atmosphere, in addition to the changes which take place in the Earth's magnetic field and the equatorial electrojet (EEJ) strength, added to the effects due to the dynamics of the neutral winds.

#### 1.2.2.2: Day Night Variation of TEC

During night time, there is no solar radiation falling on the atmosphere, so there is no appreciable energy to ionize the atoms present in the ionosphere. But the opposite process of recombination of ions takes place and so there is a decrease in ion density of atmosphere and hence reduced TEC is observed. During afternoon when the solar radiation is maximum, so ionization increases and it overtakes the process of recombination of ions and hence TEC value increases.

#### 1.2.2.3: Variation of TEC in Equatorial Regions

The daily variation in TEC at the EIA region shows its steep increase and reaches its maximum value between 13:00 and 16:00 LT, while at the equator the peak is broad i.e. it occurs for a longer duration of time and occurs around 16:00 LT. A short-lived day minimum occurs between 05:00 to 06:00 LT at all the stations from the equator to the EIA crest region. Beyond the crest region the day maximum values decrease with the increase in latitude, while the day minimum in TEC is flat during most of the nighttime hours, i.e. from 22:00 to 06:00 LT, a feature similar to that observed in the mid-latitudes. Further, the diurnal variation in TEC show a minimum to maximum variation of about 5 to 50 TEC units, respectively, at the equator and about 5 to 90 TEC units at the EIA crest region !!

Daily minimum in TEC occurs during the morning hours of about 5 to 6 LT in EIA region (between the equator and peak of the fountain) whereas there is no such downward kink in TEC in regions outside the peak of EIA. And hence TEC is almost flat during nighttime. This is a feature which is similar to that at mid-latitudes i.e. the areas which are not affected by EIA.

Secondly, we can say that rate of change of TEC is quite fast at stations in the EIA region than outside it. At equatorial station, the day maximum is broader than that at the anomaly crest station. In particular, during the month of March the late afternoon decrease in TEC is equally steeper with occasional post sunset enhancements around the anomaly crest region. During the equinoctial month of March there is a nighttime maintenance of the ionosphere with an average TEC value of about 15 to 20 TEC units in the diurnal variations at stations up to the anomaly crest region.

Near the peak of EIA, a very high latitudinal gradient is present, so it will lead to greater variation in date when converted to VTEC from STEC. Spread in TEC is minimum for stations present at equator whereas it is more prominent at stations near the crest of anomaly indicating the effect due to the presence of strong latitudinal gradients at the anomaly crest region compared to those at the equatorial station.

#### 1.2.2.4: Climatic Variation of TEC

The seasonal variation in TEC maximizes during the equinox months( equinox is that period of time when sun passes over equator and lengths of day and night become equal , this

occurs on 21<sup>st</sup> March and 22<sup>nd</sup> September) followed by winter and is minimum during the summer months. In the Indian sector, the EIA crest is found to occur in the latitude zone of 15 to 25 N geographic latitudes (5 to 15 N geomagnetic latitudes).

Contour plots of the monthly average diurnal variation of TEC at four stations across India (taken from the results of GPS Aided Geo Augmented Navigation (GAGAN) project of ISRO + AAI) are shown in Fig 1.4.

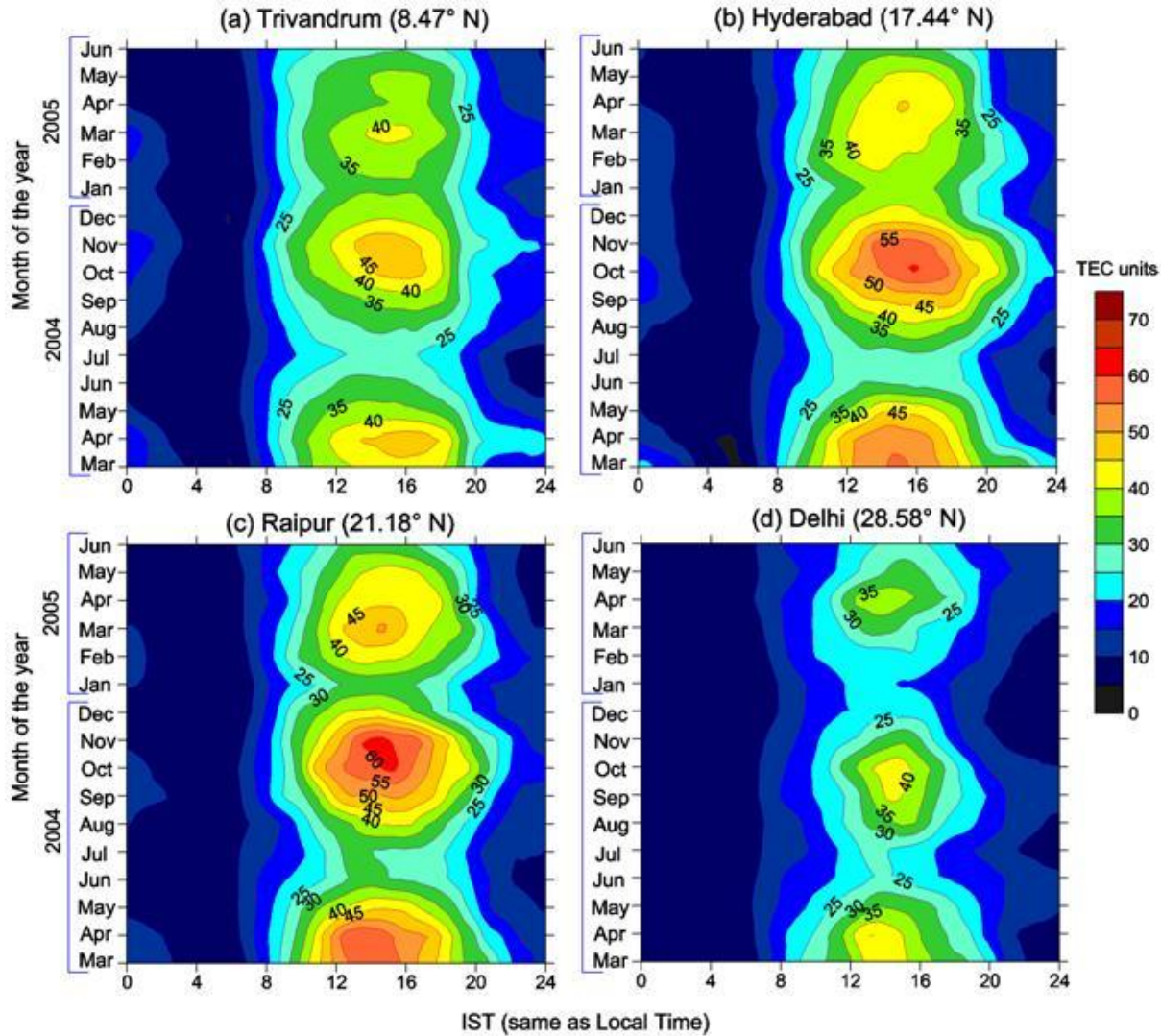


Figure 1. 4 Monthly average diurnal variation of TEC

From the Fig 1.4, we may infer that maximum peak of TEC is reached in the equinox months and is less during late summers. As expected, the maximum TEC is observed at stations near the crest of EIA region (Raipur). Also at stations farther from equator and outside the

anomaly region ionization is quite low (Delhi). Also as stated before, peak in TEC during afternoons is broader at equatorial station (Trivandrum), whereas it is sharper and more pronounced at anomaly crest regions (Raipur). It may be seen from above curves that the diurnal maximum in TEC occurs approximately between 1200 to 1600 LT, particularly at Hyderabad, Raipur and Delhi, whereas at the equatorial station Trivandrum, the occurrence of the diurnal maximum is slightly delayed and occurs around 1600 LT. At all these four stations the equinoctial maxima showing the semidiurnal variation in TEC is strongly evident, indicating the role played by the solar zenith angle variation in the changes produced by the level of production of ionization.

### 1.3: Mission Elements

Measurements at the ground station will only give us the value of the final angle of polarization. To obtain the change in polarization, we need the initial value of polarization angle which would then require us to know the orientation of the monopole. To avoid this and to make this experiment independent of the controls, we will require two beacons onboard the satellite, which will be transmitting at different frequencies and by noting the difference in the polarization angle of these two waves we will get the TEC. For carrying out the analysis, we will require the value of magnetic field over our ground station, angle between wave's propagation and earth's magnetic field, and zenith angle of the path. As value of Earth's magnetic field and its direction are known to satisfactory level, the value of polarization angle and will give us the TEC along the path of propagation of wave.

In order to study the Equatorial Ionisation Anomaly, we will require the latitudinal dependence of TEC over India. Since one ground station will only give us the TEC over that region, we will require the services of the ground stations of Youthsat. We will use the TEC values obtained at the different ground stations to study the Equatorial Ionisation Anomaly. We have hence chosen the transmission frequencies of the two beacons to be the same as that for Youthsat – 150 and 433 MHz.

#### 1.3.1: Transmitted Data

It is very essential to make the beacon independent of the On Board Computer (OBC) because only then we can use it to detect whether the satellite is alive or dead in space. The currently proposed signal that we will transmit via beacon is:

00 00 1 1000 000 01 1 | 00 10 100 00 01

which is IITBSAT INDIA in Morse Code. The signal will be created using only an analog circuit. Another social goal that can be achieved by the beacon is discussed in Section 1.5.

### 1.3.2: Antenna used on Satellite

The monopole antennae on the satellite will be serving several purposes.

- 1) One of the monopoles transmitting at 433MHz will serve as a beacon independent of the on board computer. In the worst case scenario when the OBC fails for some reason, the beacon should still be sending a simple unintelligent identification sequence to mark the presence of the satellite.
- 2) The linearly polarized waves coming from the monopole antennae will give us the TEC values.
- 3) The other monopole operating at 150MHz will be serve a social goal discussed in a later section.
  - The body of the satellite itself will serve as the ground plane for the monopoles.
  - Steel tapes coiled during launch will be used as monopole antennae on the satellite. Further details are mentioned in the Structures section of the document.

### 1.3.3: Location and Features of the Ground Station

The ground station will receive and store the beacon signal received from satellite and also calculate its polarization angle which will be used to compute TEC above the ground station. The polarization angle obtained by the crossed monopoles arrangement will be used along with Earth's magnetic field, zenith angle of satellite, angle between earth's magnetic field and way of propagation, to calculate STEC and subsequently convert it to VTEC. This data will be automatically stored and then can be retrieved for any further use.

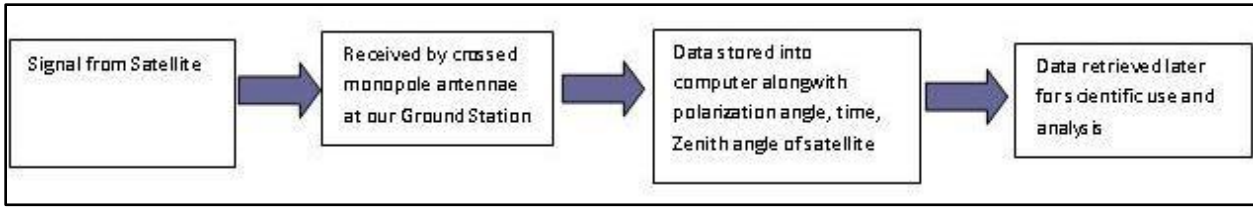


Figure 1. 5 Block Diagram of the Ground Station

#### 1.4: Requirements from other Subsystems

**Power System:** As we will be using two transmitters and one micro controller on board, do we will have a power requirement of about 2W.

**Structures:** They need to arrange for slots for our PCB cards and also to arrange for proper deployment of two monopole antennas

**OBC:** As decided earlier we won't be using the OBC services for the bacon. For the other monopole we will need the obc to send us signals in the correct protocol.

**Controls:** Not very stringent.

**Communication:** NIL

#### 1.5: A Social Goal

The main purpose of this new payload is to make our GPS and thermopile data accessible all over the country. This will enable students all over India to receive and analyze the data, and use it for their benefit. Hence we will be reaching out to more students to start such initiatives.

We will transmit our data through one of our two FSK beacons using a monopole antenna. Whoever wants to receive the data will need a ground station for receiving the data being sent by our beacon on the satellite. This will essentially consist of:

- i. Monopole antenna for receiving data
- ii. Low noise amplifier
- iii. Demodulator

##### 1.5.1: Frequency of transmission

We have to analyze two frequencies, namely 136MHz (VHF) and 434MHz (UHF).

Specifications at 136 MHz

- Power required for transmitter on satellite: 0.1W
- Elevation angle: 45deg.
- No antenna control required at ground or satellite.
- Bandwidth: 2KHz
- Contact time in 146 revolutions.: 19.8 minutes
- Data: 2.37Mb
- Data rate: 2Kbps

#### Specifications at 433 MHz

- Power required for transmitter on satellite: 1W
- Elevation angle: 45deg.
- No antenna control required at ground or satellite.
- Bandwidth: 2KHz
- Contact time in 146 revolutions.: 19.8 minutes
- Data: 2.37 Mb
- Data rate: 2Kbps

So analyzing this data obtained from the link budget analysis performed by us, it is evident that 136MHz is more feasible. It has low power consumption as well as a better noise figure.

#### 1.5.2: Monopole antenna for receiving data

Length =  $\lambda/4$ , where  $\lambda$  is the wavelength for the frequency of transmission.

For 136 MHz length = 55.14cm.

For 434 MHz length = 17.28cm.

Antenna can be either purchased or designed in lab.

#### 1.5.3: Low noise amplifiers

LNA's with a gain of around 8dB will be required for this set up. LNA's of very high quality are available in the price range of Rs12000 to 15000 and moderate quality LNA's are available at

around Rs 5000, which can be used for this purpose.

For LNA's, buying off the shelf is definitely the best option.

#### 1.5.4: FSK Demodulators

They consist of the following components:

1. IF Filter
2. Limiter
3. Discriminator
4. Integrate and Dump filter
5. Threshold detector

The block diagram for the demodulator is shown in Fig 1.6. This demodulation circuit can either be designed or purchased off the shelf, the latter of which is the more feasible option.

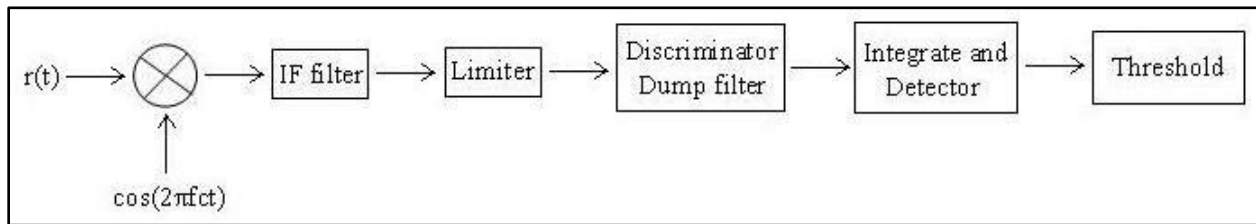


Figure 1. 6 Block Diagram for the Demodulator

Overall, this feels like a good goal to reach out to the other students in the country. This will our small effort towards enlightening the youth of today.

## **Chapter 2: Thermal Imaging: Mission Overview**

Global warming is caused by a number of gases but the most significant contribution towards the effect is by Carbon-dioxide ( $\text{CO}_2$ ). By analyzing the distribution of  $\text{CO}_2$  and its variation across the globe one can study this effect in detail. For this purpose, the satellite will attempt at making a thermal map of the earth by recording the intensity of radiation pertaining to the absorption band of  $\text{CO}_2$  (10.5 to 12.5 $\mu\text{m}$ ) and atmospheric window (13 to 17.5  $\mu\text{m}$ ) which has no absorption.

The thermal emission in the atmospheric window region will also enable us to sketch a thermal map of the earth which is of great importance when dealing with the various climatic models of the earth.

To achieve this, the satellite will use an array of Thermopiles, which are essentially thermoelectric sensors that measure the heat flux incident on them. Filters in the absorption band of  $\text{CO}_2$  and in the atmospheric window region will be used.

### **2.1: Introduction**

One of the several ways to measure heat flux is by utilizing the Seebeck effect. In Seebeck effect, a temperature difference across two metal-metal junctions is converted into a potential difference across these junctions. A thermocouple is a system of two dissimilar metals joined together, one of which is heated so as to measure the heat flux.

A thermopile is a system of several such thermocouples joined in series with each other so as to create a significant voltage drop across the junctions.

#### **2.1.1: Choice of Device**

For thermal imaging, we had the following options:

1. CCD imaging array
2. Bolometers
3. Thermopiles.

The CCD imaging array (in essence a standard IR camera) was not suitable as it required a high degree of attitude control and stabilization and a high degree of robustness in structure in order for it to render good quality images.

The bolometers required a cryogenic environment in order to give good results. Further, they were found to be devices that are not very accurate.

Hence we finally chose thermopiles as

- they were easily available
- they can be easily used
- are more accurate than bolometers at normal temperatures

### 2.1.2: Working Principle

The type of thermopile we are using in this mission is known as a differential thermopile. In this type of thermopile, heat flux incident on surface A is conducted to surface B so as to create a temperature difference across the two surfaces. The thermocouples connected across these two surfaces convert this difference in temperature to a potential difference. The potential difference thus generated is given by:

$$V = N \times S \times \Delta\theta$$

where  $N$  = no. of thermocouple junctions,

$S$  = Seebeck coefficient and

$\Delta\theta$  = temperature difference created.

This device is a linear device as the equation relating the temperature difference with heat flux is a linear differential equation.

We will now derive an expression for the temperature difference  $\Delta\theta(t)$  for a steady heat flux  $\mu$  incident on the thermopile at time  $t = 0$ .

We assume that the temperature varies only along the thickness of the thermopile, the  $x$  direction. Under this assumption a relation between  $\Delta\theta(t)$  and  $\mu$  can be derived as follows:

The differential equation governing the conduction of heat through the thermopile along one dimension is

$$\frac{\partial\theta}{\partial t} = h^2 \frac{\partial^2\theta}{\partial x^2} \quad \text{where} \quad h^2 = \frac{K}{\rho\sigma},$$

$K$  = thermal conductivity,  
 $\rho$  = density,  
 $\sigma$  = specific heat.

In this case, the initial and boundary conditions are

$$\theta_{x,0} = \theta_0,$$

$$\theta_{L,t} = \theta_0,$$

$$\frac{\partial \theta}{\partial x}_{0,t} = \mu$$

Solving the equation yields the solution as

$$\theta_{0,t} - \theta_{L,t} = \mu L - \frac{8\mu L}{\pi^2} \sum_{j=1}^{\infty} \frac{e^{-\lambda_j^2 t}}{j - 1/2^2}$$

$$\text{where } \lambda_j = \frac{h j - 1/2 \pi}{L}.$$

This shows that the device behaves as a parallel system of several first order systems, which has time constants  $\tau_0 = 4L^2/\pi^2 h^2, \tau_0/9, \tau_0/25, \tau_0/49 \text{ etc.}$  This response of the system is shown in Fig 1.10.

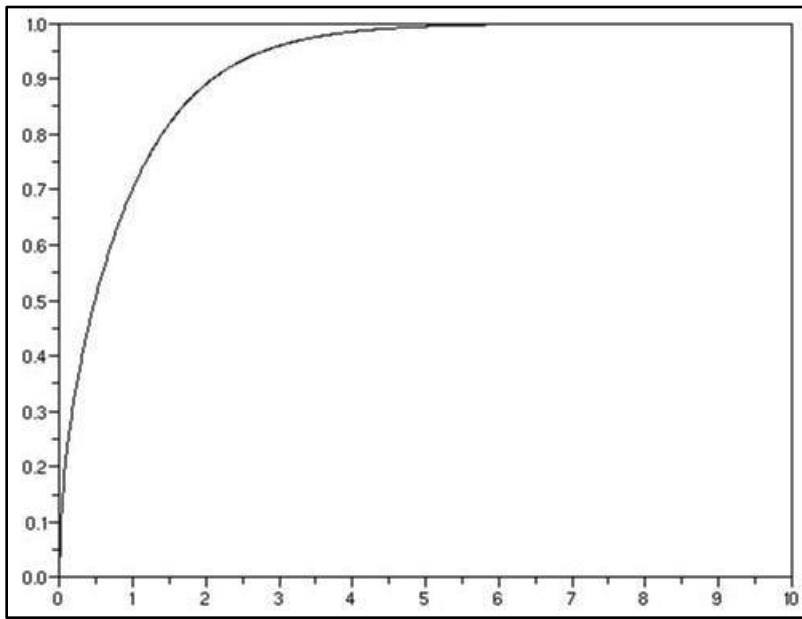


Figure 2. 1 Time response of thermopile to step input ( $\tau_0 = 1, \mu = 1, L = 1$ )

Essentially, after a significant time, the responses with smaller time constants become negligible. Thus it functions as a first order device.

### 2.1.3: Noise Levels

The thermopile generates only Johnson noise due to its resistance. This is a white noise and its RMS density is given by

$$e_n = \sqrt{4kTR} \text{ where } k = \text{Boltzmann's constant} = 1.38 \times 10^{-23} J/K$$

*T = Absolute Temperature*

*R = Resistance of thermopile*

The typical magnitudes of these noises are

$$\begin{aligned} e_n &\approx \sqrt{4 \times 1.38 \times 10^{-23} \times 300 \times 49 \times 20} V \text{ (assuming bandwidth = 20 Hz)} \\ &\approx 4 nV \end{aligned}$$

## 2.2: Mission Objectives

This experiment will have the following targets:

- Creating a complete thermal map of the earth with
  - a temperature resolution of 1° C
  - a spatial resolution of 55 km x 55 km.
- Creating a CO<sub>2</sub> map of the earth with
  - a resolution in the data of 0.05% by volume of CO<sub>2</sub>
  - a spatial resolution of 55 km x 55 km.

Overall system specifications are as follows:

- Total no. of thermopiles: 25 (for atmospheric window) + 25 (for CO<sub>2</sub>)
- Swath of each thermopile: 688 km
- Area covered by each thermopile: 688km X 688km
- Sampling time: 4s
- Revisit time: 3 days
- Memory requirements: 10.8Mb per day
- Data downlink requirements: 45Kbps

The block diagram of the system is shown in Fig 2.2.

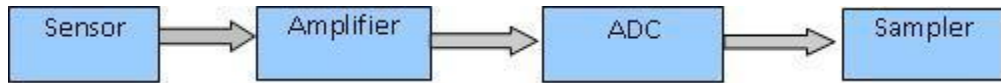


Figure 2. 2 Block Diagram of Thermopile system

### 2.2.1: Choice of Bands

We obtained the following graphs relating the spectral radiance of earth and the wavenumber (in centimeter<sup>-1</sup>) as shown in Fig 2.3.

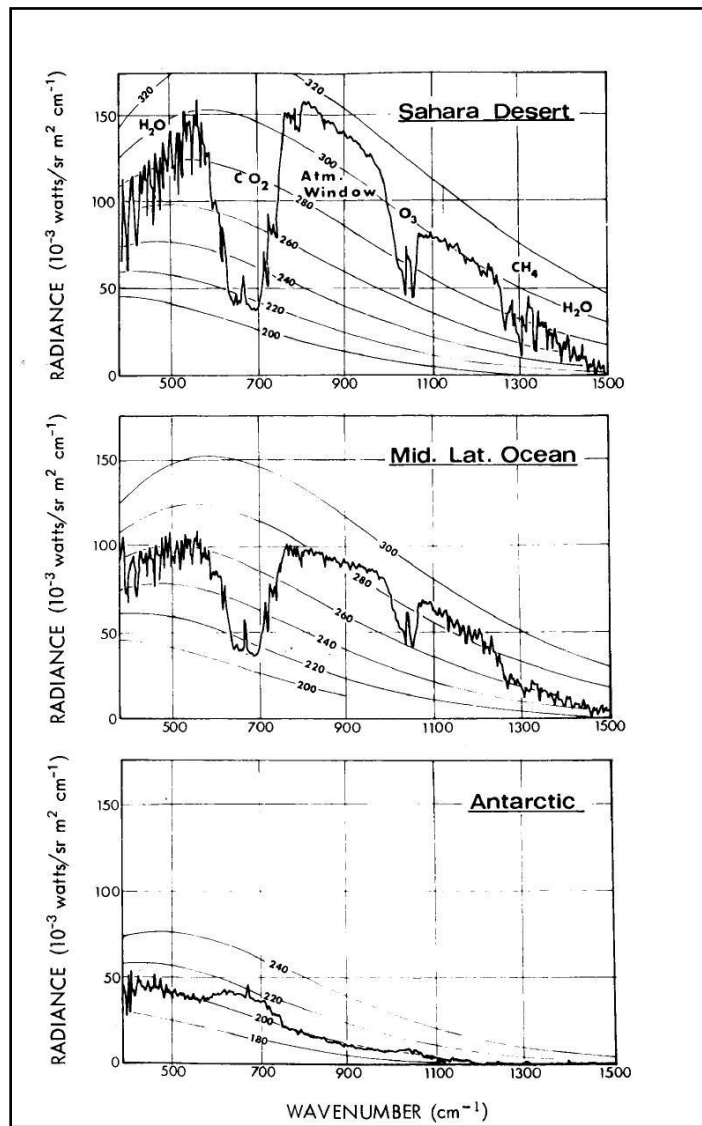


Figure 2. 3 Graph of radiance vs. wavenumber for earth's emission spectra over various regions  
Adapted from NASA technical reports, report no. SP-8067, pp. 14 publicly available on

<http://hdl.handle.net/2060/19710023628>

These graphs show that:

- All over the earth, there is a dip in the wavenumber region  $600 - 775 \text{ cm}^{-1}$ , i.e. in the wavelength range  $12.9 \mu\text{m} - 16.7 \mu\text{m}$ , due to absorption by  $\text{CO}_2$
- There is an atmospheric window in the region  $800 - 975 \text{ cm}^{-1}$  i.e. in the wavelength range  $10.3 \mu\text{m} - 12.5 \mu\text{m}$  which there is no absorption by any gas and thus we get the actual character of the radiance curve.

We can hence use the atmospheric window region to get the actual radiance curve and then the temperature of the region can be obtained by comparing it with the blackbody curves. We can also get the  $\text{CO}_2$  levels by knowing the actual amount of radiation in the absorption band and the amount which would have been had there been no  $\text{CO}_2$  cover. In other words, comparison of the flux in the  $\text{CO}_2$  band with the heat flux in the atmospheric window region will enable us to eliminate the effect of temperature in the  $\text{CO}_2$  absorption spectrum.

Hence, we have chosen the following bands of operation:

- i.  $12.9 \mu\text{m} - 16.7 \mu\text{m}$ , as absorption band
- ii.  $10.3 \mu\text{m} - 12.5 \mu\text{m}$ , as window band.

### 2.2.2: Choice of Swath

Our orbit is a 9:30 am-pm sun synchronous polar orbit. Thus we expect an orbital period of about 100 minutes. In 1 day the satellite goes around the earth about  $N = 1440/100 = 14.4$  times. If we desire to make a complete map of the earth, the swath must be chosen such that the satellite can view every point on the equator at least once everyday. Thus the swath is given by

$$\begin{aligned} S &= \frac{2\pi R_{\text{earth}}}{2N} \\ &= \frac{2 \times 3.1415 \times 6400}{2 \times 14.4} \text{ km} \\ &= 1396 \text{ km} \end{aligned}$$

However, as will be explained later in the document, the swath of each thermopile needs to be only  $\frac{1}{2}$  of this value. Thus, swath of each thermopile,  $S_{\text{thermopile}} = S/2 \sim 700 \text{ km}$ .

### 2.2.3: Expected Values of Heat Flux

With this swath, the expected values of heat flux in the different regions can be calculated as shown below:

In the window region:

$$\text{Solid Angle, } \Omega = \frac{\text{Area}}{\text{Height}^2} = \frac{700^2}{670^2} = 1.09 \text{ sr}$$
$$\therefore \text{Heat Flux} = R_{\text{avg,window}} (\text{average radiance}) \times \Omega \times \Delta \bar{v}$$
$$= 19 \text{ W/m}^2 (\text{typical}), 4 \text{ W/m}^2 (\text{min})$$

In the absorption region:

$$\text{Heat Flux} = R_{\text{avg,absorption}} (\text{average radiance}) \times \Omega \times \Delta \bar{v}$$
$$= 9.5 \text{ W/m}^2 (\text{typical})$$

The absolute value of the heat flux in this region is found to be very close to the typical value, everywhere on the earth.

## 2.3: Mission Elements

The various elements in this payload are described below.

### 2.3.1: Choice of Thermopile

Based on the requirements from a space grade sensor, the following thermopile was chosen:

Name	Vatell BF-02
Dimension	2.5 cm x 2.5 cm
Active Area	8.2 mm x 7.16 mm
Thickness	0.25 mm
Shear Stress	6.9 MPa
Sensitivity	1 mV/W/cm <sup>2</sup>

Time Constant	0.9 s
Resistance	49 Ω
Noise Figure	0.9 nV/ $\sqrt{\text{Hz}}$
Thermal Conductivity	0.25 W/mK
Max Temperature	170 °C
Cost per thermopile	320£

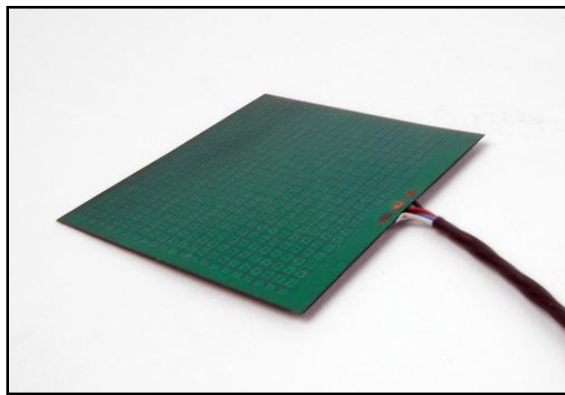


Figure 2. 4 Vatell BF-02

### 2.3.2: Associated Circuits

The amplifier circuit, as suggested by the manufacturing company is shown in Fig 2.5

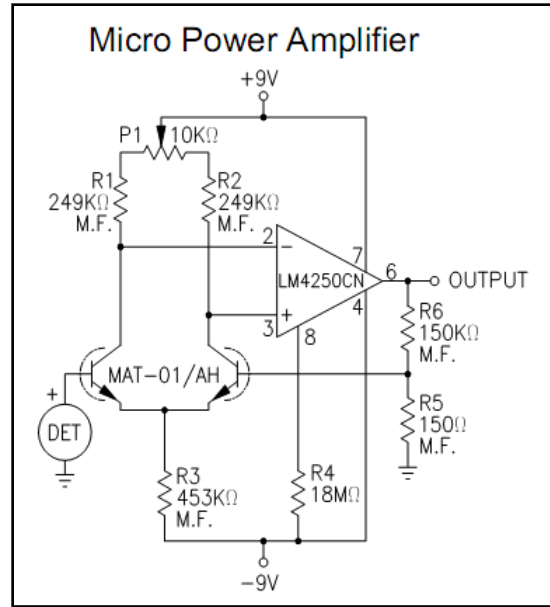


Figure 2. 5 Amplifier for thermopile

We have decided to implement the following system in our satellite.

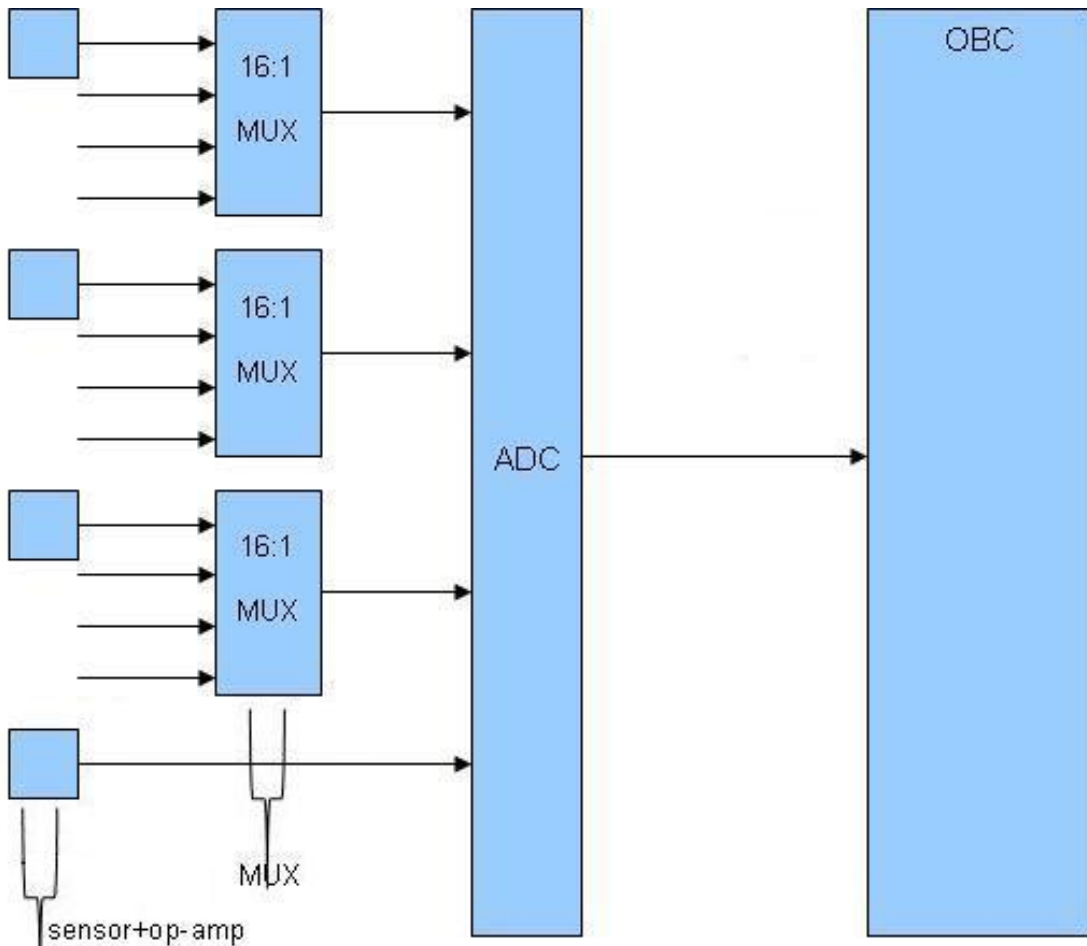


Figure 2. 6 Block Diagram for thermopile implementation

We will be using 49 thermopiles in all, among which one will be for bias elimination purposes. As of now, we have selected the following op-amps as the possible candidates.

The one extra thermopile will be used as a reference in order to remove any bias from the readings. Its output will be directly given to the OBC through its own MUX.

### 2.3.3: Collimators

The thermopiles have their fields of view collimated using a mechanical collimator shaped like a box around the thermopile of height approximately 30mm. It is required that infrared rays arriving from outside the prescribed field of view be prevented from reaching the thermopile chip through reflection or otherwise.

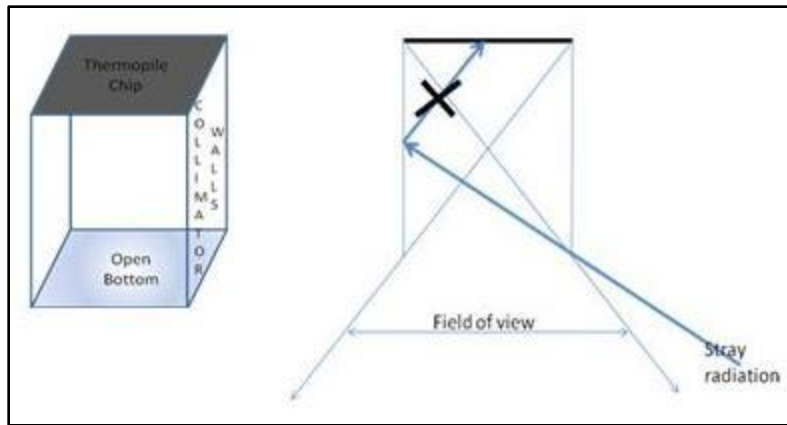


Figure 2. 7 Collimator for Thermopile

This will be achieved by

- 1) Coating the inner walls of the collimators with the filter material. This will prevent unwanted radiation in the irrelevant wavelength regions from falling on the collimator and thus keep the temperature of the collimators down to a low value.
- 2) The inner surfaces of the collimators will be coated black so that no radiation in the region of interest gets reflected onto the thermopiles.

The filter, collimator and the substrate on which the thermopile is mounted all absorb thermal radiation and hence re-radiate thermal noise by emission, thus reducing the signal to noise ratio and creating unsteadiness in the thermal noise levels. From these constraints, the scientific requirements of the experiment dictate that either (1) the onboard components do not radiate (or emit minimal radiative noise) in the wavelength range being detected by the sensor or (2) the onboard components reach a thermal steady state so that thermal noise can be eliminated from the readings by pre-calibration on earth in similar experimental conditions. Details of the thermal control and placement of the thermopiles+collimators on the nadir surface are discussed in the Structures and Thermals section.

#### 2.3.4: Filters

We plan to get the filters fabricated at LEOS for the bands discussed above:

- $12.9 \mu\text{m} - 16.7 \mu\text{m}$ , as absorption band
- $10.3 \mu\text{m} - 12.5 \mu\text{m}$ , as window band.

## 2.4: Post Processing of Data

The data received at the ground station will consist of the following:

1. Data from all the 50 thermopiles
2. Position data taken at the sampling instant
3. Attitude data taken at the sampling instant.

The schemes we propose for the analysis of such data is described below.

### 2.4.1 Method of Deconvolution

Let us assume the actual heat flux distribution at the earth's surface to be  $h(x)$ . At a position  $x_0$ , we will be measuring

$$q(x_0) = \int_{x_0-\delta}^{x_0+\delta} h(x) f(x-x_0) dx$$

where  $f(x)$  denotes the factor introduced due to the variable response of the thermopile to radiations from various directions.

Let the Laplace transform of  $h(x)$  be  $H(s)$ . We can see that

$$Q(s) = L(q(x)) = H(s) \int_{-\delta}^{\delta} e^{sx} f(x) dx$$

We would be sampling this data at a frequency  $f_{\text{samp}}$ . The Nyquist sampling theorem then tells us that we can get all components of the data varying at a frequency  $\leq f_{\text{samp}}/2$ . We can approximate the original data by some interpolation scheme. In this case, Whittaker-Shannon interpolation scheme would be quite appropriate as it would be computationally easier.

After getting the approximate original data  $q'(x)$ , we can get its Laplace transform  $Q'(s)$  and we can then approximate  $H(s)$  by

$$H'(s) = \frac{Q'(s)}{\int_{-\delta}^{\delta} e^{sx} f(x) dx}$$

We can now generate the approximate heat flux  $h'(x)$  by the inverse Laplace transform of  $H'(s)$ .

Now,  $h(x)$  is related to the temperature distribution  $T(x)$  by

$$h(x) = \frac{8hc^2\bar{V}_{avg}^3}{\frac{hc\bar{V}}{kT} - 1} \Delta\bar{V}$$

Thus, we can generate the temperature distribution from the gathered data. In order to find the spatial resolution of the final data, we observe that we are getting the components of the data with frequency  $\leq f_{samp}/2$ . Hence, we can't detect variations of temperature occurring over a region which is covered by the satellite in a time less than or equal to  $2/f_{samp}$ . Considering the limitations of pointing accuracy (0.5 degrees accuracy in attitude determination) and the limitations in the rate of data transmission, the sampling rate was chosen to be 1 reading every 4 seconds, which brings the resolution down to 55 km.

Note that we can do all this processing only in the direction of motion of the satellite. In the direction perpendicular to the direction of motion of the satellite, the following methodology is employed to achieve the desired resolution:

On the nadir surface of the satellite here will be an array of  $N$  thermopiles each with a swath of  $S/2$  and having an overlap region of width  $S/2(1-1/N)$  with the previous one. We can then apply the same principle to the readings of all these thermopiles and attain a resolution equal to  $S/N$  in the perpendicular direction.

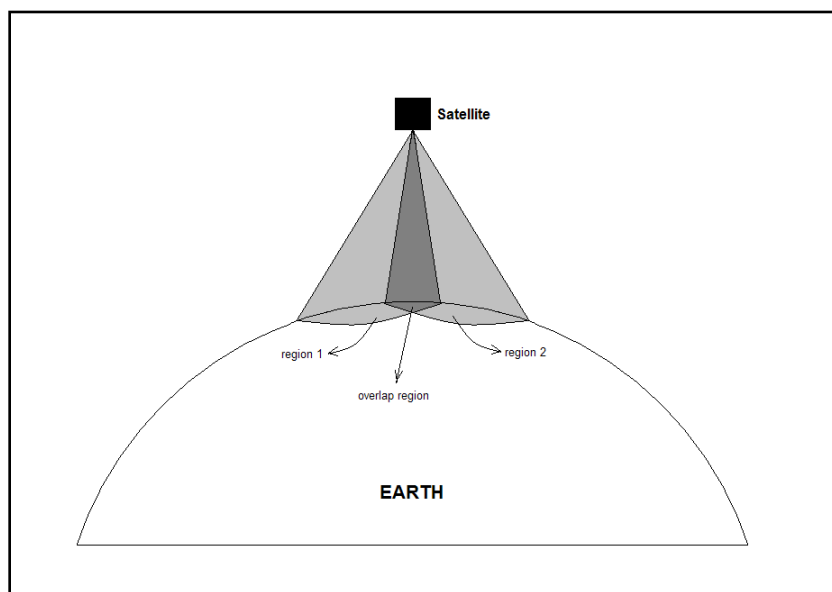


Figure 2. 8 Overlap regions of consecutive fields of view

Considering the base area available on the Nadir surface, it was decided that 25 thermopiles catering to measurements in the atmospheric window region and 25 thermopiles catering to measurements in the carbon dioxide absorption region will be used.

In order to restrict the field of views of the thermopiles to the required regions, collimators will be used in front of the sensors. These collimators will be in the form of steel plates which block the excess radiation. Fig 2.8 illustrates the situation.

#### 2.4.2: Method of Polynomial Interpolation

We also propose the following interpolation scheme to get the required data from the observed data.

Let the heat flux distribution have the expansion:

$$h(x) = \sum_{i=0}^{\infty} a_i x^i$$

Then we have from equation of  $q(x_0)$  used before, we get

$$\begin{aligned} q(x_0) &= \int_{-\delta}^{\delta} h(x + x_0) f(x) dx \\ &= \int_{-\delta}^{\delta} \left( \sum_{i=0}^{\infty} a_i (x + x_0)^i \right) f(x) dx \\ &= \sum_{k} \left( \sum_{i \leq k} \binom{k}{i} a_i \left( \int_{-\delta}^{\delta} x^i f(x) dx \right) \right) x_0^k \end{aligned}$$

Thus, if we denote the power series expansion of  $q(x_0)$  as

$$q(x_0) = \sum_j b_j x_0^j$$

Then we have that

$$b_k = \sum_{i \leq k} \binom{k}{i} a_i \left( \int_{-\delta}^{\delta} x^i f(x) dx \right)$$

Hence we can determine all  $a_i$ 's can be calculated from the knowledge of the  $b_k$ 's as they are linearly related.

## 2.5: Requirements from other Subsystems

The requirements desired from the other subsystems are defined below.

### Control Requirements

The spatial resolution is 55 km x 55 km. Thus, we require attitude determination and control so that the FOV is not be off from the required region by more than 5.5 km. This translates to an attitude accuracy of 0.5 degrees.

### Memory Requirements

Assuming that each of the thermopiles generates 10 bit data at each sampling interval, we have the total data collected in a day to be

$$D = N \text{ (no. of thermopiles = 50)} \times 86400\text{s}/4\text{s} \times 1\text{B} = 1.25\text{MB.}$$

Since the attitude and position are sampled at a much smaller rate, the memory requirement for the payload is 2.5 MB (In the worst case, data transmission might be possible only after a period of two days).

### Data transmission Rate Requirements

Since the average duration of contact with the ground station per day is 7.5 minutes, the data transmission rate required is

$$R = D/T_{\text{contact}} = 22.75\text{Kbps.}$$

## Chapter 3: Orbit Selection Criteria

### 3.1: Orbit Planning

#### 3.1.1: Calculation of Orbital elements

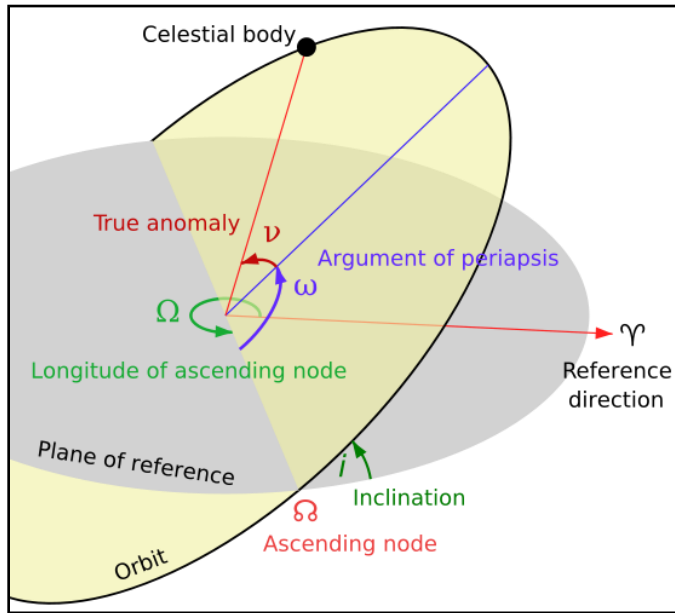


Figure 3. 1: Orbit Parameters

We are assuming our orbit to be the 9:30 am-pm Sun Synchronous orbit with altitude of 671 km, which is supposed to be launched in 1<sup>st</sup> Quarter of 2009. All our current calculations are using this orbit. None of the functions of the satellite are heavily depended on the orbit.

$$R_e = 6378.137 \text{ km}$$

$$a = 671 + 6378.137 = 7049.137 \text{ km}$$

$$e = 0 \text{ Assumed}$$

Since orbit sun synchronous therefore-

$$\omega_p = -\frac{3R_e^2}{2a^2} J_2 \omega_{sat} \cos i$$

Where-

- $J_2$  is the perturbation due to oblateness of earth : 1.08e-3
- $\omega_p$  is the period of revolution of earth around sun : 1.991e-7
- $\omega_{sat}$  is the angular velocity of satellite around earth : 1.067e-3
- $i$  is the inclination

Substituting values we get,  $i=98.118^\circ$

Since our orbit is circular therefore-

$\omega=0$  Argument of perigee

$\Omega = \text{Angle between sun and satellite at vernal equinox}$

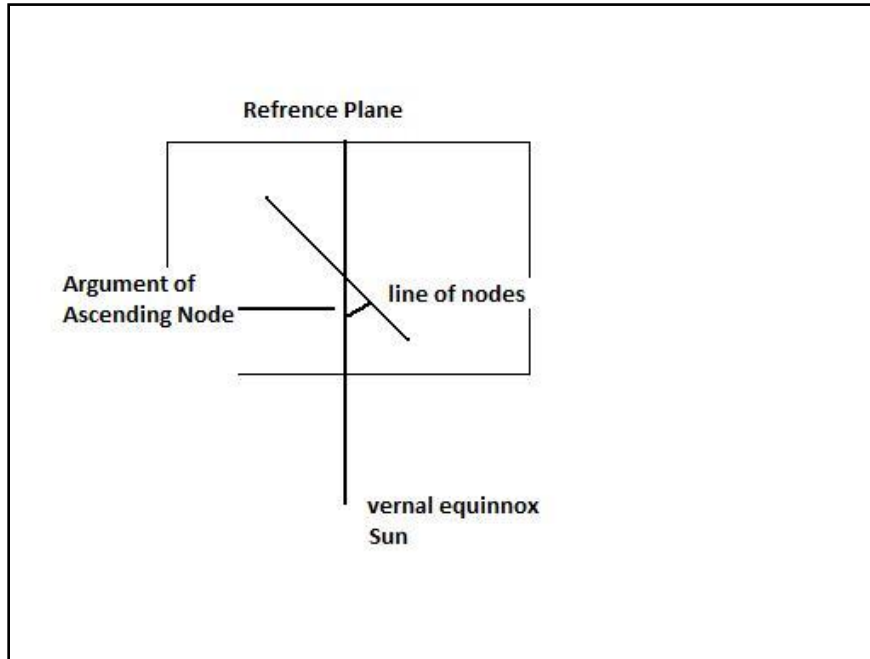


Figure 3. 2: Angle between Satellite and Vernal Equinox

At vernal equinox if sun passes overhead at a particular place on equator at noon then the point on equator corresponding to 9:30 am will be separated by  $\Omega=(12-9.5)*15=37.5^\circ$

Therefore,  $\Omega=37.5^\circ$

True anomaly ( $v$ )=Eccentric Anomaly=Mean Anomaly=0 (Depends upon time since launch)

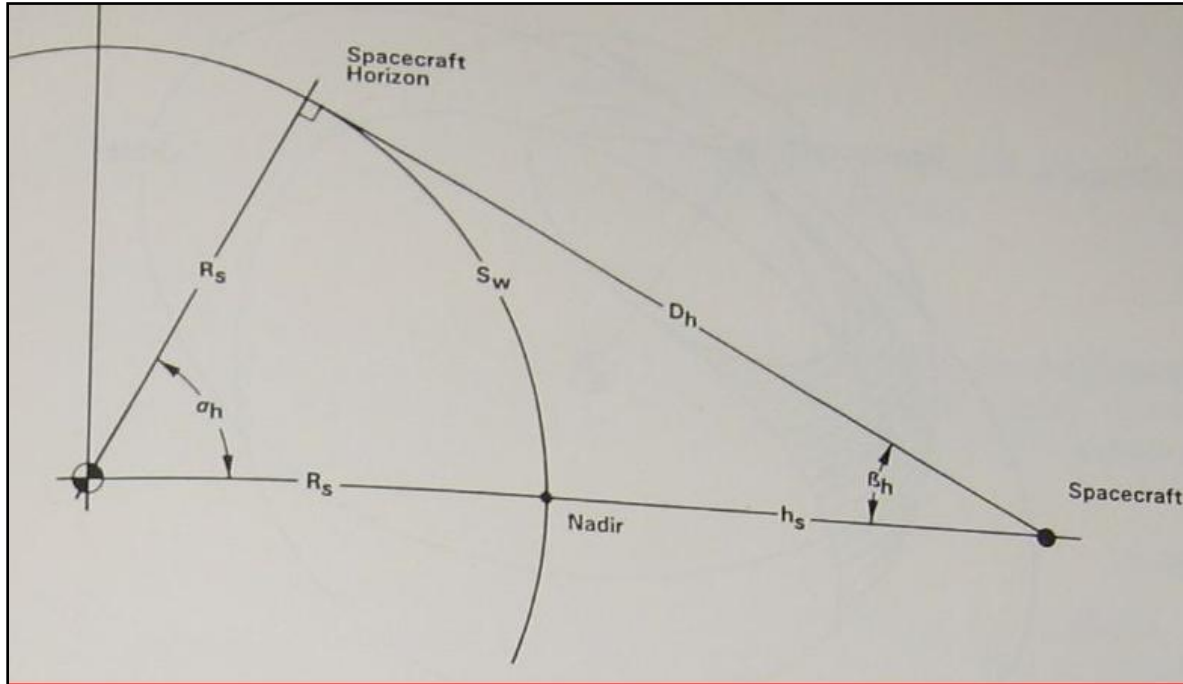
Therefore six orbital parameters are-

a	7049137 m
e	0 (Assumed)
i	$98.118^\circ$
$\Omega$	$37.5^\circ$
$\omega$	0
$v$	- (NA)

### 3.1.2: Time Period

$$T_p = \sqrt{\frac{4\pi^2 a^3}{GM}}$$

$$T_p = 5878.4 \text{ sec} = 97.97 \text{ min}$$



$$\theta = \cos^{-1} \frac{R_e}{R_e + h} = \cos^{-1} \frac{R_e}{a} = 25.2^\circ$$

$$\beta = \frac{\pi}{2} - \theta = 64.8^\circ$$

### 3.1.3: Communication Time

$$\text{Max time available} = \text{Time above horizon} = \frac{2\theta}{360} T_p = .14 T_p = 13.7 \text{ min}$$

Time available for effective communication

- Time taken to cross from -60 to +60
- $t = \frac{2\theta}{360} T_p \frac{120}{360} \cos \Delta$
- $\Delta = \text{angle from zenith}$

### 3.1.3.1: Angle from zenith

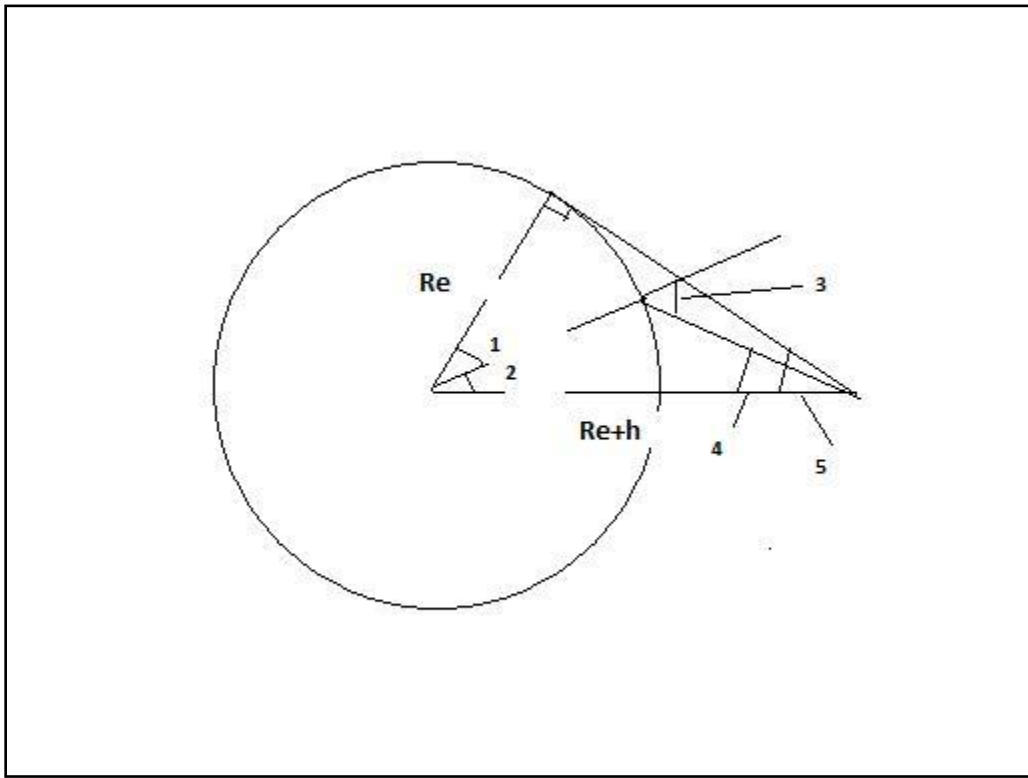


Figure 3. 3: Zenith Angle

For the Fig 3.3,

$$1+2=\theta$$

$$2=\theta_1$$

$$3=\Delta$$

$$5=\beta$$

If satellite does not pass overhead and  $\Delta$  is the zenith angle then by sine rule-

$$\frac{\sin \Delta}{R_e + h} = \frac{\sin(\Delta - \theta_1)}{R_e}$$

Solving we get

$$\cot \Delta = \cot \theta_1 - \frac{R_e}{R_e + h} \cosec \theta_1$$

where,  $\Delta$  is the angle from zenith

### 3.1.3.2: Footprint

$$A = 2\pi R_e^2 (1 - \cos \theta) = 2.4 \times 10^{13} m^2 = .047 \text{ of earth}$$

### 3.1.3.3: Ground Track

$T_p=97.97$  min which is not an integral multiple of 1 day therefore-

$\alpha$ =Angle by which earth rotates in  $T_p$  time= $24.49^\circ$

Number of revolutions per day=14.697

In one revolution ground track moves westward by  $\alpha$

Therefore in 14 revs angle travelled= $342.86^\circ$

and in 15 revs angle travelled= $367.35^\circ$

### 3.1.3.4: Revisit time

Since time period is not an integral multiple of 1 day therefore revisit time is not one day.

However after 14 revs satellite is  $17.14^\circ$  from station and since  $\Theta = 25.2$  therefore is visible from station. Similarly after 15 revs satellite is  $7.35^\circ$  from station therefore again visible.

### 3.1.3.5: Satellite passes over ground station

Day	Contact Time
1	10.812
2	9.059
3	10.519
4	1.549
5	9.639
6	9.649
7	1.549
8	10.51
9	9.063
10	1.666
11	10.814

Thus we can see that cycle almost repeats itself after 148 passes or around 10 days. On an average in one day we will have 7.4 min of contact time. The graph below shows variation of

$T_{\text{contact}}$  with no. of revolutions. All the short term and long term periodicities are apparent in Fig 3.4.

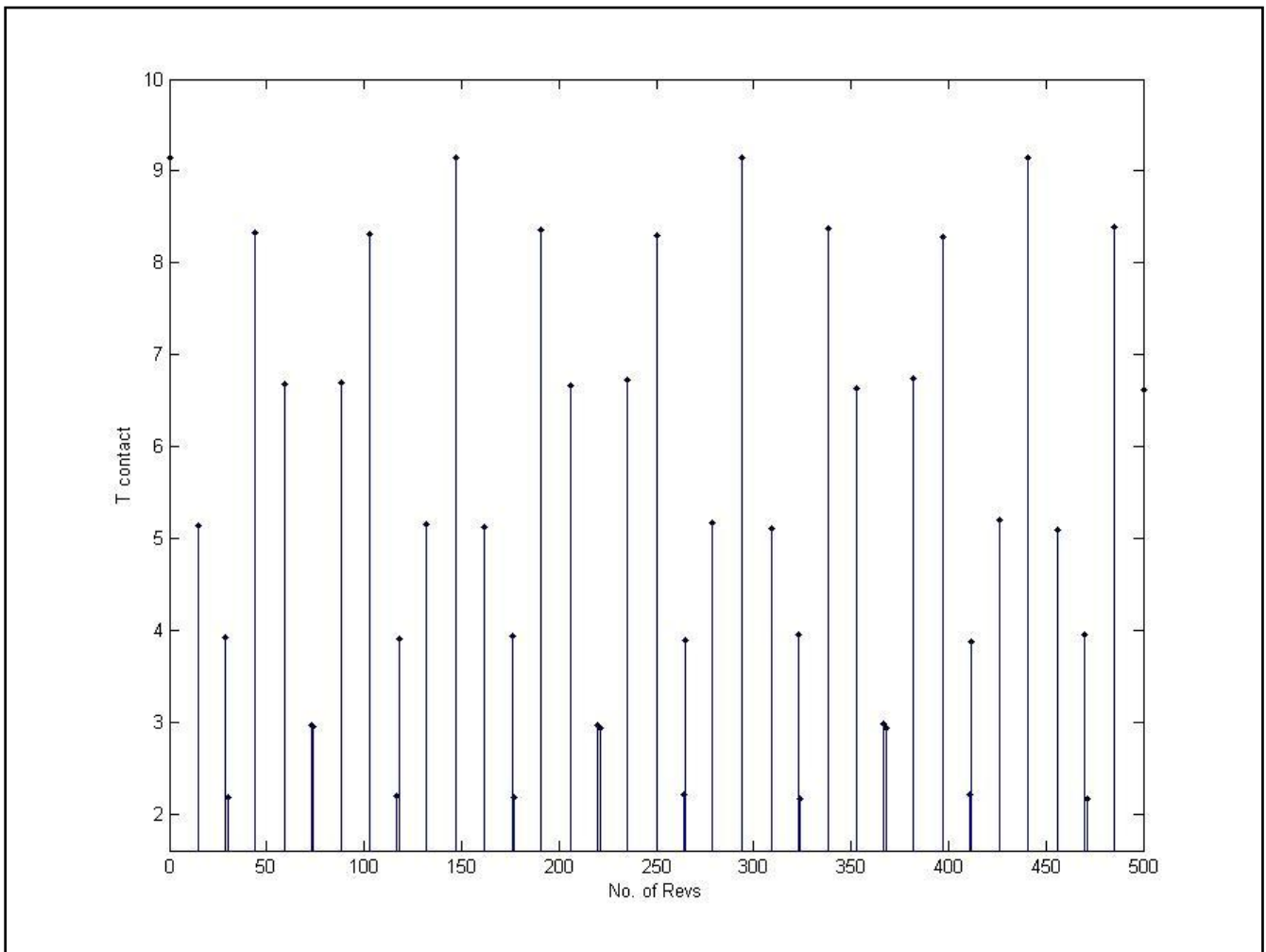


Figure 3. 4: Graph between Contact time and Number of Revolutions

### 3.1.4: Orbit Simulation Software

Software for simulation is AGI Satellite Toolkit which is industrially recognized software for generating satellite data. Software uses SGP4 algorithm as its orbit propagation algorithm.

## 3.2: Orbit Determination

### 3.2.1: Need for Orbit Determination

Many satellite operations require us to know the position of the satellite in space with certain level of accuracy. In case of our satellite we need to know the orbital position of the satellite for two reasons.

#### 1. Payload requirements

Since our satellite intends to make a thermal map of the earth therefore with each image the satellite takes we need to know the position associated with image in order to understand what part of earth is being imaged. Payload requires us to measure the position and velocity of the satellite within an accuracy of 10m and 10m/s respectively.

#### 2. Functioning of magnetometer

Magnetometer, which is a sensor for attitude determination of the satellite, measures magnetic field along the body axes of the satellite and then compares it with the inertial magnetic field given by the IGRF model to get the attitude of the satellite. For calculating the reference magnetic field from the IGRF model we need the position of satellite in space. Since the magnetic field does not change very much with distance we can assume that payload requirements are much more stringent than the magnetometer requirements.

### 3.2.2: Methods of Orbit Determination

Position of satellite in space can be determined in two ways:

1. Orbit Propagation
2. GPS Sensor

#### 3.2.2.1: Orbit Propagation

If we know the position and velocity of the satellite at the time of injection into the orbit. We can use the orbit propagation algorithms to predict the position of satellite in future times. This method has two disadvantages:

1. We can never model the perturbations on the satellite with complete accuracy.
2. We can never know the injection conditions of the satellite with sufficient accuracy.

Both of these induce errors in orbit prediction and cause the predicted values to drift from the actual values.

### 3.2.3: Global Positioning System (GPS)

#### 3.2.3.1: Introduction

GPS is a system of determination of position by receiving data from 31 satellites orbiting the earth in 6 orbits. These orbits are equally spaced at 60 degrees to each other. Each GPS satellite transmits its own unique pseudo-random code at a pre-determined frequency, namely 10.23 MHz. Each pseudo-random code consists of 1023 chips thus the signal repeats every 1 ms. This system is called the Coarse/Acquisition (C/A) mode and is primarily used for civilian purposes. There is another P(Y) system for military purposes. Besides, each satellite also transmits its own ephemeris (position and orbit of that satellite with reference to earth) data, almanac and also the GPS date and time of day. The ephemeris data is transmitted once every 30 s and takes 18 s to be transmitted.

#### 3.2.3.2: Calculation of position from these data

Calculation of position from GPS data primarily makes use of a technique called trilateration. This is a mathematical process of fixing an object's position by measuring distances from three objects of known positions.

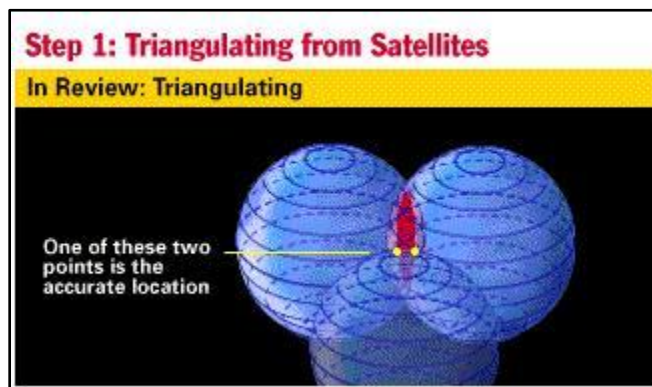


Figure 3. 5: Triangulating from satellite

Suppose that we know that we are 25000 km from a satellite whose position we know from its ephemeris data. This fixes us down to a sphere of radius 25000 km centered at that satellite. Further if we know we are 29000 km from another satellite we know we are on the circle of intersection of those two spheres. Knowing our distance from another satellite pins us down to

two points of intersection of the three spheres. One of them is usually physically unacceptable. Thus we are able to fix our position precisely.

### 3.2.3.3: Reference frames used to describe the motion of a satellite

There are mainly three reference frames used to describe the motion of a satellite around the earth:

- Earth-Centered Inertial frame (ECI)
- Earth-Centered Earth-Fixed frame (ECEF)
- Earth-Centered Orbit frame
- Orbit frame
- Body frame

They are discussed below:

- *Earth-Centered Inertial frame (ECI)*: This frame is an inertial frame whose origin is at the center of the earth, z-axis towards the North Pole, x-axis towards the vernal equinox, the point where the plane of the Earth's orbit about the Sun crosses the Equator going from south to north and the y-axis completes a right handed coordinate system.
- *Earth-Centered Earth-Fixed frame (ECEF)*: This frame is a non-inertial frame rotating with the earth i.e. it is earth-fixed. Its z-axis is fixed towards the North Pole but the x and the y axes rotate at an angular speed of about  $7.2921 \times 10^{-5}$  rad/s. The x-axis points towards the intersection of  $0^\circ$  latitude and  $0^\circ$  longitude, the y-axis completing a right handed coordinate system.
- *Earth-Centered Orbit frame*: This is a frame in which the Keplerian elements are given. This frame is thus the frame directly used to describe the motion of the satellite about the earth. Its x-axis is towards the perigee, y-axis along the minor axis of the satellite orbit and z-axis towards the normal to the plane of the orbit.
- *Orbit frame*: This frame is also a satellite fixed frame which rotates with the satellite at a rate which depends on the height of the satellite.
- *Body frame*: This frame is fixed onto the satellite and thus makes description of its motion about its center of mass very simplified. Its origin is at the COM of the satellite.

### 3.2.3.4: Measurement of position by GPS receiver

#### 3.2.3.4.1: Distance measurement

Every satellite transmits its own unique pseudo-random code. These codes are intercepted by the receiver which itself generates a same code. However there is a time difference between the signal received and that transmitted due to the path light had to cover from the satellite to us.

Symbolically if  $\Delta t$  be the time difference then

$$\Delta d = \Delta t \times c \text{ (where } c=\text{velocity of light in vacuum).}$$

The receiver measures this phase difference by delaying its signal until it matches the received signal. However to measure distance accurately, we must have extremely accurate clocks (e.g. for an error of 1  $\mu\text{s}$  in measurement of time the error in position is  $3 \times 10^8 \times 10^{-6} = 300 \text{ m!}$ ).

To get rid of this we measure the distances from more than 3 satellites. If our measurements had been accurate they should all have intersected at a single point. But due to errors in measurement they will not. Thus we correct each measurement by a correction factor so that they do intersect at a point.

However, note that by getting this correction factor we have been able to correct our clocks to atomic precision (which are actually installed on the GPS satellites).

Thus, actually the position is calculated in four-dimensional space-time i.e. we know the time also along with the position.

The reason for a pseudo-random code is that This ensures that the satellite signal is not messed up with any other stray signal or with signal from another satellite.

#### 3.2.3.4.2: Errors

The major sources of error in this measurement are as follows:

Sources of User Equivalent Range Errors (UERE)

Source	Effect
Ionospheric effects	$\pm 5 \text{ meter}$
Ephemeris errors	$\pm 2.5 \text{ meter}$
Satellite clock errors	$\pm 2 \text{ meter}$

Multi path distortion	$\pm 1$ meter
Tropospheric effects	$\pm 0.5$ meter
Numerical errors	$\pm 1$ meter

We are going to discuss each of these one by one.

i. [Ionospheric errors:](#)

The ionosphere plays a major role in modifying the signals sent by the GPS satellites.

While passing through the ionosphere, the frequency as well as the phase of the signals is distorted. These errors are completely random and cannot be predicted beforehand.

However, this effect can be used to gain various important details about the atmosphere including its moisture level, temperature, free electron density etc.

ii. [Ephemeris errors:](#)

These errors arise due to the 'backdated' ephemeris data transmitted by the satellite (it is sent out once in 30 minutes, thus doesn't account for any minute change of the orbit within those 30 minutes).

iii. [Satellite clock errors:](#)

Though the clocks on board the GPS satellites are very accurate atomic clocks, still they do have an error inherent in them. These are much more stable errors and can easily be eliminated.

iv. [Multipath distortion:](#)

This error is generally predominant at ground level where the signal can reach the observer by various paths by reflection from various nearby objects.

However, in a satellite context, this error can be observed when the signal takes several paths, by refraction in the ionosphere and phase of each is slightly different from each other.

v. [Tropospheric effects:](#)

These effects are not as important in satellite context as the satellite usually orbits high above the troposphere. But they can be measured when a satellite is receiving signal from a GPS satellite which is near the horizon.

vi. Relativistic errors:

The theory of relativity predicts that due to the constant motion of the satellites, the clocks on board the satellites go slow. Thus the frequency of the clocks must be somewhat less than the intended frequency. Actually it is set to 10.22999999543MHz instead of 10.23 MHz.

There is also another source of relativistic errors called the Sagnac effect. This is due to the fact that the measurements on the satellite are done in a non-inertial frame instead of an inertial one, whereas the Lorentz transformations are valid for only inertial frames.

Ignoring this will produce an error of about 10 m in position.

### 3.2.3.5: Potential Uses in satellite programme

#### Latitude and longitude measurement:

The primary use of a GPS receiver is of course to calculate the position of the satellite.

#### Time measurement:

The GPS system calculates the position of the body in four-dimensional space-time. Thus we are able to get the accurate present time by these measurements.

#### Measurement of atmospheric data:

Several important parameters of the atmosphere can be obtained from GPS measurements:

#### Measurement of ionospheric errors:

While passing through the ionosphere the frequency as well as the phase of the signals is modified. The equation governing the time delay of a radio wave propagating through the ionosphere is:

$$\Delta t = 40.3/(c \times f^2) \times \int N dl \dots \dots \dots \text{Seconds.} \dots \dots \dots \quad (1)$$

Where

$N$  = free electron density in ionosphere in  $\text{el/m}^2$

$c$  = speed of light in vacuum

$\int dl$  is the integral over the path followed by the signal.

Now, GPS satellites transmit data over two widely spaced frequencies, namely:

$L_1 = 1575.42 \text{ MHz}$

$L_2 = 1227.60 \text{ MHz}$

Thus if we calculate the difference between the times as measured by these two sets of frequencies there will be some difference between the two given by:

$$\begin{aligned}\delta(\Delta t) &= 40.3/c \times (1/f_1^2 - 1/f_2^2) \times \int N dl \dots \dots \dots \text{seconds} \\ &= \Delta t_1 \times f_2^2/(f_2^2 - f_1^2). \dots \dots \dots (2). \dots \dots \text{where } \Delta t_1 = \text{time delay of } L_1 \\ &\quad \text{frequency}\end{aligned}$$

For the two particular two frequencies selected for GPS satellites this simplifies to

$$\delta(\Delta t) = \Delta t_1 \times 1.546.$$

Now, we can measure  $\int N dl$  by putting back this value of  $\Delta t_1$  in (1).

By getting the values of  $\int N dl$  for various positions of the satellite we can get a fairly accurate model of vertical electron distribution profile in ionosphere.

#### Measurement of Tropospheric errors:

These can be measured by a technique called 'radio occultation' technique. This technique can be briefly summarized as follows.

When a satellite receives data from a GPS satellite that is near the horizon, the signals pass through the troposphere and are modified by it. By measuring these errors, we can make a fairly accurate estimate of various tropospheric parameters.

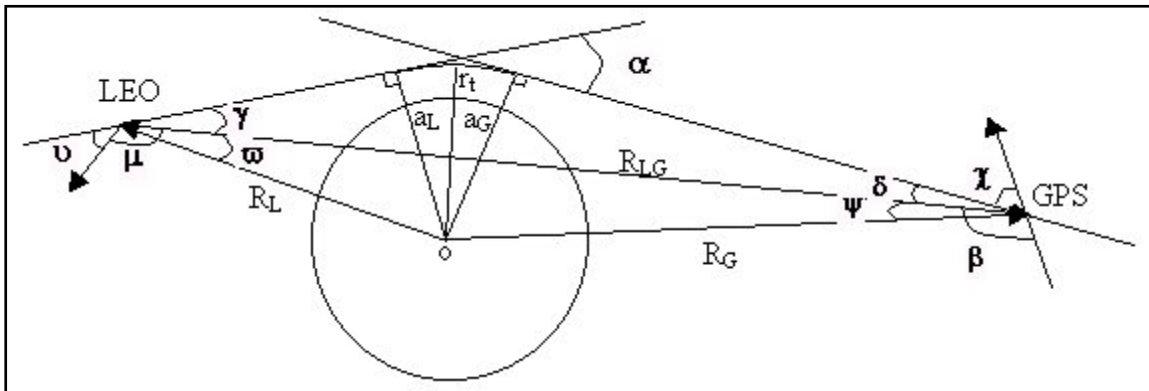


Figure 3. 6: Tropospheric Errors

#### Doppler shift observations:

The variation of  $\alpha$  with  $\omega$  primarily depends upon the vertical profile of the atmosphere. We always expect a Doppler shift in the frequency of the received signal due to relative motion between the satellite and the GPS source. But this shift depends upon the projection of the relative velocity on the line joining the two satellites, which is distorted by path through troposphere. During an occultation the variation of  $\alpha$  with  $\omega$  primarily depends upon the vertical profile of atmospheric refractive index.

The refractive index of atmosphere is given by

$$N = (n - 1) \times 10^6 = 77.6 \times P/T + 3.73 \times 10^5 \times P_w/T^2 - 40.3 \times 10^5 \times N_e/f^2$$

where  $N$ : refractivity

$P$ : atmospheric pressure [mbar]

$P_w$ : water vapor [mbar]

$n_e$ : electron number density per cubic meter [number of electron/m<sup>3</sup>]

$f$ : transmitter frequency [Hz]

$w$ : liquid water content [g/m<sup>3</sup>]

#### Attitude measurement by GPS data:

With the help of extremely sophisticated GPS receivers placed along three axes of a satellite we can directly measure the attitude of the satellite to a fair degree of accuracy. The necessary requisites of a GPS receiver for this purpose are:

1. high precision

## 2. dual-frequency receiver

For example, an admissible error of  $1^\circ$  in the attitude measurement needs an accuracy of about .5 cm in the measurement of position which is too optimistic.

Another way to measure attitude which is more commonly used is to place 3/4 antennas on the satellite on the axes. The signals from these antennas simultaneously fed to the receiver which then measures attitude by interferometric computations.

### 3.2.3.6: GPS Sensors

Receiver	T(°C)	Mass (gm)	Dimensions (mm)	Power (W)	Position (m)	Velocity (m/s)	TTFF (s)
SSTL SGR 05	-25 to +50	20	70 x 45 x 10	0.2 - 0.8	10	0.15	
CMC receiver	0 to +40	1200	235 x 154 x 71	6	0.1	N/A	
SSTL SGR 20*	-20 to +50	1000	160 x 160 x 50	5.5 - 7	15	1.5	
Turbo Star	N/A	N/A	212 x 212 x 44	15	N/A	N/A	
AAD*	-80 to +80	175	110 x 70 x 50	N/A	N/A	N/A	
UBLOX chip	Deter mined by extern al hardw are	Determined by external hardware	8 x 8	50m	n/a (as of now)	n/a (as of now)	1
Jupiter (rockwell)	n/a	n/a	n/a	n/a	25	0.1	18

Of these the SGR series and the UBLOX seem to be the best options. The SGR is very costly. UBLOX price is still not certain.

### 3.2.3.6.1: The SGR series

#### 3.2.3.6.1.1: SGR-05 GPS Receiver

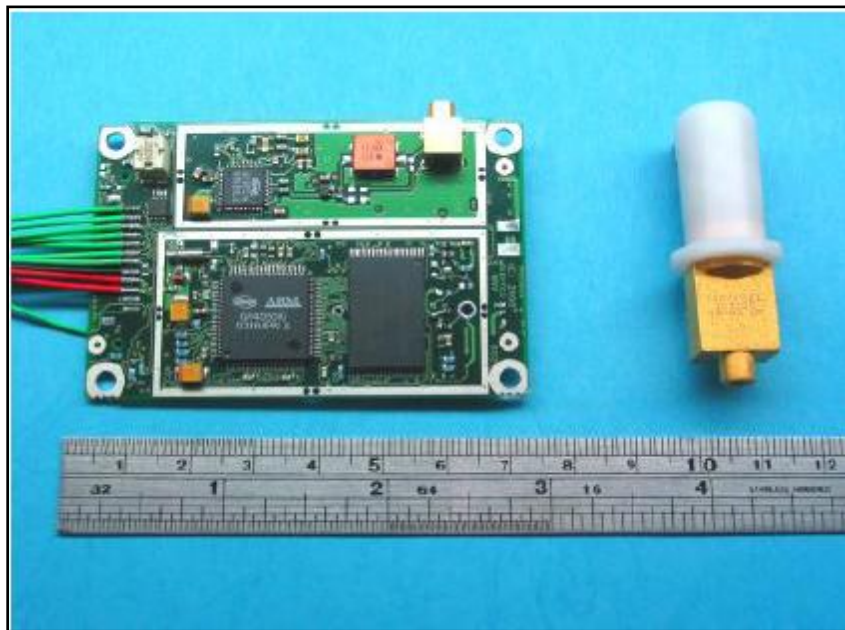


Figure 3. 7: SGR-05

#### Applications

- Positioning and orbit determination
- Time-stamping, onboard clock synchronization
- Low budget or very small satellites, micro and nanosatellites

#### Characteristics

- 12 channels receiving L1 C/A code
- 1 antenna
- Time (UTC): 1 $\mu$ s
- Position (2s): 10 m
- Velocity (2s): 0.15 ms  $^{-1}$
- Dynamic Capability: 8 kms  $^{-1}$ , 2 g
- Time to First Fix (TTFF): 60 s warm start; 9 minutes cold start.

- Interfaces: 3.3V TTL UART channels, 5 V power and pulse per second.

#### Physical & Power

- SGR05U OEM Dimensions: 70 x 45 x 10 mm
- SGR05U Mass: 20 g
- 0.50-0.8 W @ 5 V Also lower power mode (TBC)

#### Environmental (Acceptance Level)

- Vibration: 15 g rms
- Temp: SGR05U: 0° C to +50° C  
SGR05P: -20°C to +50°C
- Radiation: > 11 kRad (Si) tolerance demonstrated. SEE results available.

The SGR05 is a spacecraft orbit determination and timing subsystem designed for miniature LEO applications. The SGR05 provides GPS standard time, position, and velocity measurements in a compact and low power unit at low cost. Two grades of the SGR05 are available: SGR05U is a lower cost receiver which is sold as a standard COTS hardware product and SGR05P is a more complete package, supplied with all the acceptance documentation, parts traceability and support expected of a professional space product. Both grades of receiver are supplied with firmware suitable for operation in space.

#### TYPICAL MEASUREMENT PRECISION

Pseudorange	0.9 m	Doppler Velocity	0.5 m/s
Carrier-smoothed range	0.15 m	Carrier range rate velocity	0.03 m/s
Carrier Phase noise	1.5 mm	Filtered velocity	0.01 m/s

### 3.2.3.6.1.2: SGR-10 GPS Receiver

#### Applications

- Positioning and orbit determination
- Time-stamping, on-board clock synchronisation
- Small and large satellites
- Manoeuvring space vehicles
- Inertially stabilized satellites

#### Characteristics

- 24 L1 C/A code channels
- 2 antennas
- Time(UTC): 1
- Position (95%):10m
- Velocity(95%):0.15ms<sup>-1</sup>
- Dynamic Capability:8kms<sup>-1</sup>, 2g
- Time to first Fix (TTFF):50 s warm start; 3.5 mins cold start
- Interfaces: 28V power, RS422, CAN, PPS

Qualification / Heritage	
•SGR-10s flown on	Thai-Paht (1998), Tsinghua-1 (2000), TiungSat-1, (2000), AISAT-1 (2002), NigeriaSat-1 (2003), UK-DMC (2003)
• SGR-10 qualified and delivered for NASA-OSC's DART rendezvous mission	

Figure 3. 8: Heritage of SRG-10

The SGR-10 is a spacecraft orbit determination sub-system designed for small and large LEO satellite applications. The SGR-10 provides GPS standard time, position, velocity in a compact qualified unit, proven in orbit on numerous missions. The SGR-10 has 24 channels enabling a

very fast time to first fix, and supports two antennas to improve visibility under changing vehicle orientations.

## Features

- SGR chipset is based on high performance commercial Zarlink GPS chipset and ARM60B 32 bit RISC processor.
- Radiation susceptibility of parts has been evaluated in a joint SSTL/ESA programme. The SGR has been designed to be tolerant to radiation and has countermeasures against Single Event Upsets and Latch-ups (SEU/SEL).
- Telemetry and telecommand independence from the primary processor is provided by a separate TTC Node.
- Primary interfaces to the SGR comprise of RS422 (point-to-point) and CAN bus (industrial multi-node Controller Area Network).
- Code stored in Flash memory to enable rapid booting and future functional upgrades, even once in orbit.
- Windows program provided to monitor and control the SGR and to view and process logged data from the SGR.
- Testing and PA plans available. Environmental and Acceptance Testing and PA plans can be tailored to suit customer.

## PERFORMANCE

	Typical (95%)	Max (95%)
Orbital Position (3-D)	10 m	20 m
Orbital Velocity (3-D)	0.15 m/s	0.25 m/s
Time	0.5 $\mu$ s	1 $\mu$ s
Time to First Fix (cold)	200 s	350 s
Time to First Fix (warm)	50 s	90 s

## TYPICAL MEASUREMENT PRECISION

Pseudorange	0.9 m	Doppler Velocity	0.5 m/s
Carrier-smoothed range	0.15 m	Carrier range rate velocity	0.03 m/s
Carrier Phase noise	1.5 mm	Filtered velocity	0.01 m/s

### 3.2.3.6.1.3: SGR-20 GPS Receiver

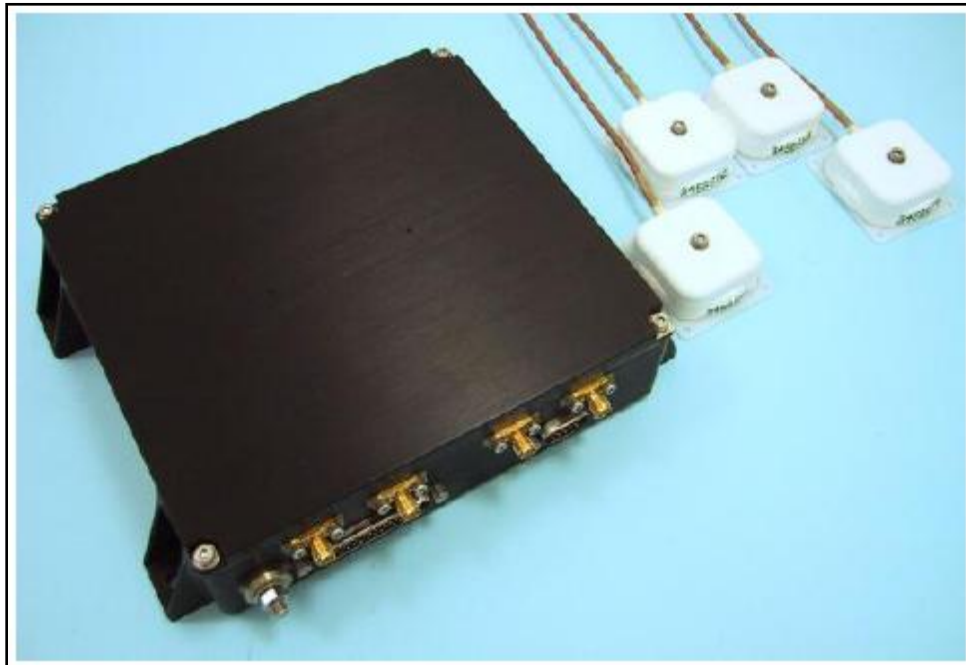


Figure 3. 9: SGR-20

### Application

- Positioning and orbit determination
- Time-stamping, on-board clock synchronization
- Attitude determination
- Small and large satellites
- Manoeuvring space vehicles
- Inertially stabilised satellites

## Characteristics

- 24 L1 C/A code channels
- 4 antennas
- Time(UTC): 1
- Position (95%):10m
- Velocity(95%):0.15ms<sup>-1</sup>
- Attitude determination: 0.5-1degree
- Dynamic Capability:8kms<sup>-1</sup>, 2g
- Time to first Fix (TTFF):50 s warm start; 3.5 mins cold start
- Interfaces: 28V power, RS422, CAN, PPS

## Qualification / Heritage

- SGR-20 flown on:  
UoSAT-12 (1999),  
ESA's PROBA (2001)  
BILSAT-1 (2003), Topsat (2005)
- SGR-20 qualified and delivered for  
Spacehab International Space  
Station application
- SGR-10 (subset of SGR-20) flown  
on Thai-Paht (1998), Tsinghua-1  
(2000), TiungSat-1, (2000), AISAT-  
1 (2002), NigeriaSat-1 (2003), UK-  
DMC (2003), China-DMC (2005)
- SGR-10 used on NASA-OSC's  
DART rendezvous mission

Figure 3. 10: Heritage of SGR-20

The SGR20 is a spacecraft orbit determination subsystem designed for small and large LEO satellite applications. The SGR20 provides GPS standard time, position and velocity in a compact qualified unit, proven in orbit on numerous missions. The SGR20 has 24 channels enabling a very fast time to first fix, and supports multiple antennas to improve visibility under changing vehicle orientations and attitude determination.

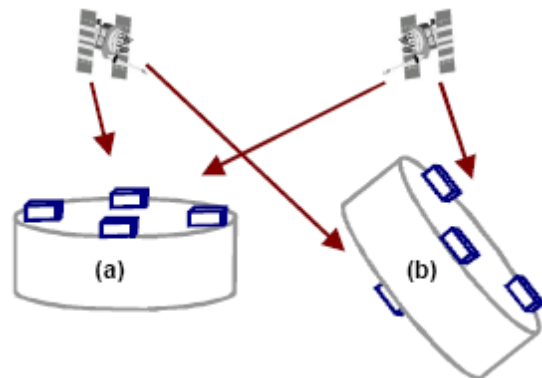
## POSITIONING PERFORMANCE

	Typical (95%)	Max (95%)
Orbital Position (3-D)	10 m	20 m
Orbital Velocity (3-D)	0.15 m/s	0.25 m/s
Time	0.5 µs	1 µs
Time to First Fix (cold)	200 s	350 s
Time to First Fix (warm)	50 s	90 s
Attitude determination	0.5 – 1°	TBD

## TYPICAL MEASUREMENT PRECISION

Pseudorange	0.9 m	Doppler Velocity	0.5 m/s
Carrier-smoothed range	0.15 m	Carrier range rate	0.03 m/s
Carrier Phase noise	1.5 mm	Filtered velocity	0.01 m/s

- For attitude determination, configuration of antennas is important.
- Three-four antennas required to determine attitude, placed on 0.2 – 2 metre baseline pointing spacewards.
- Multipath should be reduced by avoiding too many protrusions on antenna facet.
- Fourth antenna could be mounted underneath to improve visibility, see (b).



### 3.2.3.6.2: UBLOX

UBX-G5010

u-blox 5 GPS single chip with SuperSense®

GALILEO-ready



The UBX-G5010 GPS single chip boasts an acquisition performance of under 1 second. The chip features the award-winning SuperSense® -160 dBm indoor GPS sensitivity, power needs of less than 50 mW and a footprint smaller than 100 mm<sup>2</sup>. These features make the UBX-G5010 ideal for cell phones, PDAs, personal navigation devices, cameras, media players and other battery-operated portable devices.

Engineering samples will be available in Q1 2008.

Highlights:	Features:
<ul style="list-style-type: none"><li>• Ultra-fast acquisition: Under 1 second time-to-first-fix (TTFF)</li><li>• Massively parallel GPS engine with 50 channels and over 1 million correlators</li><li>• -160 dBm SuperSense Indoor GPS</li><li>• Cost-optimized architecture: No external LNA and Flash EPROM needed</li><li>• Low power consumption</li><li>• Supports A-GPS services including AssistNow Online and Offline</li><li>• GALILEO ready</li><li>• &lt; 100 mm<sup>2</sup> footprint</li><li>• Small bill of material: As few as 19 external components</li></ul>	<ul style="list-style-type: none"><li>• 32 channel dedicated acquisition engine</li><li>• 18 channel correlator engine</li><li>• Complies with RRLP, RRC, OMA/SUPL and proprietary protocols</li><li>• Exceeds performance requirements for international A-GPS standards including 3GPP TS 25.171, TIA 916 and E911 Phase II</li><li>• Wide clock frequency range</li><li>• Supports different XTAL and TCXO frequencies</li><li>• Flexible voltage supply options; no external LDO (low drop-out regulators) required</li><li>• Supports SBAS: WAAS, EGNOS, GAGAN and MSAS</li></ul>

- Connectivity: USB, 2 UARTs, SPI, DDC ( $I^2C$  compliant)
  - RoHS compliant (lead-free)

	Series	Voltage Range (V)	Thickness (mm)	50-channel engine	KickStart	SuperSense	FW Update / FLASH	UART	USB	SPI	DDC	AssistNow Online	AssistNow Offline	Dead Reckoning	Raw Data	Precision Timing	1PPS	CFG Pin	Reset Input	Antenna Supply	Antenna Supervisor
LEA-5H	PRO	2.7-3.6	3.0	✓	✓	✓	✓	1	1		1	✓	✓			✓	✓	1	✓	✓	
LEA-5S	PRO	2.7-3.6	3.0	✓	✓	✓		1	1		1	✓	✓			✓	✓	1	✓	✓	
LEA-5A	PRO	2.7-3.6	3.0	✓		✓		1	1		1	✓	✓			✓	✓	1	✓	✓	
LEA-5T	PRO	2.7-3.6	3.0	✓	✓	✓	✓	1	1		1	✓	✓			✓	✓	1	✓	✓	

**Table 1: Features of the LEA-5 Series**

## **Part B – Making of the Satellite: Subsystems**

### **Chapter 4: Communication**

#### **4.1 Introduction**

The main objective of the communication team of the student sat is to provide a working downlink for the data collected onboard the satellite. In this report we have looked at the various alternatives that are available to us to achieve our desired objectives.

The report is divided into five parts based on the above plan of action

- Antenna frequency
- Modulation
- Link budget
- Onboard antenna
- Ground station antenna

#### **4.2 Antenna frequency**

The following frequencies are available for amateur use according to the rules and regulations of the Government of India. Amateur Service is permitted in the following bands by the Government of India:

1820-1860 kHz

3500-3700 kHz

3890-3900 kHz

7000-7100 kHz

14000-14350 kHz

18068-18168 kHz

21000-21450 kHz

24890-24990 kHz

28000-29700 kHz

144-146 MHz

434-438 MHz

1260-1300 MHz

Among them, three frequencies are chosen for further studies for our downlink frequency. They are:

- a) 434 MHz
- b) 866 MHz
- c) 902 MHz

The main reason behind selection of each of these frequencies is those industrial grade components are easily available at these operating frequencies. Also, as we move into still higher frequency bands the free space loss increases much beyond tolerable margins leading to negative system link margins.

Signal attenuation at different frequencies have been studied below.

#### 4.2.1 Transmitting frequency 434 MHz

- Ionospheric losses : 0.4 dB
- Free space losses : 153.2 dB
- Atmospheric losses : 2.1 dB

#### 4.2.2 Transmitting frequency 868 MHz

- Ionospheric losses : 0.3 dB
- Free space losses : 159.2 dB
- Atmospheric losses ~ 2.1 dB

#### 4.2.3 Transmitting frequency: - 902 MHz

- Ionospheric losses : 0.8 dB
- Free space losses : 159.1 dB
- Atmospheric losses ~ 2.1 dB

We are unsure whether it is possible to get a permission of 902 MHz for student satellite purpose. If permission is not available, then we will try to go for 1260MHz. This will help in reducing the dimensions of patch antenna.

### 4.3 Modulation

The main problem in radio systems is to transmit information with little use of power and bandwidth as possible and at the same time maintaining the simplicity of the equipments. Modulation is when the carrier wave in a signal is changed to channel it is transmitted over. The carrier wave can be modulated in three different ways by changing the phase. In satellite communication the amplifier is near saturation and if we want to reinforce a modulated carrier wave, we have to keep the amplitude or the envelope for the carrier wave constant. So the best option is to go with modulation techniques that employ a change in the frequency and phase. In this report we have a look at all the different modulation techniques that were considered by our team and the advantages and disadvantages of those techniques.

#### 4.3.1 ASK

Advantages:-

- a) It is the easiest to accomplish.
- b) Its noise rejection is good.

Rejected as:-

- a) It is not a constant envelope modulation technique which may lead to unpredictable variation of the signals amplitude.
- b) It does not support intelligent data transmission.

#### 4.3.2 PSK

(binary or quadrature)

Advantages:-

- a) It supports high bit rates.
- b) It is a constant envelop modulation technique.
- c) It is robust even in the presence of noise.

Rejected as:-

- a) It is too complex to accomplish.
- b) We do not require that high data rates.
- c) The encoding and decoding of the signal would require complex algorithms (both on the OBC and the ground station) as the transmitted and received signals would have to be synchronized so

that a pulse which is sent as a zero is not recognized as a one and vice versa. And this phase difference would depend on the path length traveled by the pulse.

#### 4.3.3 GMSK

Advantages :

- a) It has all the properties of FSK and most of PSK.
- b) It has a low bandwidth bit rate product which would enable us to transmit more data in less bandwidth.
- c) It's interband interference is less.

Rejected as:-

- a) It isn't easily available.
- b) There is the problem of inter symbol interference ( though this can be minimized using a separate component on board).
- c) The transmitter requires extra power to overcome the noise generated due to inter symbol interference. Also the receiver would become quite complex.

#### 4.3.4 FSK

Advantages:

- a) It is a constant envelop modulation
- b) It is robust enough for our purpose
- c) There is no need for 100 % synchronization.
- d) The bandwidth – bit time product is quite high compared to GMSK , so no inter symbol interference takes place.

Disadvantages:

It does not support as high data rates as QPSK

- a) The bandwidth efficiency is less
- b) There may be a problem of interband interference as well.

## 4.4 Antenna

### 4.4.1 Antenna fundamentals

An antenna is a conductive element which converts electrical energy into an electromagnetic field (transmit), or converts an electromagnetic field into electrical energy (receive). An important feature is the property of reversibility, the same antenna can be used with the same characteristics as transmit or as a receive antenna. An antenna is characterized by its center frequency, bandwidth, polarization, gain, radiation pattern and impedance. These factors have been studied below.

#### 4.4.1.1 Resonant frequency

The resonant frequency is related to the electrical length of the antenna. The electrical length is usually the physical length of the wire divided by its velocity factor (the ratio of the speed of wave propagation in the wire to  $c_0$ , the speed of light in a vacuum). Typically an antenna is tuned for a specific frequency, and is effective for a range of frequencies usually centered on that resonant frequency. However, the other properties of the antenna (especially radiation pattern and impedance) change with frequency, so the antenna's resonant frequency may merely be close to the center frequency of these other more important properties.

#### 4.4.1.2 Gain

Gain as a parameter measures the directionality of a given antenna. An antenna with a low gain emits radiation with about the same power in all directions, whereas a high-gain antenna will preferentially radiate in particular directions. Specifically, the Gain, Directive gain or Power gain of an antenna is defined as the ratio of the intensity (power per unit surface) radiated by the antenna in a given direction at an arbitrary distance divided by the intensity radiated at the same distance by an hypothetical isotropic antenna .We should remember that gain does not imply that the power is amplified by the antenna . It just gives an idea regarding the power distribution of an antenna and how directional it is.

#### 4.4.1.3 Radiation pattern

The radiation pattern of an antenna is the geometric pattern of the relative field strengths of the field emitted by the antenna. The radiation pattern of an antenna is typically represented by a three dimensional graph, or polar plots of the horizontal and vertical cross sections.

#### 4.4.1.4 Impedance

As an electro-magnetic wave travels through the different parts of the antenna system it may encounter differences in impedance ( $E/H$ ,  $V/I$ , etc). At each interface, depending on the impedance match, some fraction of the wave's energy will reflect back to the source, forming a standing wave in the feed line. The ratio of maximum power to minimum power in the wave can be measured and is called the standing wave ratio (SWR). A SWR of 1:1 is ideal. A SWR of 1.5:1 is considered to be marginally acceptable in low power applications where power loss is more critical, although an SWR as high as 6:1 may still be usable with the right equipment. Minimizing impedance differences at each interface (impedance matching) will reduce SWR and maximize power transfer through each part of the antenna system.

#### 4.4.1.5 Bandwidth

The bandwidth of an antenna is the range of frequencies over which it is effective, usually centered on the resonant frequency.

#### 4.4.1.6 Polarization

The polarization of an antenna is the orientation of the electric field (E-plane) of the radio wave with respect to the Earth's surface and is determined by the physical structure of the antenna and by its orientation. It has nothing in common with antenna directionality terms: "horizontal", "vertical" and "circular". Thus, a simple straight wire antenna will have one polarization when mounted vertically, and a different polarization when mounted horizontally. Reflections generally affect polarization. For radio waves the most important reflector is the ionosphere - signals which reflect from it will have their polarization changed unpredictably. For signals which are reflected by the ionosphere, polarization cannot be relied upon. For line-of-sight communications for which polarization can be relied upon, it can make a large difference in signal quality to have the transmitter and receiver using the same polarization; many tens of dB

differences are commonly seen and this is more than enough to make the difference between reasonable communication and a broken link.

#### 4.4.2 Types of Antennae

##### 4.4.2.1 The microstrip patch

###### 4.4.2.1.1 Introduction to patch

These types of antennas are popular because of their low profile and because they easily can be fitted to different geometries. They are typically used at frequencies from 1 to 100 GHz. The patch antenna consists of a rectangular metal plate printed onto a dielectric substrate with ground plane on one side.

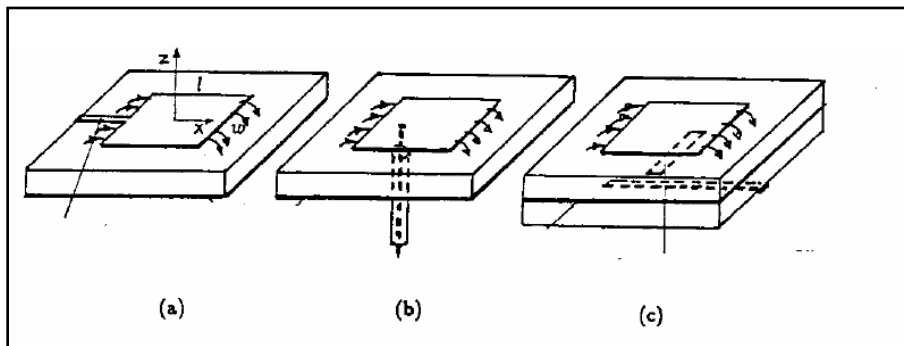


*Figure 4. 1: Microstrip Patch Antenna*

###### 4.4.2.1.2 Important Correlations

###### 4.4.2.1.2.1 Length and width

The following are the formulae which were used to calculate the length and width

$$a) W = c/(2 * f_r) * \sqrt{(2/(\epsilon_{sr} + 1))}$$

Where  $W$  = width of the patch

$f_r$  = resonant frequency = 434 MHz

$\epsilon_{sr}$  = dielectric constant of substrate = 2.2 of RT Duroid 5870

$$b) \epsilon_{sr} (\text{effective}) = (\epsilon_{sr} + 1)/2 + (\epsilon_{sr} - 1)/2 * (1 + 12 * h / W)^{-0.5}$$

where  $h$  = height of the substrate = 1.59 mm

c) effective wavelength in dielectric = wavelength / sqrt (epsr effective) =

d) L (effective) = wavelength (effective) /2

e) delta L =

$$0.412 * [( \text{epsr effective} + 0.3 ) * (W/h + 0.264)] / [ ( \text{epsr effective} - 0.258) * (W/h + 0.8) ]$$

f) L = L (effective) – 2 \* delta L

#### 4.4.2.1.2.2 Bandwidth

$$\text{Bandwidth} = 3.77 * ( \text{epsr} - 1 ) / \text{epsr}^2 * W / L * ( t / \text{wavelength eff.} )$$

#### 4.4.2.1.2.3 Input Impedance

$$\text{Input Impedance} = 90 * ( \text{epsr}^2 ) / ( \text{epsr} - 1 ) (L/W)^2 \text{ ohms}$$

#### 4.4.2.1.2.4 Mass of patch

##### MATERIALS:

Ground plane: Assuming aluminium - (Density = 2.7 g/cc)

Substrate: RT Duroid 5880 (Density = 2.2 g/cc)

##### MASS:

Substrate:  $26 \times 26 \times 0.125 \text{ to } 0.15 \times 2.2 = 185.9 \text{ g to } 223.08 \text{ g}$

Ground plane:  $26 \times 26 \times 0.01 \times 2.7 = 18.252 \text{ g}$

Mass of patch :  $22 \times 22 \times 0.01 \times 2.7 = 13.068 \text{ g}$

Total mass of patch = 217.22 – 254.4

#### 4.4.2.1.2.5 Voltage Standing Wave Ratio (VSWR)

Radio communication theory, [7], states that the antenna impedance,  $Z_L$ , has to be matched to the transmission line,  $Z_0$ . The reason for this is that maximum power transfer between source and load occurs when the system impedances are matched. It also improves the signal-to noise-ratio for the system and reduces amplitude and phase errors.

The match can be described by the reflection coefficient

$$\Gamma(f) = \frac{Z_L(f) - Z_0}{Z_L(f) + Z_0} \quad (3-1)$$

and the voltage standing wave ratio:

$$VSWR(f) = \frac{1 + |\Gamma(f)|}{1 - |\Gamma(f)|} \quad (3-2)$$

The reflection coefficient varies from -1, for short load, to +1, for open load, and becomes 0 for matched impedance load

VSWR is a measure of impedance mismatch between the transmission line and its load. The higher the VSWR is, the greater the mismatch. For a good match the voltage standing wave ratio should be under 2 for a specified frequency. When VSWR is 2.0 it is equal to 90 % power absorption.

The VSWR obtained from simulation was in the range 9 - 17. Though this is a high figure, nothing can be commented as yet as we have not decided our transmission line impedance which will depend upon the cables that we use and our actual system parameters.

#### 4.4.2.1.3 Specifications of the Patch Antenna

##### 4.4.2.1.3.1 Downlink frequency: 434 MHz

- Center frequency or resonant frequency : 434 MHz
- Dimensions of ground plane : 260 mm \* 260 mm
- Dimensions of patch : 220 mm \* 220 mm
- Substrate : RT Duroid 5880
- Thickness of substrate : 1.59 mm
- Beamwidth : 90 degrees
- Percentage bandwidth : 0.58

- Gain : 1 – 6 dBi
- Input impedance : 363 ohms
- VSWR : 2.69
- Feed point: The feeding will be through a coaxial cable. The feed point will be at a distance of 39 mm from the centre of the patch. The reason for choosing coaxial feed probe over microstrip line feed is that the latter causes an increase in the level of undesired radiations and also leads to an increase in the radiation from the feed line leading to an increase in the cross polar level.
- Axial ratio: The axial ratio (ideally) would be 1 as we are opting for circular polarization.
- Mass of patch antenna: 217.22 grams – 254 grams

#### 4.4.3.1.3.2 Downlink frequency 868 MHz

- Center frequency or resonant frequency : 868 MHz
- Dimensions of ground plane : 123 mm \* 144 mm
- Dimensions of patch : 116 mm \* 137 mm
- Substrate : RT Duroid 5880
- Thickness of substrate : 1.59 mm
- Beamwidth : 90 degrees
- Percentage bandwidth : 0.54 %
- Gain : 1 – 6 dBi
- Input impedance : 363 ohms
- VSWR : not yet simulated
- Feed point : not yet simulated
- Axial ratio : The axial ratio ( ideally ) would be 1 as we are opting for circular polarization.
- Mass of patch antenna: 71 ~ 80 grams

## 4.5 Link budget analysis

### 4.5.1 Satellite

Spacecraft transmitter power output : 2 watts

Spacecraft total transmission line losses : 2 dB

Spacecraft Antenna Gain : 1 dBi

Spacecraft EIRP : 2 dBW

4.5.2 Transmitting Frequency: 434 MHz

4.5.2.1 Downlink Path

Spacecraft Antenna Pointing Loss : 0.2 dB

Polarization Loss : 0.2 dB

Path loss : 153.2 dB

Atmospheric loss : 2.1 dB

Ionospheric Loss : 0.8 dB

Rain loss : 0 dB

Isotropic Level at the Ground Station: -154.5 dBW

4.5.2.2 Ground Station

Groundstation Antenna pointing loss : 0.4 dB

Groundstation Antenna Gain : 16 dBi

Groundstation Total Transmission Line Losses : 2.2 dB

Groundstation Effective Noise Temperature : 515 K

Groundstation Figure Of Merit ( G/T) : -13.3 dB/K

Groundstation Signal-to-noise Power Density (S/No) 60.4 dBHz

Data Rate : 33 KBps

4.5.2.3 Eb/No method

Eb/No for downlink : 20.6 dB

Required Eb/No = 10.5

System link Margin : 9.1 dB

4.5.2.4 SNR Method

Signal power at Ground Station : -141.1 dBW

Groundstation receiver Bandwidth : 24000 Hz ( 1 percent of the bandwidth of patch )

Receiver Noise power : -157.7 dBW

SNR at Ground Station : 16.6 dB

Required SNR : 10.0

System Link Margin : 6.6 dB

#### 4.5.3 Transmitting Frequency: 868 MHz

##### 4.5.3.1 Downlink Path

Spacecraft Antenna Pointing Loss : 0.2 dB

Polarization Loss : 0.2 dB

Path loss : 159.2 dB

Atmospheric loss : 2.1 dB

Ionospheric Loss : 0.8 dB

Rain loss : 0 dB

Isotropic Level at the Ground Station: -160.5 dBW

##### 4.5.3.2 Ground Station

Groundstation Antenna pointing loss : 0.4 dB

Groundstation Antenna Gain : 16 dBi

Groundstation Total Transmission Line Losses : 2.2 dB

Groundstation Effective Noise Temperature : 515 K

Groundstation Figure Of Merit ( G/T) : -13.3 dB/K

Groundstation Signal-to-noise Power Density (S/No) : 54.4 dBHz

Data Rate : 33 KBps

##### 4.5.3.3 Eb/No method

Eb/No for downlink : 14.5 dB

Required Eb/No = 11.5 dB

System link Margin : 3 dB

##### 4.5.3.4 SNR Method

Signal power at Ground Station : -147.1 dBW

Groundstation receiver Bandwidth : 24000 Hz ( 1 percent of the bandwidth of patch )

Receiver Noise power : -157.7 dBW

SNR at Ground Station : 10.6 dB

Required SNR : 10.0

System Link Margin : 6.6 dB

## Chapter 5: Attitude and Orbit Control System

### 5.1 Introduction

The primary objectives of this subsystem are,

- 1) To determine the attitude of the satellite with the sampling rate and precision as specified by the payload and/or as required for attitude control of the satellite
- 2) To control the attitude of the satellite in the given orientation with the accuracy as required by the payload.
- 3) These are to be done subject to system constraints like power, weight, size etc.

The attitude determination is conventionally done using an array of sensors like Magnetometer, Sun-sensor, Earth sensor, Star sensor and GPS. Considering the severe constraints on Weight, Power and size we decided to use a Sun sensor and a magnetometer to determine the attitude of the satellite.

A Digital Magnetometer is inexpensive and comes as a chip. This can be mounted on a chip and gives digital output. The attitude accuracy of the order of  $0.1^\circ$  as well as the components of the earth's magnetic field along the axes of the magnetometer are obtained. However, this does not give a unique vector in the Orbit reference frame but a cone. Hence, it needs to be augmented with a sunsensor.

The accuracy of attitude determination using a sunsensor depends on the quality of suns-sensor used. Accuracy as high as  $0.1^\circ$  can be obtained using a digital sunsensor available in the market while a simple sunsensor based on interpretation of the current distribution obtained from the solar panels gives only accuracy of the order of  $5^\circ$ . This issue is dealt with in detail in later part of the chapter.

The data obtained from both the sensors is used by Kalman Filter or an extended Kalman Filter to obtain more accurate estimate of the attitude of the satellite. The Kalman Filter is based on the attitude dynamics model of the satellite. Hence, obtaining an accurate attitude dynamics model is important. The attitude determination is done at the sampling rate as required by the payload. The same data can be used as a feedback for the controller. The satellite is gravity gradient stabilized using a gravity gradient boom. This stabilizes the satellite at zero value of all the Euler angles. The angular position of the satellite is expected to deviate from zero only by small angle.

However to obtain the desired orientation of the satellite at all time, an active damping of the liberations of the satellite is essential. This is done using magnetic damping by the magnetorquer coils and the linear control law. These magnetorquers are also used for attitude maneuvers, if required and for detumbling the satellite after launch from the Launch Vehicle.

All the above issues will be dealt with from design perspective in the following chapter.

Control requirements that have been given to us by the Payload team are-

Orbit Determination Accuracy-

Position-10m

Velocity-10m/s

Attitude Determination Accuracy-

Roll – 0.5 deg

Pitch – 0.5 deg

Yaw – 0.5 deg

Attitude Control along Roll, Pitch and Yaw necessary

## 5.2 Sensors

The attitude determination using sensors can be subdivided into reference sensors and inertial sensors.

### 5.2.1 Reference sensors

#### 5.2.1.1 Star Sensor

The Star Sensor provides the control algorithm with information about the orientation of the sensor with respect to one or more stars in a known constellation of stars. In other words it provides the control system with one of two orientation vectors necessary to determine the attitude in an unambiguous fashion. So far, available systems would clearly exceed at least one budget (mass) assigned to the attitude subsystem.



*Figure 5. 1: Static Earth Horizon Sensor*

#### 5.2.1.2. Sun Sensor

A current position acquires the spacecrafts orientation with respect to the sun. In order to measure a vector to the sun it is necessary to measure the sun's position in two planes.

#### 5.2.1.3 Horizon Sensor

The horizon sensor as a reference sensor is similar to the star sensor. But instead of providing a vector to a field of stars it images the earth's horizon in an infrared optical band and determines the satellite's position with respect to the horizon image. A simpler version of the horizon sensor is an infrared sensor which tells the control algorithm if the earth (or any other infrared source for that matter) is in the field of view of the sensor. A disadvantage of this simple method is the very limited accuracy for attitude determination.

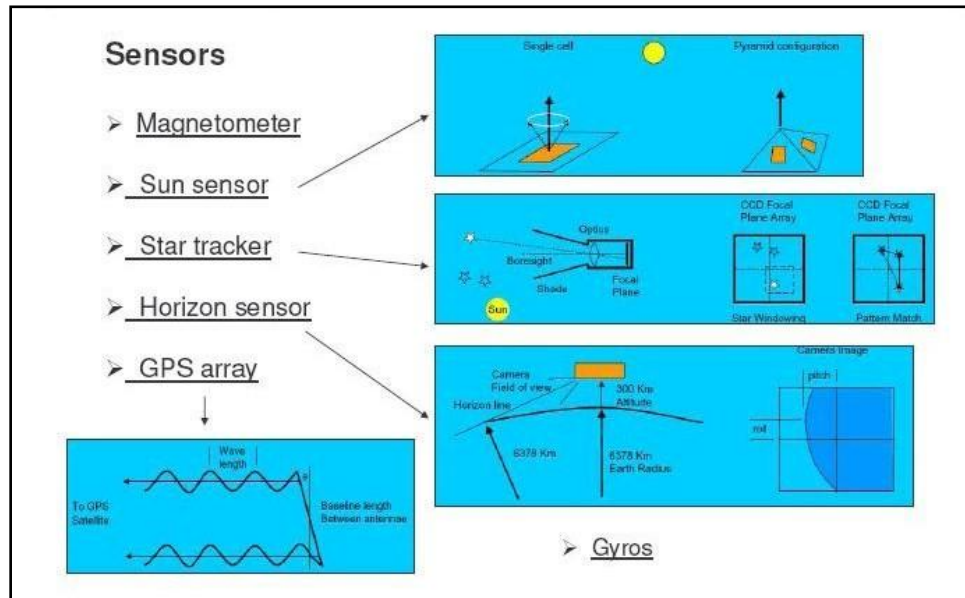


*Figure 5. 2: Different Sensors*

#### 5.2.1.4 Magnetometer

A magnetometer measures the orientation and strength of the magnetic field of the Earth inside

the spacecraft. The controller requires an additional reference vector to unambiguously acquire the satellites attitude. It also requires information about the current position of the satellite due to the variation of the geomagnetic field along one orbit.

### 5.2.2 Inertial sensors

Inertial sensors have in common that they have to be updated by a reference typically from one of the above reference sensors, since they all show a drift in the angle measurement which is the necessary information for the attitude algorithm. This drift is due to the integration of an erroneous spin rate measurement.

#### 5.2.2.1 Gyroscopes

Gyroscopes (gyros) are inertial sensors, i.e. they measure angular rates or angular acceleration opposed to angles to a reference. Gyros, in whichever form ever, are typically used for high accuracy attitude determination on larger scientific platforms. While electronic gyros can be manufactured very lightweight and reliable, mechanical gyros are somewhat bulky and heavy and will exceed the mass budget. It should be considered though for the piezo-gyros that, accessories are necessary for conditioning of the weak output signal. Piezo-electric gyros can have drifts up to 20% resulting in large errors if not updated frequently. The different forms are:

Optical: a laser beam sent into opposite directions into a light conducting ring creates measurable interference as a function of angular rates.

Mechanical: High spin wheels alter their measurable orientation about one axis in an inertial frame when a torque about another perpendicular axis is applied.

Electronical: Piezo sensors react with a measurable internal voltage when acceleration is imposed that results from angular velocity.

The acquisition of the current position can be done by an on-board GPS receiver. This will be backed up by data from NORAD Two-Line Element Sets.

### 5.2.3 Sensors chosen for our use

From the listed sensors we decided to choose Magnetometer and Sun sensor for attitude determination on the basis of cost, reliability, accuracy and use in other student satellites.

#### 5.2.3.1 Magnetometer

##### 5.2.3.1.1 Introduction

A magnetometer is a scientific instrument used to measure the strength and/or direction of the magnetic field in the vicinity of the instrument. It measures the orientation and strength of the magnetic field of the Earth inside the satellite. A magnetometer can only be used in orbit close to earth where the magnetic field is strong and well modeled. This is feasible for our satellite.

Measurements are done in three dimensions, by three independent orthogonal sensors. The Earth's magnetic field is thus measured in the sensor frame. The measurements from the magnetometer are compared with the modeled magnetic field. As the magnetometer gives an output in Body frame, and the model is in Orbit frame, the relation between these frames can be used to calculate the attitude of the satellite.

##### 5.2.3.1.2 Reference frames

1. Inertial Frame - An inertial frame is used for attitude applications. The X direction points from the focus of the orbit to the vernal equinox,  $\hat{o}_1$ , the Z direction is in the orbital angular velocity direction, and Y is perpendicular to X and Z.
2. Orbital Frame -The orbital frame is located at the mass center of the spacecraft, and the motion of the frame depends on the orbit. This frame is non inertial because of orbital acceleration and the rotation of the frame. The  $\hat{o}_3$  axis is in the direction from the spacecraft to the Earth,  $\hat{o}_2$  is the direction opposite to the orbit normal, and  $\hat{o}_1$  is perpendicular to  $\hat{o}_2$  and  $\hat{o}_3$ . In circular orbits,  $\hat{o}_1$  is the direction of the spacecraft velocity. The three directions  $\hat{o}_1$ ,  $\hat{o}_2$ , and  $\hat{o}_3$  are also known as the roll, pitch, and yaw axes, respectively.
3. Body Frame - Like the orbital frame, the body frame has its origin at the spacecraft's mass center. This frame is fixed in the body, and therefore is non-inertial. The relative orientation between the orbital and body frames is the basis of attitude dynamics and control.

4. Principal Axis - Principal axes are a specific body-fixed reference frame. This axis system has its origin at the mass center, and is oriented such that the moment of inertia matrix is diagonal and known as the principal moments of inertia.

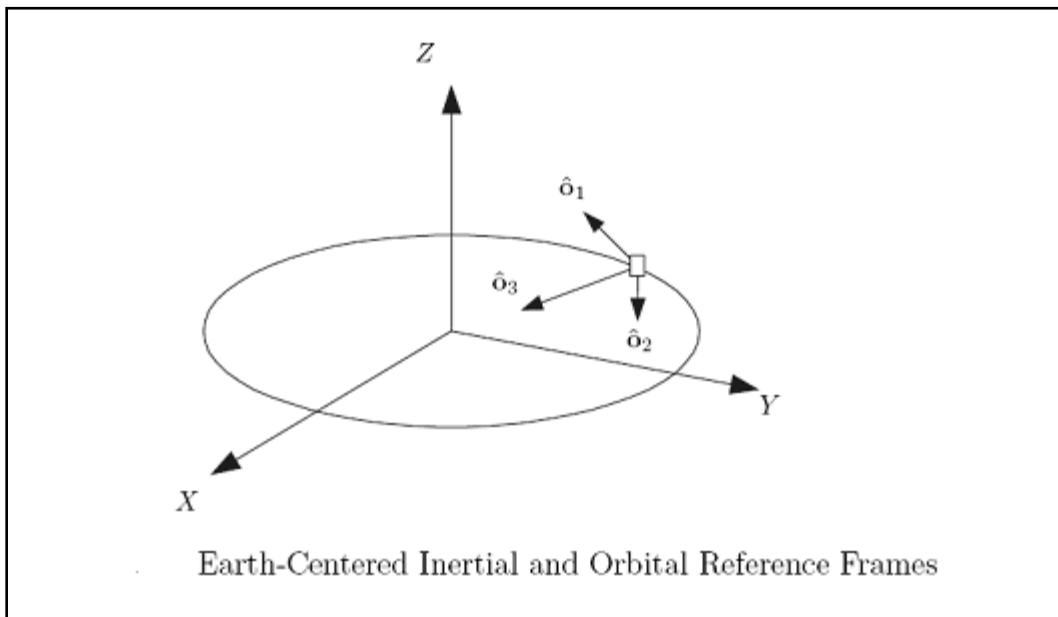


*Figure 5. 3: Inertial and Orbital Reference Frames*

#### 5.2.3.1.3 Earth's Magnetic Field

Attitude determination of the satellite using a magnetometer depends on local magnetic field. Therefore it is essential to understand the earth's magnetic field for correct attitude determination. The magnetic field around the Earth resembles that of a uniformly magnetized sphere, or a dipole, which is tilted as shown in the figure below. The fact that it approximates a tilted dipole was discovered in 1600 by William Gilbert, and was published in his treatise *De Magnete*. In 1635, Gellibrand was the first to show that the geomagnetic field is both time and position dependent.

The strength of the magnetic field is approximately 30000 nT at the equator and 60000 nT at the poles on the surface of the Earth. The magnetic dipole axis, designated as  $\hat{m}$  in the figure above, is located at  $79.8^\circ$  N latitude and  $107.0^\circ$  W longitude, in the year 1999. The magnetic dipole axis is currently at an inclination angle of  $11.5^\circ$  with the equatorial plane. The axis is drifting westward at about 0.2 degrees /year, and the strength is decreasing by 0.05% per year.

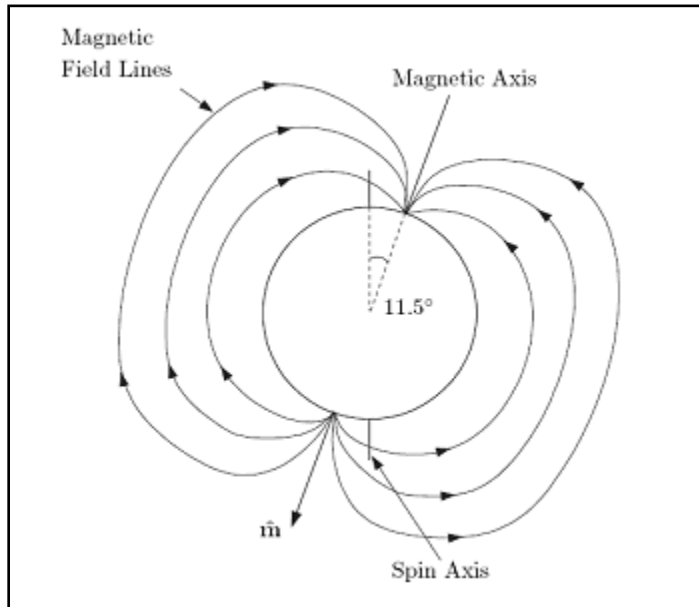


*Figure 5. 4: Geomagnetic Field*

#### Variations in Earths Magnetic field

- Temporal Variations - Temporal variations are described as disturbances in the geomagnetic field which result from the changing positions of the Earth and the Sun
- Diurnal Variations Diurnal variations are one type of temporal variation. These variations occur in the day-to-night magnetic field intensity.
- Secular Variations - Secular variations in the magnetic field occur gradually over very long periods of time. The secular variations are very small, but after a few years their accumulation is enough to make the magnetic field models outdated.

#### 5.2.3.1.4 Analytic Models

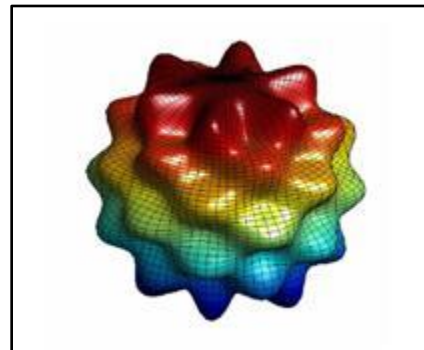


*Figure 5. 5: Bumpy Sphere*

Spherical Harmonic Model

The **B** field in tangential coordinates is calculated as

$$\begin{aligned}
B_r &= \frac{-\partial V}{\partial r} = \sum_{n=1}^k \left( \frac{R_\oplus}{r} \right)^{n+2} (n+1) \sum_{m=0}^n (g^{n,m} \cos m\phi + h^{n,m} \sin m\phi) P^{n,m}(\theta) \\
B_\theta &= \frac{-1}{r} \frac{\partial V}{\partial \theta} = - \sum_{n=1}^k \left( \frac{R_\oplus}{r} \right)^{n+2} \sum_{m=0}^n (g^{n,m} \cos m\phi + h^{n,m} \sin m\phi) \frac{\partial P^{n,m}(\theta)}{\partial \theta} \\
B_\phi &= \frac{-1}{r \sin \theta} \frac{\partial V}{\partial \phi} \\
&= \frac{-1}{\sin \theta} \sum_{n=1}^k \left( \frac{R_\oplus}{r} \right)^{n+2} \sum_{m=0}^n m(-g^{n,m} \sin m\phi + h^{n,m} \cos m\phi) P^{n,m}(\theta)
\end{aligned}$$

where

$$\begin{aligned}
g^{n,m} &\equiv S_{n,m} g_n^m \\
h^{n,m} &\equiv S_{n,m} h_n^m
\end{aligned}$$

and

$$S_{n,m} = \left[ \frac{(2 - \delta_m^0)(n-m)!}{(n+m)!} \right]^{1/2} \frac{(2n-1)!!}{(n-m)!}$$

The Kronecker delta,  $\delta_j^i = 1$  if  $i = j$  and 0 otherwise. In addition  $P^{n,m}$  is defined by

$$\begin{aligned}
P^{0,0} &= 1 \\
P^{n,n} &= \sin \theta P^{n-1,n-1} \\
P^{n,m} &= \cos \theta P^{n-1,m} - K^{n,m} P^{n-2,m}
\end{aligned}$$

where

$$K^{n,m} = \begin{cases} \frac{(n-1)^2 - m^2}{(2n-1)(2n-3)} & n > 1 \\ 0 & n = 1 \end{cases}$$

The resulting field is equivalent to that of a bumpy sphere.

#### 5.2.3.1.5 International Geomagnetic Reference Field (IGRF)

Spherical harmonic analysis is used to compute the International Geomagnetic Reference Field (IGRF), which defines the theoretical undisturbed geomagnetic field at any point on the Earth's surface. The geomagnetic field used in the satellite model is the IGRF model created by the IAGA (International Association of Geomagnetism and Aeronomy).

$$V(r, \theta, \phi) = a \sum_{n=1}^{\infty} \sum_{m=0}^n \left(\frac{a}{r}\right)^{n+1} (g_n^m \cos(m\phi) + h_n^m \sin(m\phi)) P_n^m(\cos(\theta))$$

Here ‘V’ is the potential function of the field about the Earth (given in spherical Coordinates in ECEF frame), ‘a’ is the mean radius of the Earth. The  $P_n^m(\cos(\theta))$  are Schmidt quasinormalized associated Legendre functions of degree ‘n’ and order ‘m’. And ‘g’ and ‘h’ are the constant Gaussian.

The IGRF model currently in use is IGRF 10 which will expire in 2010 and is hence suitable for our mission.

N.B. – We have currently used this model to make a simulation of the magnetic disturbance torques.

#### 5.2.3.1.6 Orbit estimator

There exists numerous orbit estimators but Because of the requirement of low computation consumption a simple estimator is proposed

By using the rotation matrix for transforming between earth centered orbit to ECEF frame i.e.

$$\mathbf{R}_{oc}^e = \mathbf{R}_z(-\Omega + \theta) \mathbf{R}_x(-i) \mathbf{R}_z(-\omega)$$

the orbit estimator becomes

$$\mathbf{R}_{oc}^e = \mathbf{R}_z(-\Omega + \theta) \mathbf{R}_x(-i) \mathbf{R}_z(-\omega) \mathbf{r}^{oc}$$

where

$$\mathbf{r}^{oc} = a \begin{bmatrix} \cos E - e \\ \sqrt{1 - e^2} \sin E \end{bmatrix}$$

is the vector from the center of the Earth to the satellite decomposed in the Earth-Centered Orbit frame. Effects due to the non spherical Earth,  $\Omega_{J2}$  and  $\omega_{J2}$ , the Sun,  $\Omega_{sun}$  and  $\omega_{sun}$ , and the Moon,  $\Omega_{moon}$  and  $\omega_{moon}$ , will degrade the estimator’s accuracy over time. Because of this, these perturbations have been implemented into the estimator and gives rise to a more complicated but more accurate estimator given by

$$\begin{aligned}\mathbf{R}_{oc}^e &= \mathbf{R}_z(-\Omega_0 + (\dot{\Omega}_{J2} + \dot{\Omega}_{moon} + \dot{\Omega}_{sun})t + \theta_0 + \omega_{ie})\mathbf{R}_x(-i) \cdot \\ &\quad \mathbf{R}_z(-(\omega_0 + (\dot{\omega}_{J2} + \dot{\omega}_{moon} + \dot{\omega}_{sun})t))a \left[ \frac{\cos E - e}{\sqrt{1 - e^2 \sin E}} \right]\end{aligned}$$

#### 5.2.3.1.7 Attitude determination from magnetometer readings

The magnetometer measures the Earth's magnetic field in the sensor frame. To get the best result, the sensor and the satellite axes should be parallel, or at least have a known configuration relative to another. The measurements from the magnetometer are compared with the modeled magnetic field. As the magnetometer gives an output in Body frame, and the model is in Orbit frame, the relation between these frames can be used to calculate the attitude of the satellite. This gives us the roll angle ( $\theta$ ), the pitch angle ( $\phi$ ) and the yaw angle ( $\psi$ ).

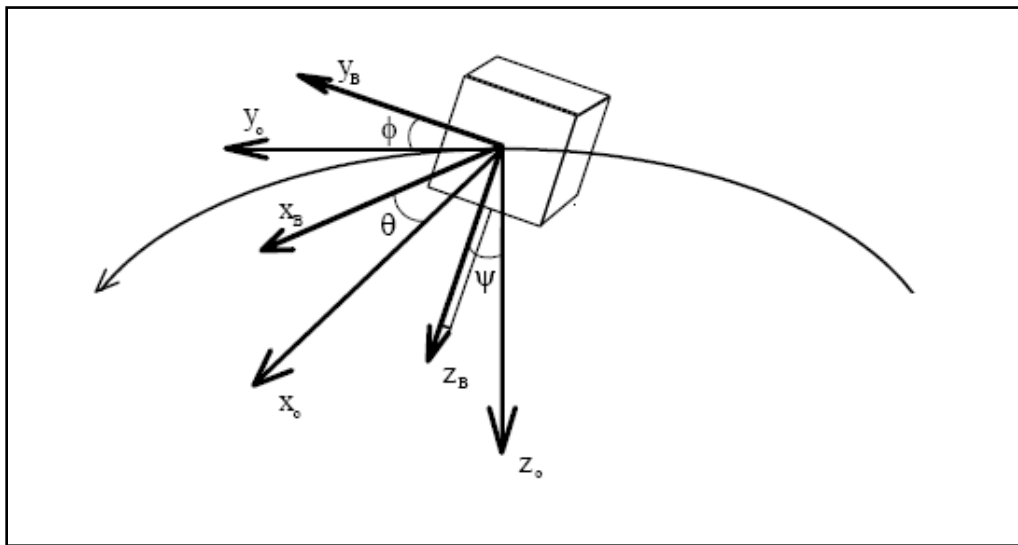


Figure 5. 6: Angles measured by the magnetometer

The accuracy of the magnetometer is limited mainly by two factors:

- A disturbance field due to spacecraft electronics - In orbit, the measured magnetic field is not only originating from the Earth. The satellite, with its electronic circuits, may also influence the magnetometer and degrade the estimation. To overcome this, one has to consider shielding when implementing the hardware. In addition, a different alignment of single components can increase or decrease the disturbance greatly.
- External disturbances - The ionosphere is not a uniform field. Electrical currents within the ionosphere induce unpredictable magnetic disturbances. How this influence the

magnetometer is not known. Not only is the magnetometer inaccurate, the model, which the measurements are compared to, also has errors. These errors decrease with increased complexity of the model. A better model will decrease the errors, but demand more resources of the processor running the ADCS. Also, errors in the orbit estimator, i.e. the estimated position of the satellite, will introduce errors.

#### 5.2.3.1.8 Types of magnetometers

##### 5.2.3.1.8.1 Vector Magnetometers

Types of low field vector magnetometers include induction air coil magnetometers, fluxgate magnetometers, and Superconducting Quantum Interference Device (SQUID) magnetometers.

1. Induction Coil Magnetometer - The induction coil is one of the most widely used vector measurements, as well as one of the simplest. It is based on Faraday's law, which states that a changing magnetic flux,  $\Phi$ , through the area enclosed by a loop of wire causes a voltage to be induced which is proportional to the rate of change of the flux. Two types of induction coil configurations for measuring field strength are air core loop antennas and rod antennas. These both operate using the same assumptions and techniques.
2. Fluxgate Magnetometer - A fluxgate magnetometer is extremely popular for use in many applications. Characteristically, it is small, reliable, and does not require much power to operate. It is able to measure the vector components of a magnetic field in a 0.1 nT to 1 mT range. These are the magnetometers of choice for satellite attitude systems. The fluxgate magnetometer is a transducer which converts a magnetic field into an electric voltage. Fluxgates are configured with windings through which a current is applied. If there is no component of the magnetic field along the axis of the winding, the flux change detected by the winding is zero. If there is a field component present, the flux in the core changes from a low level to a high level when the material goes from one saturation level to another. From Faraday's law, a changing flux produces a voltage at the terminals of the winding proportional to the rate of change of the flux. *These are mostly used satellites.*
3. SQUID Magnetometer - The SQUID (Superconducting Quantum Interference Device) magnetometer works on the principle that the magnitude of a superconducting current flowing between two superconductors separated by a thin insulating layer is affected by the presence of a magnetic field. These magnetometers are the most sensitive devices available

to measure the magnetic field strength. However, one disadvantage is that only the change in the magnetic field can be measured, instead of the absolute value of the field

#### 5.2.3.1.8.2 Vector Gaussmeters

1. Hall Effect Gaussmeter - The Hall effect gaussmeter is the most widely used sensor for measuring strong magnetic fields. It is based on the Hall effect, which states that under the influence of a magnetic induction field, a moving charge experiences a force that is at a right angle to the field vector and the velocity vector of the charge. Hall effect devices can be made out of conductors such as copper, but using semiconducting materials such as gallium arsenide, indium antimonide, or indium arsenide produces the most stable Hall coefficients. The most favored material is indium arsenide because it has a low temperature coefficient of sensitivity, low resistance, and a relatively good sensitivity.
2. Magnetoresistive Gaussmeter - Magnetoresistive gaussmeters work because the resistivity of a ferromagnetic material changes under the influence of a magnetic field. The amount of change is based on the magnitude of the magnetization, as well as the direction of flow of the current to measure resistivity.

#### 5.2.3.1.8.3 Scalar Magnetometers

Scalar magnetometers measure the magnitude of the magnetic field. This measurement is accomplished by using the atomic and nuclear properties of matter.

Scalar magnetometers have very high resolution and accuracy, and are almost independent of orientation to the magnetic field.

A few limitations exist with scalar magnetometers, however. They require the magnetic field to be constant throughout the sensing element area, and have a limited measurement range, which is typically  $20 \mu\text{T}$  to  $100 \mu\text{T}$ . In addition, while the orientation of the magnetic field does not affect the reading of the sensor, there are a few limitations of the direction of the magnetic field vector relative to the sensor in order for a measurement to be taken.

#### 5.2.3.1.8.4 Comparison between various types of magnetometers

Instrument	Range (mT)	Resolution (nT)	Comment
Induction Coil	$10^{-10}$ to $10^6$	Variable	Cannot measure static fields
Fluxgate	$10^{-4}$ to 0.5	0.1	General-purpose vector magnetometer
SQUID	$10^{-9}$ to 0.1	$10^{-4}$	Highest sensitivity magnetometer
Hall Effect	0.1 to $3 \times 10^4$	100	Best for fields above 0.1T
Magnetoresistance	$10^{-3}$ to 5	10	Good for mid-range applications
Proton precession	0.02 to 0.1	0.05	General-purpose scalar magnetometer
Optically pumped	0.01 to 0.1	0.005	Highest resolution scalar magnetometer

*Figure 5. 7: Comparison between various magnetometers*

#### 5.2.3.1.9 Problem with 3 axis magnetometer and the need for an additional sensor

While using a magnetometer, the controller requires an additional reference vector to unambiguously acquire the satellites attitude. As the magnetometer measures the earth's magnetic field (a vector) and determines the attitude in comparison with this, the magnetometer would not detect any angular change along this axis. Thus an additional sensor is needed to completely determine attitude. Mostly a sun sensor is used, but sometimes a GPS device is used in addition to the magnetometer.

#### 5.2.3.1.10 Magnetometer Comparison

##### HMC6343



Here are some other specifications:

The HMC6343 utilizes Honeywell's Anisotropic Magnetoresistive (AMR) technology that provides advantages over other magnetic sensor technologies. The sensors feature precision sensitivity and linearity, solid-state construction with very low cross-axis sensitivity designed to measure both direction and magnitude of Earth's magnetic fields. Honeywell's Magnetic Sensors are among the most sensitive and reliable low-field sensors in the industry.

## MOUNTING CONSIDERATIONS

### Stencil Design and Solder Paste

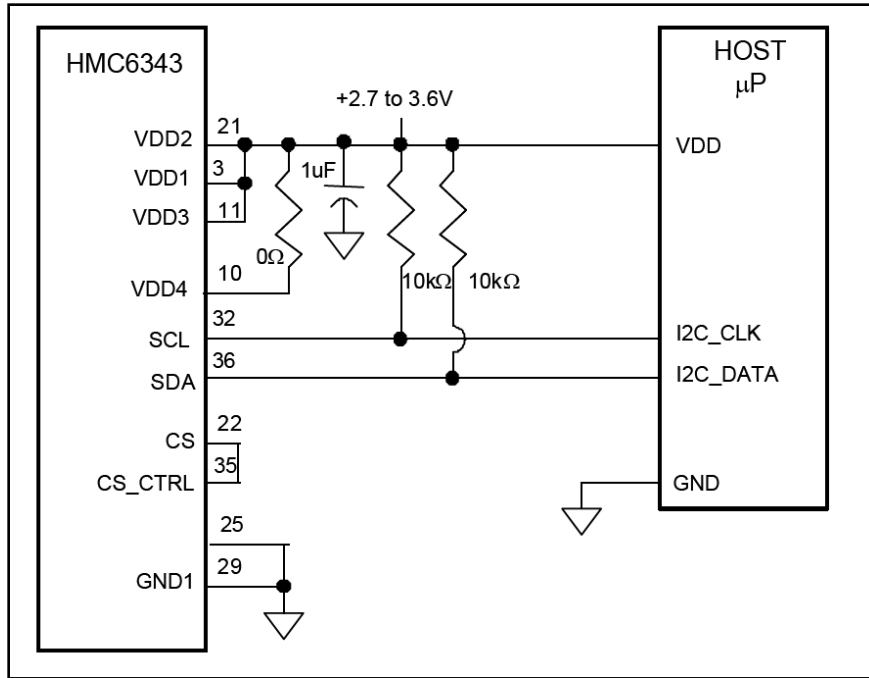
A 4 mil stencil and 100% paste coverage is recommended for the electrical contact pads. The HMC6343 has been tested successfully with no-clean solder paste.

### Pick and Place

Placement is machine dependant and no restrictions are recommended, and have be tested with mechanical centering. Placement force should be equivalent 1206 SMT resistors and enough force should be used to squeeze the paste out from the package/contact pad overlap and to keep the package pin contacts vertical.

## BASIC DEVICE OPERATION

The Honeywell HMC6343 magnetoresistive sensor circuit is a trio of magnetic sensors, accelerometers, and analog support circuits to measure magnetic fields. Additionally a microcontroller is integrated for computation of direction and calibration. With power supply applied, the sensor converts any incident magnetic field in the sensitive axis direction to a differential voltage output. In addition to the bridge circuit, the sensors have on-chip magnetically coupled offset straps for incident field adjustment.



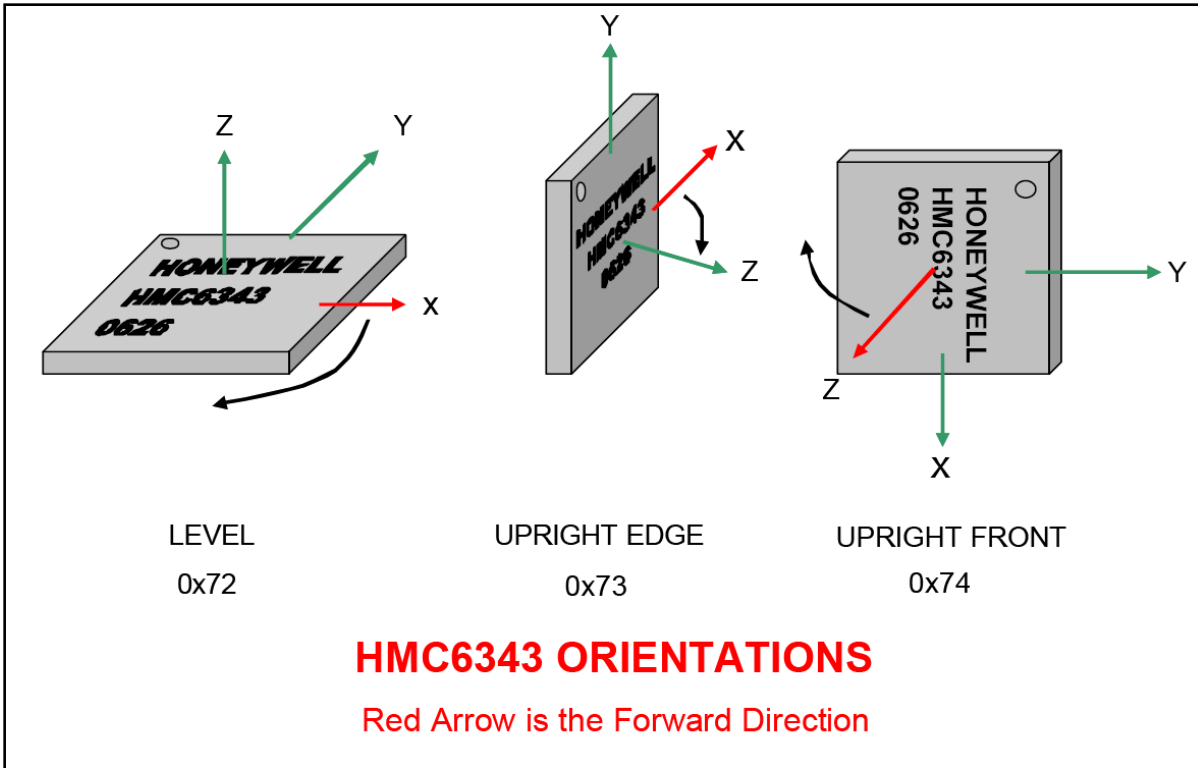
## Operational Modes

The HMC6343 has three operational modes; Sleep, Standby, and Run. Sleep mode is defined as having the analog circuitry powered off, and has the lowest power consumption while power is applied to the VDD pins. Standby mode has the HMC6343 fully powered, but with no measurements performed and the processor is waiting for commands to perform.

Run mode is fully engaged in continuous measurements at the set rate, and ready to receive further commands. The operational mode settings are stored in EEPROM register 0x04, and shown further the HMC6343 protocol definition.

## Mounting Orientations

The HMC6343 provides for three standard mounting orientations, with a flat horizontal orientation the factory set default. For vertical mounting, there are two upright orientations with either the X-axis or the Z-axis designated as the forward reference directions. To change the forward reference direction, send the appropriate command byte (0x72, 0x73, or 0x74) for level or upright orientations, and reset the processor (or cycle power). To enjoy other orientations, you can add or subtract 90 degree increments of deviation angle as required from the three choices. The figure below shows pictorially the orientations.



### User Hard-Iron Calibration

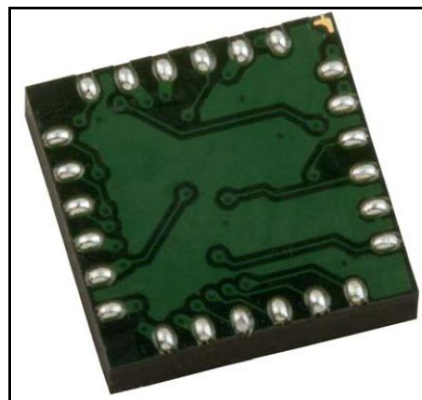
The HMC6343 provides a user calibration routine with the 0x70 command permitting entry into the calibration mode and the 0x7F command to exit the calibration mode. During the calibration procedure, the compass and the platform to which the compass is attached is rotated at a reasonably steady speed through 360 degrees. This process should at least take one minute for best accuracy. For best HMC6343 calibration, the rotation should include as much pitch and roll orientations possible. The calibration time window is recommended to be from 60 seconds up to 3 minutes depending on the end user's platform.

The calibration routine collects these readings to correct for hard-iron distortions of the magnetic field. These hard-iron effects are due to magnetized materials nearby the HMC6343 part that in a fixed position with respect to the end user platform. An example would be the magnetized chassis or engine block of a vehicle in which the compass is mounted onto. Upon exiting the calibration mode, the resulting magnetometer offsets and scaling factors are updated.

Characteristics	Conditions*	Min	Typ	Max	Units
<b>Power Supply</b>					
Supply Voltage	VDD Referenced to GND	2.7	3.3	3.6	Volts
Current	All VDD pins connected together Run Mode (10Hz Output) Standby Mode Sleep mode	3.5 4.5 10	4.5 5.5 1.0	5.5 1.0 10	mA mA $\mu$ A
<b>Compass Function</b>					
Field Range	total applied magnetic field		$\pm 1$	$\pm 6$	gauss
Heading Accuracy	At Level $\pm 15^\circ$ tilt $\pm 60^\circ$ tilt		2.0 3.0 4.0	3.0	$\pm$ deg RMS
Heading Resolution	Output Data		0.1		degrees
Update Rate	Run Mode (1, 5, 10Hz)	1	5	10	Hz
Tilt Range	From Horizontal		$\pm 80$		degrees
Tilt Accuracy	$0^\circ$ to $\pm 15^\circ$ $\pm 15^\circ$ to $\pm 60^\circ$		$\pm 1$ $\pm 2$		degrees
Tilt Resolution	Output Data		0.1		degrees
<b>Offset Straps</b>					
Resistance	Measured from OFF+ to OFF-	5	8	11	ohms
Offset Constant	DC Current Field applied in sensitive direction		10		mA/gauss
Resistance Tempco	$T_A = -40$ to $125^\circ\text{C}$	1800	2700	4500	ppm/ $^\circ\text{C}$
<b>General</b>					
Operating Temperature	Ambient	-40		80	$^\circ\text{C}$
Storage Temperature	Ambient, unbiased	-55		125	$^\circ\text{C}$
Weight			0.32		grams
ESD Voltage				400	V
MSL	Moisture Sensitivity Level	3			-

\* Tested at  $25^\circ\text{C}$  except stated otherwise.

## HMC6352



The Honeywell HMC6352 is a fully integrated compass module that combines 2-axis magneto-resistive sensors with the required analog and digital support circuits, and algorithms for heading computation.

## Operational Controls

HMC6352 has two parameters; Operational Mode and Output Mode, which control its operation. The Operational Mode control byte is located at RAM register byte 74(hex) and is shadowed in EEPROM location 08(hex). This byte can be used to control the continuous measurement rate, set/reset function, and to command the HMC6352 into the three allowed operating modes; Standby, Query, and Continuous.

## Operational Modes

Standby Mode: (Operational Mode=0) This is the factory default mode. The HMC6352 waits for master device commands or change in operational mode. Receiving an “A” command (get data) will make the HMC6352 perform a measurement of sensors (magnetometers), compute the compensated magnetometer and heading data, and wait for the next read or command. No new measurements are done until another “A” command is sent. This mode is useful to get data on demand or at random intervals as long as the application can withstand the time delay in getting the data.

Query Mode: (Operational Mode=1) In this mode the internal processor waits for “A” commands (get data), makes the measurements and computations, and waits for the next read command to output the data. After each read command, the HMC6352 automatically performs another get data routine and updates the data registers. This mode is designed to get data on demand without repeating “A” commands, and with the master device controlling the timing and data throughput. The tradeoff in this mode is the previous query latency for the advantage of an immediate read of data.

The above two modes are the most power conserving readout modes.

Continuous Mode: (Operational Mode=2) The HMC6352 performs continuous sensor measurements and data computations at selectable rates of 1Hz, 5Hz, 10Hz, or 20Hz, and updates the output data bytes. Subsequent “A” commands are un-necessary unless re-

synchronization to the command is desired. Data reads automatically get the most recent updates. This mode is useful for data demanding applications.

#### Output Data Modes

The read response bytes after an “A” command, will cause the HMC6352 will return two bytes with binary formatted data. Either heading or magnetometer data can be retrieved depending on the output data selection byte value. Negative signed magnetometer data will be returned in two’s complement form. This output data control byte is located in RAM register location 4E(hex) and defaults to value zero (heading) at power up.

**Heading Mode:** The heading output data will be the value in tenths of degrees from zero to 3599 and provided in binary format over the two bytes.

**Raw Magnetometer Modes:** These X and Y raw magnetometer data readings are the internal sensor values measured at the output of amplifiers A and B respectively and are 10-bit 2’s complement binary ADC counts of the analog voltages at pins CA1 and CB1. The leading 6-bits on the MSB are zero filled or complemented for negative values. The zero count value will be about half of the supply voltage. If measurement averaging is implemented, the most significant bits may contain values of the summed readings.

**Magnetometer Modes:** These X and Y magnetometer data readings are the raw magnetometer readings plus offset and scaling factors applied. The data format is the same as the raw magnetometer data. These compensated data values come from the calibration routine factors plus additional offset factors provided by the set/reset routine.

#### Removal of Hardiron Effects:

#### User Calibration

The HMC6352 provides a user calibration routine with the “C” command permitting entry into the calibration mode and the “E” command to exit the calibration mode. Once in calibration mode, the user is requested to rotate the compass on a flat surface at least one full circular rotation while the HMC6352 collects several readings per second at various headings with the emphasis on rotation smoothness to gather uniformly spaced readings. Optimally two rotations

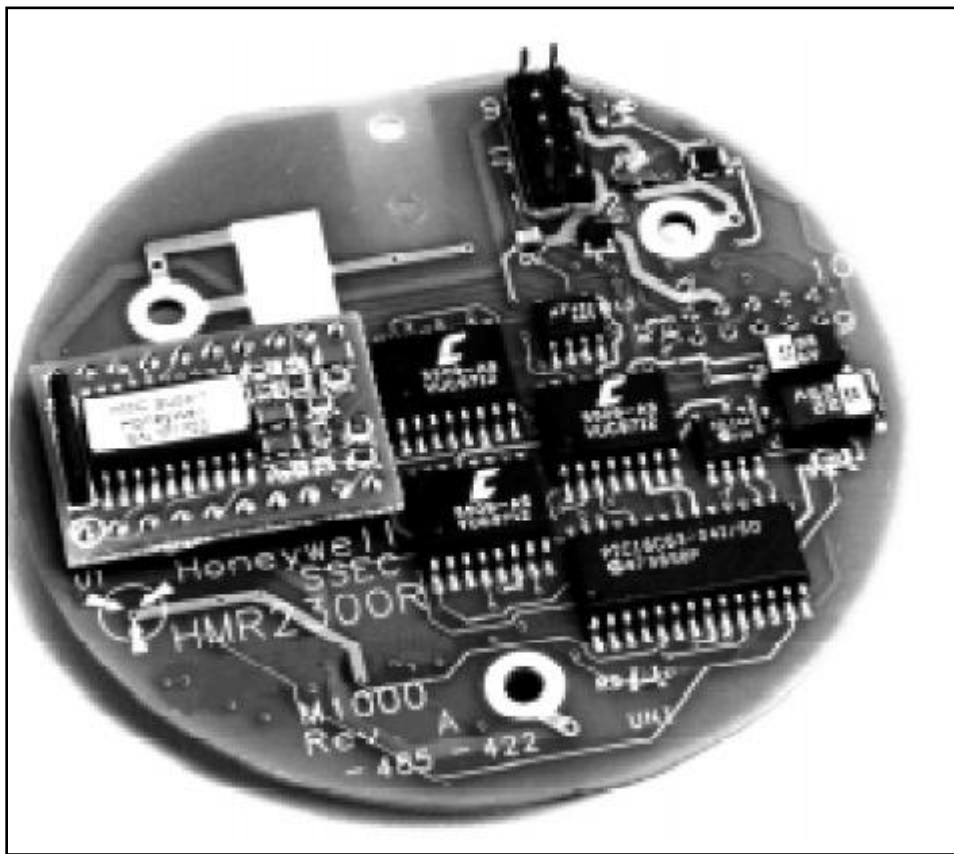
over 20 seconds duration would provide an accurate calibration. The calibration time window is recommended to be from 6 seconds up to

3 minutes depending on the end user's platform. The calibration routine collects these readings to correct for hard-iron distortions of the earth's magnetic field. These hardiron effects are due to magnetized materials nearby the HMC6352 part that in a fixed position with respect to the end user platform. An example would be the magnetized chassis or engine block of a vehicle in which the compass is mounted onto. Upon exiting the calibration mode, the resulting magnetometer offsets and scaling factors are updated

Characteristics	Conditions <sup>(1)</sup>	Min	Typ	Max	Units
Supply Voltage	Vsupply to GND	2.7	3.0	5.2	Volts
Supply Current	Vsupply to GND Sleep Mode (Vsupply = 3.0V) Steady State (Vsupply = 3.0V) Steady State (Vsupply = 5.0V) Dynamic Peaks		1 1 2	10	µA mA mA mA
Field Range <sup>(2)</sup>	Total applied field	0.10	-	0.75	gauss
Heading Accuracy	HMC6352		2.5		degRMS
Heading Resolution			0.5		deg
Heading Repeatability			1.0		deg
Disturbing Field	Sensitivity starts to degrade. Enable set/reset function to restore sensitivity.	20			gauss
Max. Exposed Field	No permanent damage and set/reset function restores performance.			10000	gauss
Operating Temperature	Ambient	-20		70	°C
Storage Temperature	Ambient	-55		125	°C
Peak Reflow Temperature	For Lead-Free SMT Reflow	230	-	240	°C
Moisture Sensivity	Max 240°C		MSL3		-
Output	Heading, Mag X, Mag Y				
Size	6.5 x 6.5 x 1.5				mm
Weight			0.14		grams

(1) Tested at 25°C except stated otherwise.  
(2) Field upper limit can be extended by using external resistors across CA1/CA2 and CB1/CB2.

## HMR2300r



### FEATURES

- Strapdown Magnetometer Replaces Bulky Fluxvalves
- Microprocessor Based Smart Sensor
- Range of  $\pm 2$  Gauss— $<70$  mGauss Resolution
- Readings can Achieve Heading Resolution of  $0.02^\circ$
- Rate Selectable—10 to 154 Samples/Sec.
- Small Size: 2.83 in.—Fits in ML-1 Style Enclosure
- Repeatable and Reliable—MTBF >50,000 hours

The HMR2300r strapdown magnetometer provides an excellent replacement of conventional fluxvalve sensors, commonly used in aviation systems today. The HMR2300r offers higher reliability (MTBF >50,000 hours) that reduces maintenance and repair cost. Since the design is strapdown, as opposed to a gimballed fluxvalve, it has no moving parts

to damage or wear out during severe flight conditions.

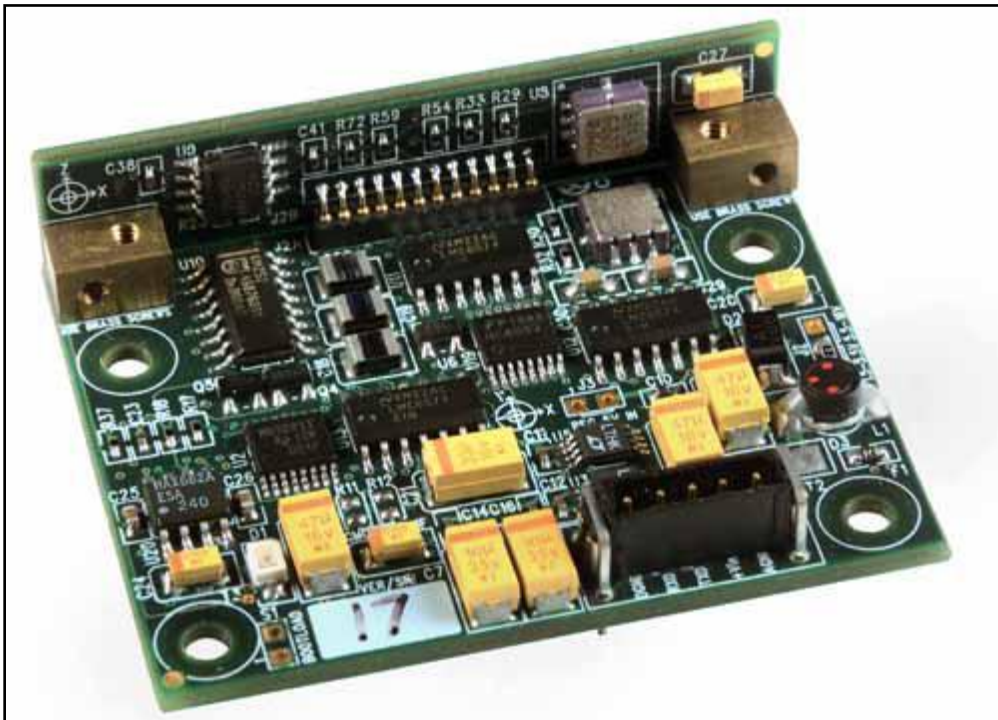
Honeywell's three-axis strapdown magnetometer detects the strength and direction of the earth's magnetic field and communicates the x, y, and z component directly via serial bus. The HMR2300r is compliant with applicable MIL-STD- 810E requirements for military and commercial flight systems.

Characteristic	Conditions	Min	Typ	Max	Unit
Supply Voltage	Pin 9 referenced to pin 5	6.5		15	Volts
Supply Current	V <sub>supply</sub> =15V (with 120 Ω termination)		45	55	mA
Operating Temperature	Ambient	-40		85	° C
Storage Temperature	Ambient, unbiased	-55		125	° C
Field Range	Full scale (FS)—total applied field	-2		+2	Gauss
Linearity Error	Best fit straight line ±1 Gauss		0.1 1	0.5 2	%FS
Hysteresis Error	3 sweeps across ±2 Gauss @ 25 ° C		0.01	0.02	%FS
Repeatability Error	3 sweeps across ±2 Gauss @ 25 ° C		0.05	0.10	%FS
Gain Error	Applied field for zero reading		0.05	0.10	%FS
Offset Error	Applied field for zero reading		0.01	0.03	%FS
Accuracy	RSS of all errors ±1 Gauss		0.12 1	0.52 2	%FS
Resolution	Applied field to change output	67			µGauss
Axis Alignment	Variation to 90 degrees		±1	±2	degree
Noise level	Output variation in fixed field		0.07	±0.13	mGauss
Temperature Effects	Coefficient of gain Coefficient of offset (with S/R=ON)		-0.06 ±0.01		%/° C
Power Supply Effect	From 6 to 15V with 1 Gauss applied		150		ppm/V
Vibration (operating)	5 to 10Hz for 2 hrs. 10Hz to 2KHz for 30 min.		10 2.0		mm g force
Max. Exposed Field	No perming effect on zero reading			10	Gauss
Weight	Board only			40	grams

**QUALITY AND ENVIRONMENTAL CONDITIONS—TABLE 6**

<b>Parameter</b>	<b>Method and Test Levels</b>
Printed Circuit Board	Conforms to IPC-6011 and IPC-6012, Class 3, using FR-4 laminates and prepreg per IPC-4101/21.
Assembly and Workmanship	Conforms to J-STD-001, Class 3, and IPC-A-610, Class 3, respectively.
Electrostatic Sensitive Devices	The HMR2300r shall be treated as an Electrostatic Sensitive Device (ESD) and precautionary handling and marking shall apply.
Mean Time Between Failure (MTBF)	The MTBF of the HMR2300r is 25,000 hours minimum under the environmental conditions specified.
Altitude	The HMR2300r is capable of withstanding altitudes per MIL-STD-810E, Method 520.1, Procedure III.
Fungus	The HMR2300r is constructed with non-nutrient materials and will withstand, in both operation and storage conditions, exposure to fungus growth per MIL-STD-810E, Method 508.4
Shock	The HMR2300r will perform as specified following exposure to shock IAW MIL-STD-810E, Method 513.4, Table 516.4, Procedure I, V, and VI. Functional shock (20g, 11ms, 3 shocks in both directions of 3 axes) and crash hazard shock (40g, 11ms, 2 shocks in both directions of 3 axes).
Vibration	The HMR2300r will perform as specified during exposure to random vibration per MIL-STD-810E Method 514.4, Category 10, Figure 514.4, random vibration, 4 Hz - 2000 Hz ( $0.04g^2/Hz$ to $0.0015 g^2/Hz$ ), 3 hr./axis operating.
Salt Fog*	The HMR2300r, when clear coated, will operate as specified after 48 hrs. exposure to a salt atmosphere environment per MIL-STD-810E, Method 509.3, Procedure I *User must provide polyurethane clear coat to board.
Explosive Atmosphere	The HMR2300r will not ignite an explosive atmosphere when tested IAW MIL-STD-810E, Method 511.3, Procedure I.
Humidity	Method 507.3, Procedure III.
Temperature	10 cycles at $-54^\circ C$ to $+71^\circ C$ operating (approx. 4 hours/cycle including stabilization time).
EMI	The HMR2300r will meet the requirements of MIL-STD-461C, Notice 2, and MIL-STD-462, Notice 5.

## HMR 3500



The HMR3500 TruePoint™ compass module is a 3-axis digital compass solution with a customizable coordinate system for mounting in any desired orientation. Three

Anisotropic Magneto-Resistive sensors and three MEMS accelerometers are combined to provide compass heading as well as pitch and roll angles.

It is a Compass Module includes 3-axis Anisotropic Magneto-Resistive (AMR) sensors, 3-axis MEMS accelerometers, a temperature sensor, and 16-bit microprocessor with onboard Analog to Digital Converter (ADC).

## FEATURES BENEFITS

- Precision Compass Accuracy Resolution
- Tilt Compensated
- Small Size for Tight Mounting Conditions, Minimal Layout Constraints
- Hard and Soft Iron Compensation Routines
- User Driven Calibration to Null Stray Fields. A Single Routine for both Hard and Soft Iron Corrections
- World Magnetic Model Included
- 40° to +85°C Operating Temp Range Wide Variety of Power Sources Light Weight
- 3.0 oz with Aluminum Housing, 0.6 oz PCB only
- Customizable Coordinate System
- 24 Custom Coordinate Orientations
- All Solid State Components
- Rugged for User Defined Orientation Plane

## CIRCUIT DESCRIPTION

The HMR3500 circuit design starts with a microprocessor powered by power supply sub-circuit that takes the input voltage and creates regulated power for the various other circuits in the HMR3500. Two 2-axis MEMS accelerometers are mounted horizontally and vertically to combine into a 3-axis tilt sensing sub-circuit. Each accelerometer outputs a Pulse-Width-Modulated (PWM) digital signal that the microprocessor measures for pitch and roll angles.

Besides an integral temperature sensor, a 2-axis and 1-axis magnetic sensor devices are mounted horizontally and vertically to create a 3-axis measurement of the incident magnetic field upon the

sensors. Each sensor output is amplified and sent to a multiplexed input ADC residing inside the microprocessor. After digitizing, the magnetic signals are corrected for hard and soft-iron magnetic errors created by the environment to which the compass is attached.

Heading computation uses the magnetic and tilt information inputs after compensation for errors. From the basic magnetic heading, a declination value may be added to arrive at a geographic north referenced heading. An index offset value may also be added to correct for mechanical installation misalignment on the target platform.

This is not a magnetometer its a compass.

<b>SPECIFICATIONS</b>					
Characteristics	Conditions	Min	Typ	Max	Units
<b>Heading</b>					
Accuracy	(Clean Magnetic Environment) Level Pitch $0^\circ$ to $\pm 30^\circ$ Roll $0^\circ$ to $\pm 30^\circ$	-	0.5 0.5 0.75	1.0 1.5 1.5	(1 $\sigma$ )
Resolution			0.1		deg
Repeatability	3 sweeps, $0^\circ$ to $360^\circ$ , level		0.2		deg rms
<b>Pitch and Roll</b>					
Roll Range	Default orientation, rotation about X-axis		$\pm 180^\circ$		deg
Pitch Range	Default orientation, rotation about Y-axis		$\pm 80^\circ$		deg
Accuracy	Roll $\pm 30^\circ$ , Pitch $\pm 30^\circ$		0.5	1.0	deg rms
Null Accuracy <sup>1</sup>	Level		$\pm 0.5$		deg
Resolution	Level, 1-sigma, 100 readings		0.04		deg
Roll Repeatability	Roll $\pm 70^\circ$ Pitch $\pm 70^\circ$		0.2 0.2		deg rms
Pitch Repeatability	Roll $\pm 70^\circ$ Pitch $\pm 70^\circ$		0.1 0.1		deg rms
<b>Magnetic Field</b>					
Range	Maximum Magnetic Flux Density		0.7		gauss
Resolution	1-sigma, 100 readings		0.45		milli-gauss
Dip Angle	Earth's Vertical Field Component	-70		+70	deg
Linearity			0.2		%FS
<b>Electrical</b>					
Input Voltage	Standard Product	2.5	5.0	5.2	volts DC
Power	Input Voltage 2.5 to 5.2V		300		mW
<b>Digital Interface</b>					
UART	ASCII	4800	9600	38,400	Baud
Update Rate	Continuous Heading Updates	0.05	10	25	Hz
Format	Bi-directional binary packet data protocol.		RS-232		-
<b>Physical</b>					
Dimensions	Circuit Board Assembly		1.97 x 1.65 x 0.52		inches
Weight	HMR3500 PCB only HMR3500 with case, no cable		0.6 3.0		ounce ounces
Connector	5-pin, 2mm pin spacing				-
<b>Environment</b>					
Temperature	Operating Storage (OEM only)	-40 -55	- -	+85 +125	°C °C

<sup>1</sup> Null zeroing prior to use of the HMR3500 and upon exposure to temperature excursions beyond the Operating Temperature limits is required to achieve highest performance.

\* Tested at 25°C unless stated otherwise.

Now for the question of 2 x 2 axis or a 3 axis magnetometer various factors need to be considered.

- The 2 x 2 axis magnetometer will have a redundant axis which can be used in case one axis gets spoilt. But what are the chances that only 1 axis of a chip will get spoilt where as the

other is in perfect condition. But this configuration is useful in the case on some failure that one chip is spoilt we have another chip to rely on

- There is a possibility that the 2 x 2 architecture is a little more difficult to implement as compared to using a single chip
- Although the 2 x 2 option is cheaper but only by 100 \$. So this should not be a deciding factor
- Is there any problem with keeping them so close to each other? Can they be affected by each other's magnetic field?
- Power consumed by 2 x 2-axis magnetometers is much more than that by just one.
- Resolution of the 3-axis magnetometer is many times greater than that of the 2-axis one.

What Honeywell has to say ” Electronic compass solutions solve for magnetic heading by measuring the earth's horizontal magnetic field. By keeping the two-axis modules approximately level, maximum heading accuracy is achieved. For applications where compass modules will not be level, a three-axis, tilt compensated compassing solution is recommended. These three-axis compass modules perform an “electronic gimbaling” function by adding the third magnetic axis and a tilt sensor for a gravity vector reference. Tilt sensors are made of either fluidic sensors or MEMS accelerometers. Quality of the tilt measurement contributes to precision compass outputs”

### HMR vs HMC

The HMCs are chips that need to be put on PCBs whereas the HMR are entire systems. Hence flexibility is lost. But they can be more reliable.

From the reports, “Commercially available magnetometers” and “Comparison of Magnetometers” we have finalized HMR 3000 for our satellite. This magnetometer has accelerometers incorporated in it so that it directly gives the value attitude

### HMR3000 specs

Weight	92g
--------	-----

Dimensions	1.5*4.2*.88
Accuracy	Heading-0.5deg Pitch-0.4 deg Roll-.6 deg
Power	6V,35 mA
Interface	Serial, RS232 protocol
Cost	800\$

### 5.2.3.2 Sun Sensor

To augment the attitude information we have also decided to use photodiodes as Sun Sensors. These typically have an accuracy of 1 deg in attitude prediction, this accuracy however can be increased by using a better mathematical model for attitude detection.

#### 5.2.3.2.1 Sun sensor types

The three basic classes of sun sensors are analog sensors, which have an output signal that is a continuous function of the sun angle; Sun presence detector, which provides a constant output when the sun is in the FOV; and digital sensor, which provides an encoded, discrete output which is a function of the sun angle.

##### 5.2.3.2.1.1 Analog Sun sensors

Analog sensors are often called cosine detectors because a common type is based on the sinusoidal variation of output current of a solar cell with sun angle. More specifically, the output current is proportional to the cosine of the angle of the angle of incidence of the solar radiation.

$$I(\theta) = I(0) \cos \theta$$

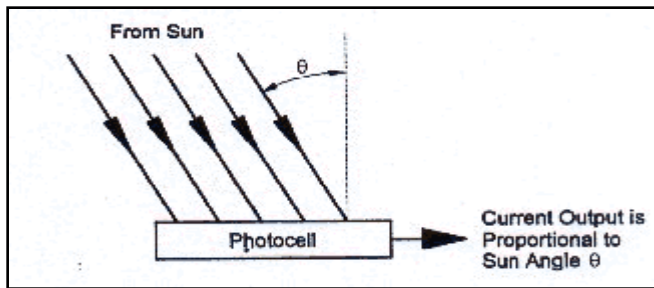


*Figure 5. 8: Analog Sun Sensor*

Unlike the other sensors, the cosine detector uses the onboard solar cells of the satellite without the need of additional hardware. Since the output<sup>1</sup> of cosine detectors is temperature dependent, it will be necessary to measure the temperatures at the sun sensors and compensate for temperatures in the sun sensor data.

A second analog sensor type uses a bar or mask to shadow a portion of one or more photocells. Different configurations can yield a two-axis sensor or a one-axis sensor with varying FOVs, accuracies, and resolutions. These sensors are commercially available.

- Two-Axis Sun Sensors: With two axis sun sensors it is possible to determine the direction of the sun using only one sensor<sup>2</sup>. In this design four rectangular photo-voltaic cells are used in a closed casing with an opening in the top part. In this sensor the output of each photo-voltaic cell will have to be measured and compared with each other to determine the angle of the incoming sunlight. Instead of using four detectors an alternative would be to use a CMOS camera chip for the same purpose.

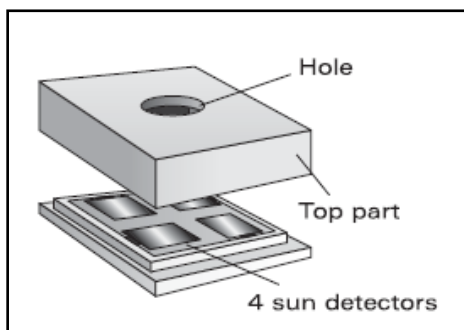


*Figure 5. 9: Two Axis Sun Sensor*

---

<sup>1</sup> current in the case of solar cells as sun sensors.

<sup>2</sup> when the sun is in the FOV, though more may be required to get a complete  $4\pi$  st coverage.

- One-Axis Sun Sensors: One example of a one-axis sun sensor uses two overlapped triangular pieces of silicon detectors, placed inside a aluminum housing. A quartz window with a slit is placed above the detectors and allows only a line of sunlight to hit the detectors. Another uses a bar cast a shadow and the in this way it is possible to measure the direction of the sunlight in both cases by determining the difference of the output of the two detectors. If this type of sun sensor would be used on the satellite, it would be necessary to use at least two of these on the side facing the sun, to determine the position of the sun in three dimensions.

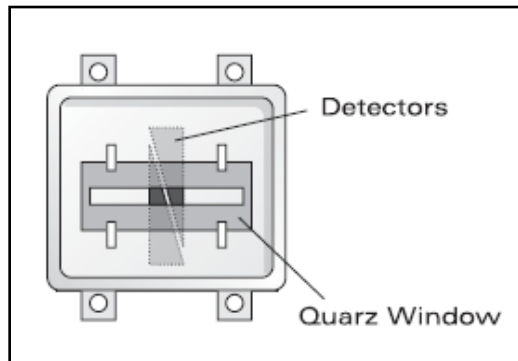


*Figure 5. 10: One Axis Sun Sensor*

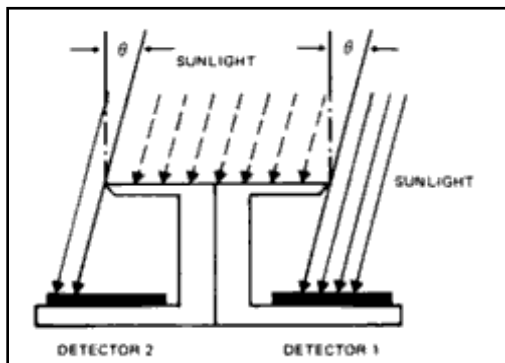


*Figure 5. 11: Sun Sensor to work*

A benefit of the single-axis and two-axis sun sensors is, that they are independent of the temperature they are exposed to, as they use the difference between their single sensor parts, which all are exposed to the same temperature.

#### 5.2.3.2.1.2 Sun Presence detector

Sun presence detectors are used to protect instrumentation, to activate hardware, and to position the spacecraft or experiments. Ideally, Sun presence detector provides a step function response that indicates when the sun is in the FOV of the detector.

*In accordance to our mission parameters, we would not be requiring Sun presence detectors.*

#### 5.2.3.2.1.3 Digital Sun sensors

A one-axis digital sun sensor generates an output which is a digital representation of the angle between the sunline and the normal to the sensor face. The sun illuminates a pattern of slits. The slits are divided into a series of rows with a photocell beneath each row. The different types of rows are as follows.

- Automatic threshold adjust
- Sign bit
- Encoded bits
- Fine bits.

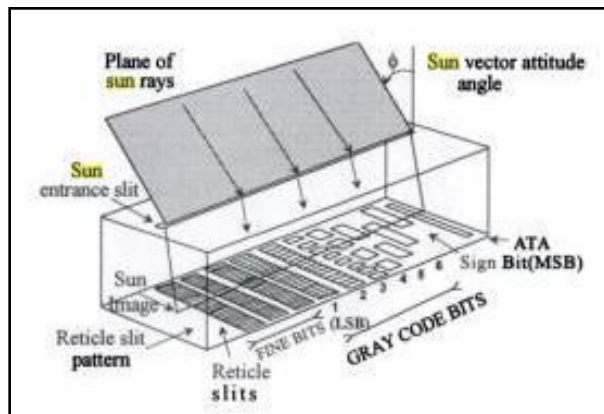


Figure 5. 12: Digital Sun Sensor

Since the photocell voltage is proportional to  $\cos\theta$  ( $\theta = \text{sun angle}$ ), a fixed threshold is inadequate. Thus we use the ATA slit, which is half the width of other slits.

The sign bit determines which side of the sensor the sun is on. The encoded bits provide a discrete measure of the linear displacement of the sun image relative to the sensor center line.

The code most widely used is the Gray code, which results in a smaller error than the corresponding binary code.

Fine Sun sensors use analog information in addition to the digital information. By knowing the intensity of sunlight striking neighboring pixels, the direction of the centroid of the Sun can be computed to within a few arc seconds.

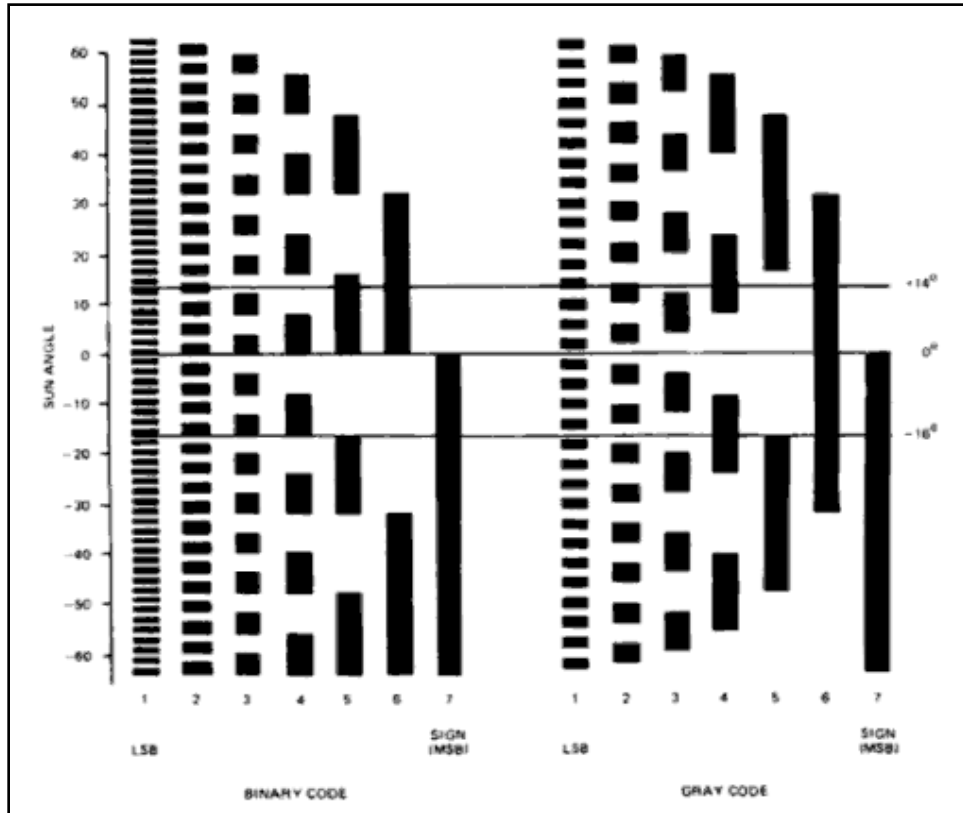


*Figure 5. 13: The pattern for a +64° FOV digital sun sensor with a 1° LSB*

Two axis sun sensors consist of two measurement components mounted at right angles, yielding a 64° by 64° or 128° by 128° FOV. Full  $4\pi$  sr coverage for two axis sensors is obtained by using five or more 128° by 128° sensors. The sensor with the highest output ATA is selected (effectively the smallest angle relative to optical null)<sup>3</sup>.

---

<sup>3</sup> and hence least error.

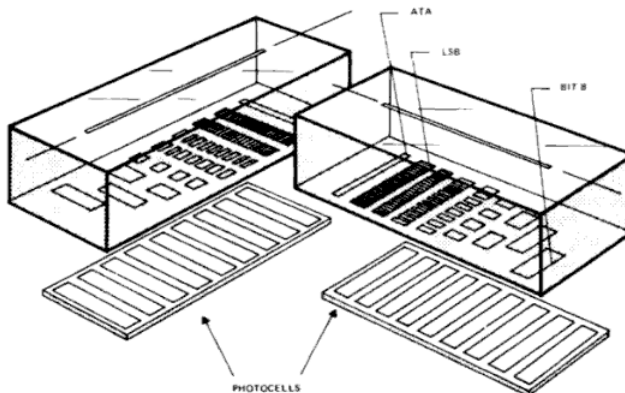


*Figure 5. 14: Multiple Digital Sunsensors at work*

The accuracy of a digital sun sensor is limited by the angular diameter of the Sun, which is approximately  $0.5^\circ$  at 1 AU.

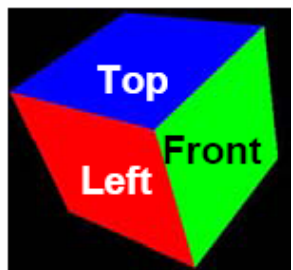
#### 5.2.3.2.2 Our options

As mentioned above, to achieve complete attitude determination, we require two independent sensors. With a magnetometer as the first, a Sun sensor would be our best option as the second sensor. The Sun sensor owes its versatility to many factors. Unlike the Earth, the angular radius of the Sun is small enough ( $0.267^\circ$  at 1 AU) for point-source approximations to be valid for most applications. This simplifies both sensor design and algorithms. Also, the Sun is sufficiently bright so as to permit use of simple equipment without discerning amongst sources. The major disadvantage with sun sensors is that they can not be used when the satellite is in eclipse.

Amongst Sun sensors, we have the following choices.

#### 5.2.3.2.3 Solar Cells as Sun sensors

The solar cells on a satellite act as cosine detectors. By measuring the current produced by 3 solar panels that share an apex, the sun vectors (a single unit vector directing on the sun), can be



calculated.

In reference with the adjacent figure, assuming identical solar cells,

$$I_{\text{left}} = I_{\max} \cos(\Phi) \sin(\theta)$$

$$I_{\text{front}} = I_{\max} \cos(\Phi) \sin(\theta)$$

$$I_{\text{top}} = I_{\max} \cos(\theta)$$

$\theta$  = the angle to the normal of the top face

$\Phi$  = the angle to the normal of the front face

$v_s^B$  = sun vector

$$v_s^B = \begin{pmatrix} \cos \phi \sin \theta \\ \sin \phi \sin \theta \\ \cos \theta \end{pmatrix}$$

$$v_s^B = \begin{pmatrix} X & 0 & 0 \\ 0 & Y & 0 \\ 0 & 0 & Z \end{pmatrix} \cdot \begin{pmatrix} I_{left} \\ I_{front} \\ I_{top} \end{pmatrix} \cdot \frac{1}{I_{max}}$$

Where X, Y and Z equal 1 or -1 depending on the solar panel's location: on the positive or negative side of the satellite.

We require an Amplifier circuit, current sensor, analog to digital converter, and the interfacing circuit to the microcontroller.

The advantage of this method is that power consumption and mass requirement is very small. But on the down side, they are extremely inaccurate, with  $1^\circ$  of accuracy<sup>4</sup> in FOV of  $30^\circ$ . The accuracy drops further as  $\theta$  approaches  $90^\circ$ .

Also, the variation of current with respect to temperature comes into play. Radiation reflected from the Earth<sup>5</sup> also introduces an error.

However, better accuracies can be achieved by using better mathematical models<sup>6</sup>.

A second option would be to use six cosine detectors<sup>7</sup> instead. This reduces the error due to Earth albedo. Earth albedo is Sun light reflected from the Earth and is near  $(30 \pm 5)$  % of the solar flux<sup>8</sup>.

Also, the solar panels used for the power supply can be used as secondary sun sensors. In this way some redundancy is added to sun sensors on the five sides with solar panels. The solar panels can use the same algorithms used for the primary sun sensors.

Earth albedo corrections would have to be done for both cases, along with a temperature correction.

*This is a very good option for our purpose; and should be seriously considered.*

<sup>4</sup> 'Attitude Determination – Advanced Sun Sensors for Pico-satellites' pdf by Yonatan Winetraub and Dr Anna B. Heller

<sup>5</sup> Earth albedo (see below)

<sup>6</sup> see appendix

<sup>7</sup> such as silicon photodiodes (planar)

<sup>8</sup> Larson and Wertz, 1992

#### 5.2.3.2.4 Manufacturing/ purchasing 2-axis Sun sensors

2-axis analog and digital sun sensors are readily available. At least five  $128^\circ$  by  $128^\circ$  FOV sensors would be required for full  $4\pi \text{ sr}$  coverage. The cost of five fine sun sensors is moderately high<sup>9</sup>. Analog and digital 2-axis sun sensors can also be manufactured, as commercially available Sun-sensors cannot be customized. High accuracies can be achieved with some manufactured designs.

Two-axis sun sensors need to be placed on the panels, and hence occupy the place of solar cells and hence less power is delivered to the batteries. The mass and power consumption of some commercially available Sun sensors is quite high.

*Manufacturing of 2-axis sun sensors should be considered because the payloads call for high accuracy attitude determination.*

*Purchasing should only be considered if both implementation of solar cells as Sun sensors and manufacturing of two-axis Sun sensors fail, due to the cost<sup>10</sup>.*

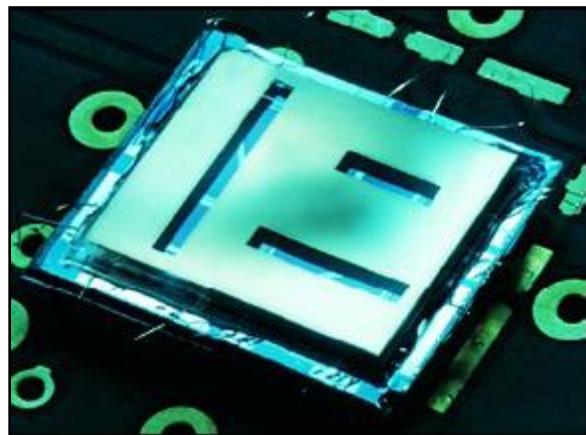


*Figure 5. 15: MIC Sun Sensor*

Shown above is the MIC (Micro Electronics Institute) Sun sensor mounted on a PCB. They are extremely lightweight, small and power saving.

---

<sup>9</sup> Cost is proportional to accuracy and FOV

<sup>10</sup> Small sun-sensor from Optical Energy Technologies inc

- $\pm 0.5^\circ$  Two axis sun readout accuracy over  $100^\circ$  field of view
- Weight: less than 40 grams
- Earth Albedo error minimization
- Power: less than 50 mwatts or zero watts if  $\pm 1^\circ$  albedo error is acceptable
- Price: \$16,000- each

### 5.3 Kalman Filter

The Kalman filter based on model of system dynamics, which makes use of the data from magnetometer and sunsensor to estimate the attitude of the satellite precisely needs to be developed and implemented. If the Kalman Filter does not give the desired performance, we need to develop an extended Kalman filter based on non-linear system dynamics. Once, again this entails good computational power available on board. However, the system dynamics is approximately periodic with a period equal to orbital time period. Hence, we can develop and load the OBC with a few models of kalman filter which can handle the job for entire orbit. Then we just need to switch between different models.

### 5.4 Actuators

The control branch, which is the actuator part of the system, can be subdivided in passive and active control mechanisms, although it has to be noted that only active mechanisms truly allow control.

#### 5.4.1 Active Actuators

##### 5.4.1.1 Thrusters

Offset thrusters actuate the satellites attitude by imposing a torque on the spacecraft. Typically thrusters are used for attitude control on bigger and heavier satellites.



A tiny blip of thrust in one direction, and a few tens of seconds later, an opposing blip of thrust is needed to keep orientation errors within limits. The tight mass budget will make it difficult to carry any propellant on-board for attitude control. The tight power budget prohibits the use of ion thrusters.

##### 5.4.1.2 Momentum Wheels

The mechanism based on momentum wheels is sometimes referred to as dual spin stabilization. Momentum wheels generate torque by acceleration of a spinning mass. This actuator requires momentum dumping when saturation is reached, i.e., when the maximum momentum storage capacity is reached. In this case another control mechanism must be able to compensate the reverse torque generated by the dumping process. So far, momentum wheels have only been manufactured for Mini- and Micro-Satellites.



*Figure 5. 16: Smallest Momentum Wheel*

The smallest momentum wheel that has been found during the initial research was Dynacon's MicroWheel200. It has the following specifications:

Size: 102 x 94 x 89 mm

Mass: 0.77kg (minimum)

Power: 3,2W + 1W (for optional rate sensor), 14/28V

It should be noted that this option is not feasible for a micro satellite.

## 5.4.2 Passive Actuators

### 5.4.2.1 Passive Permanent Magnet

A passive permanent magnet installed on a satellite simply aligns the spacecraft with the geomagnetic field vector. Limitations of this system arise from the fact that the magnetic field undergoes dramatic changes during one polar orbit.

### 5.4.2.2 Magnetorquers

Magnetorquers is principally a set of controllable electromagnets, which are capable of aligning an arbitrary vector inside the satellite with the geomagnetic field. A disadvantage is the requirement of implementing a model of the earth's magnetic field on the onboard computer.

Additionally, this system requires information about the current position. However, this requirement appears to be manageable.

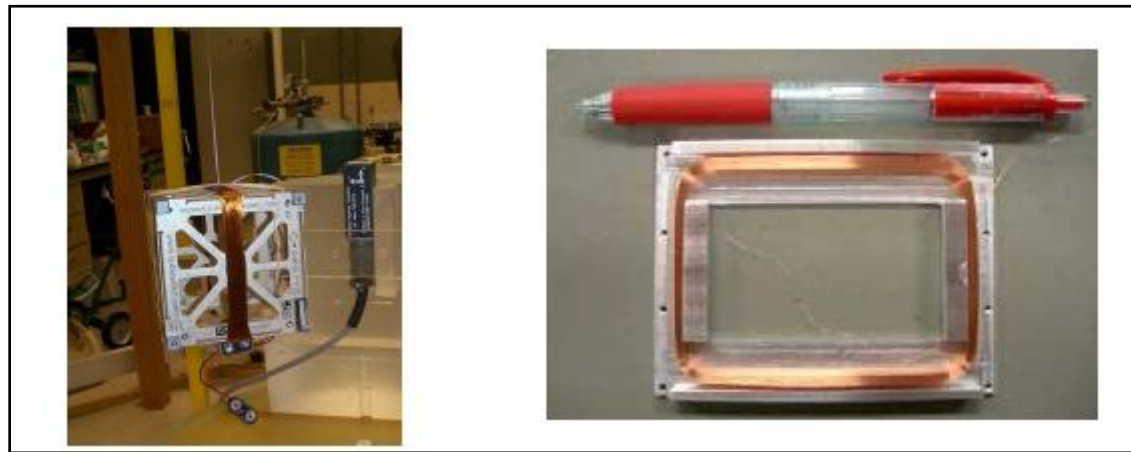


Figure 5. 17: Magnetorquers

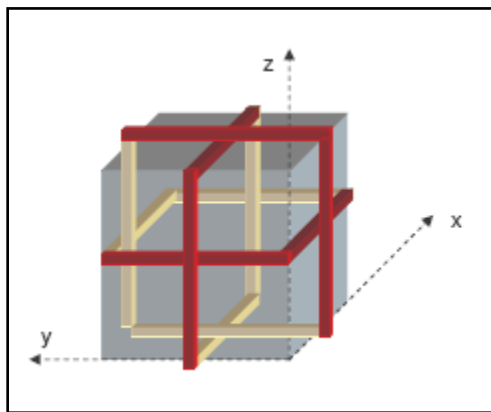


Figure 5. 18: Magnetorquer around our satellite

#### 5.4.2.3 Gravity Gradient Boom

A gravity gradient boom aligns the satellite with the earth's center of mass ideally. The stabilizing mechanism is initiated by a single in-orbit manipulation of the moments of inertia of the spacecraft. A boom, which constitutes a mass, has to be deployed after orbit insertion. After this deployment sequence, if the tensor of inertia is looked after carefully, the spacecraft will ‘fall’ into a stable position with the boom pointing towards the earth. However, the generated torques are extremely small. A small damping of the satellites motion might make a detumbling process based on this technique very time consuming. Also, a deployment of a gravity gradient boom always constitutes a single point of failure (SPOF) and is thus often avoided in the mission

design.

#### 5.4.2.4 Spin Stabilization

Spin stabilization is the passive form of a momentum wheel. The complete satellite is spun about the principal axis of inertia with the highest momentum of inertia. However efficient this mechanism may be at spin rates of about 20 up to 50 RPM.

#### 5.4.3 Actuators chosen for our use

From the list of actuators above we have chosen GGB and Magnetotorquer for our satellite for simplicity and ease in manufacturing

##### 5.4.3.1 Magnetotorquer

Magnetotorquer is the primary active actuator for our satellite. Three torquers are required for three axis attitude control of the satellite.

###### 5.4.3.1.1 Hardware Design

The design of the magnetotorquers is based on the assumption the all three coil have same properties. This means that the mass of each coil is equal to one third of the total mass.

The coils will be positioned around the solar panels, on the outside of the satellite as shown in the figure

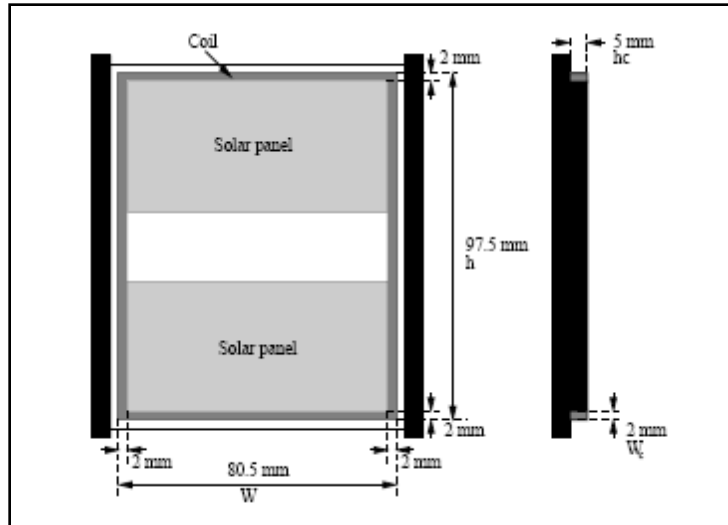


Figure 5. 19: Magnetotorquer Design

### Design Constraints

Maximum Dimensions	300*200 mm
Max Power/Torquer	1W
Minimum Temp	-100 C
Max Temp	100 C
Normal Temp	15 C
Magnetic torque req.	10e-5*( See Calculations in appendix)

### Coil Material

Torque varies inversely with square root of resistivity

Weight varies directly with density.

Also material properties should not vary too much with temperature.

For material of torque wire between Cu and Al , Cu has been chosen simply because it has been used as material for torquers in both ISRO satellites and some of the other student satellites which we have studied.

### Wire Thickness

Wire thickness is extremely critical because:

$$\tau \sim t^{1.5}$$

Therefore thicker the wire diameter more will be the torque produced.

For our calculations we have used wire diameter of .2743 mm before making the torquer we will test for wires of different thickness and see if its feasible to make the torquer out of a thicker wire.

Relative permeability ( $\mu_r$ ):

Torque varies directly with  $\mu_r$  currently we have assumed  $\mu_r = 1$  but as the material for the satellite gets finalized we will be able to get better estimate of  $\mu_r$

#### 5.4.3.1.2 Calculations of torque parameters

Symbols and their values

Torque= $\Gamma$ ;

P=power;

R=resistence;

n= number of turns

i=current;

m=magnetic moment ;

B=Earth's magnetic field = $3 \times 10^{-5}$ T;

d= diameter of Cu wire= $0.2743 \times 10^{-3}$ m ;

b= 20cm (assuming a cubic satellite of side length b) ;

$\rho$ =resistivity of Cu = $1.7 \times 10^{-8} \Omega m$ ;

$\sigma$ = density of Cu wire = $8900 \text{ kg/m}^3$ ;

$\Theta$ =angle between B and m

$\mu_r = 1$ ;

W=weight of the cu wire

Formulae used:

$$\vec{\Gamma} = \vec{m} \times \vec{B} ;$$

$$m = \mu_r n i A$$

$$i = \sqrt{P/R} ;$$

$$R = 4\rho L / \pi d^2;$$

$$A = ab ; \quad L = 2n(a+b); \quad V = \sqrt{PR}$$

$$W = (L \times \pi d^2 \times \sigma) / 4;$$

#### 5.4.3.1.2.1 Magnetic moment

$$m = \mu_r n i A$$

$$m = K_1 \sqrt{Pn}$$

$$K_1 = \mu_r d ab \sqrt{\pi / 8\rho(a + b)}$$

$$K_1 = 0.112 \text{ (S.I units);}$$

$$m = 0.112 \sqrt{Pn}$$

#### 5.4.3.1.2.2 Weight

$$W = (L \times \pi d^2 \times \sigma) / 4;$$

$$W = K_2 n$$

$$K_2 = ((a+b) \times \pi d^2 \times \sigma / 2);$$

$$K_2 = 6.91 \times 10^{-4} \text{ (S.I. units);}$$

$$W = (0.526 n) \text{ gram}$$

#### 5.4.3.1.2.3 Voltage

$$V = \sqrt{PR}$$

$$V = K_3 \sqrt{Pn}$$

$$K_3 = \sqrt{\frac{8P\rho n(a + b)}{\pi d^2}}$$

$$K_3 = 0.588 \text{ (S.I. units);}$$

$$V = 0.588 \sqrt{Pn} \text{ volts}$$

#### 5.4.3.1.2.4 Torque

$$\vec{\Gamma} = \vec{m} \times \vec{B}$$

$$\Gamma = mB\sin\theta$$

$$\Gamma = 0.112\sqrt{Pn}(3 \times 10^{-5})\sin\theta$$

$$\Gamma = .336 \times 10^{-5} \sqrt{Pn} \sin\theta$$

Based upon our Max torque req. and Power available no. of turns comes out to be:

Torque=1e-5 Nm

m=.3333

Power(W)	No. of turns	Weight(g)	Votage(V)
1	10	5.26	1.69
.5	20	10.5	1.69
.1	100	52	1.69
.05	200	105	1.69

Therefore it is possible to get the desired torque with much less power req. The penalty is in the form of weight. Thicker wire results in a heavier torquer.

Other parameters which we need to consider during the detailed design of the torque:

- 1)Temperature variation of the various parameters of the torque.
- 2)Time constant of the torque.

#### 5.4.3.1.3 Calculations for maximum torque req.

Max GG Torque

$$\text{Torque}(\Gamma) = (3\mu_g/2R^3)[I_z - I_x]\sin 2\theta$$

$$\Gamma_{max} = (3\mu_g/2R^3)[I_z - I_x]$$

Here

$$\mu_g = GM = (6.67 \times 10^{-11}) \times (6 \times 10^{24}) = 4.002 \times 10^{14} (\text{S.I. units})$$

G=Gravitational constant ,M=Mass of the Earth;

m=mass of satellite ;

$m_t$ =tip mass of GGBoom=0.250 kg

l=length of one side=0.30 m

L=Length of tether wire(Boom Length)=10 m

R=Distance of satellite from the centre of the earth=6400+670 km

=7070 km

Assuming CUBIC SATELLITE

$$I_z = ml^2/6$$

$$I_x = (ml^2/6) + m_t L^2$$

$$\Gamma_{max} = -(3\mu_g/2R^3) m_t L^2$$

$$\Gamma_{max} = -(3 \times 4.002 \times 10^{14} / 2 \times (7070 \times 10^3)^3) (0.250 \times 10^2)$$

$$\Gamma_{max} = 4.24 \times 10^{-5} (\text{S.I. units})$$

Other torques are smaller

$$\Gamma_{max} = 10^{-5}$$

For  $\theta = \pi/2$  ;  $B = 3 \times 10^{-5} T$

Max torque required=1/3( $\Gamma_{max}$ )

#### 5.4.3.1.4 Specifications

Dimensions	30*20 cm
Weight	34.55*3
Material	Cu
Wire Diameter	.2743 mm
Power	.1 W
Voltage	4.157V
Number of turns	50
Magnetic moment	0.3421 Am <sup>2</sup>

#### 5.4.3.2 Gravity Gradient Boom

Gravity gradient Boom provides passive stabilization of the satellite. GGB on a student satellite has following advantages:

- No penalty Power and On-Board-Computer resources
- Gives good coarse stability of attitude, which can then be augmented using an active controller
- The stabilization attained even in case of failure of active control is good enough
- The Linear control law with the linearization at the equilibrium position is bound to work well. In case of satellite without GGB, an advanced control law, based on Non-linear dynamics of the satellite will be essential.

From Linearization of the system dynamics about equilibrium position of zero Euler angles, we arrive at the following conditions for stability of the system.

$$1) \quad I_y > I_x > I_z$$

$$2) \quad I_y < I_x + I_z$$

Also, Amplitude of pitch oscillations  $\propto \frac{1}{I_x - I_z}$

The GGB tip mass and length is such that the above conditions are satisfied when the boom is deployed.

#### 5.4.3.2.1 GGB Design

A good GGB is expected to satisfy the following characteristics,

*Specs for GGB:*

- 1) The boom is deployed with a certain impulse and the tip mass comes to rest when the thread becomes taut
- 2) Occupies the minimum Nadir surface
- 3) The natural frequency of the first mode is not attained during the operation of the satellite  
(This has to be ensured with the damping provided by the active controller)
- 4) Minimum oscillation due to gravity gradient torque (This determines the rigidity of the boom)

- 5) Minimum total weight of the BOOM-BOX (This requires appropriate compromise between the boom-length and tip mass)
- 6) The connecting tether should have good thermal conducting and radiation reflecting properties to avoid bending due to temperature gradient
- 7) The connecting tether should be kink-free and should be able to regain a taut shape on deployment
- 8) A simple and reliable deployment mechanism on receiving the signal from OBC is essential (as suggested by ISRO, conventionally used Pyrotechnic based mechanisms should be avoided to avoid the thermal complications that may result thereof)
- 9) The base mounting should be compatible with the requirements of the Integration
- 10) The attachment between various parts i.e between tip-mass and connecting tether; connecting tether and base should be able to withstand space-grade requirements like Vibrations at launch
- 11) Any other requirements of the system Dynamics due to Coriolis forces experienced during boom deployment

#### 5.4.3.2.2 Various Concepts for GGB

We here present three concepts that we have for making a GGB,

##### 5.4.3.2.2.1 Original Design

The boom is a metallic tether of Copper Beryllium coated with a highly reflecting material, to keep the temperature gradient small. If the stiffness that the Cu-Be alloy provides is low causing small natural frequency, other suitable metal alloy can be used. This tether is wound on a metallic spindle of high density material. The spindle forms the tip mass of the GGB on deployment. The spindle with tether wound on it is placed inside a box, which has a hole for tether. This box is mounted on a spring base, from which it gets impulse for deployment. The other end of the tether is fixed to the satellite. The following figure shows the schematic of the GGB

#### 5.4.3.2.2.2 Heritage Methods

##### 5.4.3.2.2.2.1 Storable Tubular Extendible Member

One of the most successful mechanisms is the Storable Tubular Extendible Member (STEM) developed by the De Havilland Aircraft of Canada, Ltd. The boom is formed from strip of material that gets formed into a circular shape on deployment, such that the edges of the strip overlap. The resulting bending strength is almost similar to that of a seamless tube of same diameter and wall thickness. The element is stored in the strained flattened condition by winding it onto a drum. (See Fig. 5.1) There are mechanical guide rollers that continuously transform the boom from its natural circular section to a flattened condition when the boom is being retracted.

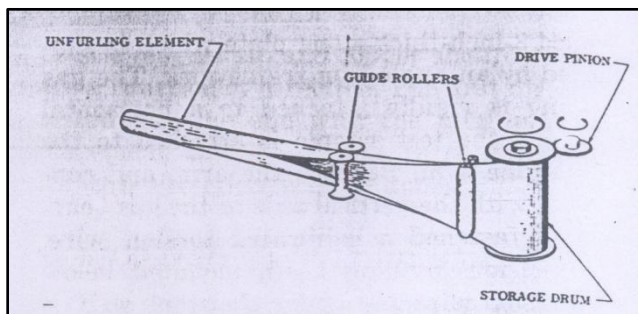


*Figure 5. 20: Stem Principle*

The boom may be extended or retracted by rotating the storage drum in the appropriate direction. Since retracting the boom means supplying strain energy to the material to flatten it, hence the motor is required to supply more power for retraction. Whereas, in the case of extension, the material is going towards its natural tendency to become a circular section, hence very little power is required. The motor is mainly used to give the correct extension velocity as desired by the control system.

In the application of STEM-type rods for gravity-gradient missions, it was recognized that thermal distortion of the STEM's could be detrimental to the performance of the system. The pointing accuracy of the system could suffer due to asymmetrical solar pressure loading and aerodynamic pressure at low altitudes. Some of the ways to decrease the temperature difference between the side facing the solar radiation and the side looking at cold space, which is responsible for the rod end deflection, are:

- Decrease rod radius
- Increase rod material thickness

- Increase rod material conductivity
- Decrease rod surface solar absorptivity

Since it was not possible to play with the configurations of the STEM rods, the optimum way was to coat the exterior surface of the rod with a low-absorptivity coating. Hence silver plate was selected to coat the beryllium-copper rods since the absorptivity of polished silver is very less. Finally, the STEM rods were produced on which extremely thin coatings (0.0002 inch) of silver were applied on the 0.002-inch thick beryllium-copper walls.

#### 5.4.3.2.2.2 Very Long Deployable Booms

It was realized that booms of very great length were necessary for high altitude passive stabilization of large vehicles. The STEM rods couldn't be used for very great length because of large thermal bending. The extent to which surface reflectivity can be increased is limited and trying to increase the thermal conductivity of the material of the boom is problematic. Hence to reduce the thermal gradient, thick walled light metal tubing was used. The studies in Lockheed improved the existing booms with better thickness-to-diameter ratio and higher thermal conductivity with the use of Aluminum and Lockalloy (BeAl).

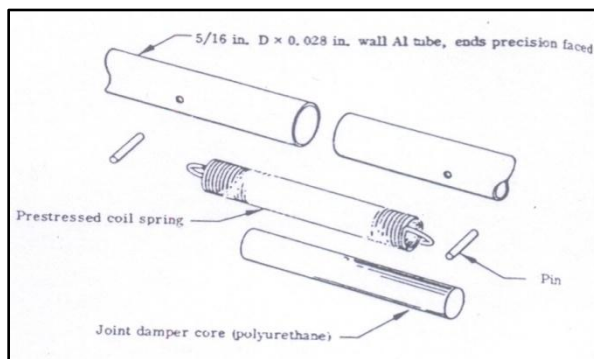


*Figure 5. 21: Self-deploying preloaded joint*

The booms were made up of many foldable segments joined together by self-deploying preloaded joints. (See Fig. 5.2) A prestressed coil spring within each joint serves the multiple functions of:

- Making the joint self-deploying
- Preloading the joint so that it is effectively rigid after deployment
- Serving a guide to align the precision-faced tubing ends after deployment

The coil spring prestress level is chosen large enough so that gravity-gradient torques can never exceed the preload. Captured within the spring is a viscoelastic deployment damper which in the temperature range of space becomes very stiff and viscous and it serves to retard the deployment and dissipate the stored energy of the springs. The folded boom shown in Fig 5.15, is made up of 5-foot segments which would become a 90-foot boom on deployment.

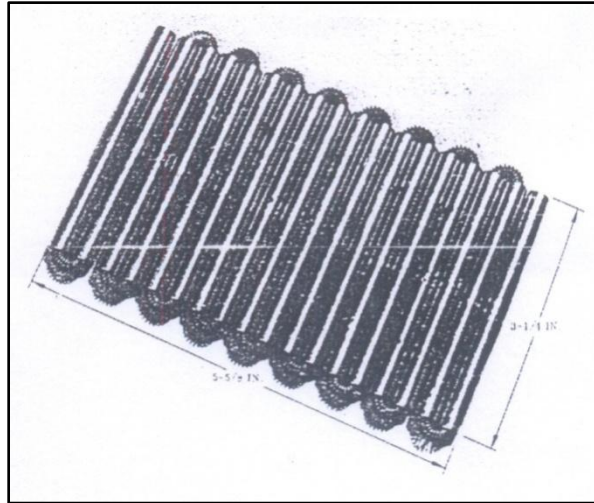


*Figure 5. 22: Folded Boom*

Vacuum is expected to have very little degrading effects on the rubber damping or the retarder material. Weight loss due to vaporization in vacuum (outgassing) was predicted to be very small because of low vapour pressure due to very large molecular weights of the polymers. Radiation shielding has been provided by burying the rubber portion of the damper within the thermal skin of the damper.

Some of the modern day student satellites have used the flexible spiral rulers as the gravity-gradient booms.

## 5.5 Controller

The control for the satellite consists of following phases of the mission,

- 1) Detumbling the satellite after launch and bringing it to a particular orientation for boom deployment
- 2) Regulation of attitude of the satellite at zero Euler angles
- 3) Flip over maneuver in case satellite is stabilized with boom pointing away from earth

Besides these there can be special modes of operation in case of failures, power-saver mode, backup required. These can be considered to be implemented if the need for the same is felt at the later stages of the project.

Detumbling the satellite essentially involves dissipation of energy or damping the spinning motion of the satellite, until it reaches a state where boom can be deployed safely. This is commonly done using the magnetorquers. Other student satellites have made use of the so called B-dot controller for this purpose. However, we intend to synthesize a control law our selves and check its performance by simulation of the same. This as well as dynamics of the satellite during the boom deployment need to be looked into. In these phases the dynamics of the satellite is nonlinear. We make use of quaternion instead of Euler angles to describe the kinematics of the satellite, since there exists a singularity at pitch angle  $90^0$ , when Euler angles are used.

After the boom is deployed the satellite is stabilized with its nadir surface pointing towards earth and all the euler angles at zero. The orientation of the satellite is perturbed due to aerodynamic drag caused by residual atmosphere; solar pressure, gravity gradient torques etc. This is counter acted by the gravity gradient torque which tends to align the boom to point towards the center of the earth. However this action is very slow and pointing precision of the order of  $0.5^0$  to  $1^0$  is required at all instants. Hence we make use of active attitude control by using magnetorquers as the actuators. The objective of the control law governing the magnetorquers is to regulate the attitude of the satellite at zero values of the euler angles as required by the payload.

### 5.5.1 Control law

Here we present the derivation of a control law we recently worked out. More such control law can be synthesized and their performance can be checked using the MATLAB/Simulink simulations.

The linearised equations of dynamics of the satellite are obtained as,

$$\begin{pmatrix} 0 & B_z & -B_y \\ -B_z & 0 & B_x \\ B_y & -B_x & 0 \end{pmatrix} \begin{pmatrix} M_x \\ M_y \\ M_z \end{pmatrix} = \begin{pmatrix} I_x & 0 & 0 \\ 0 & I_y & 0 \\ 0 & 0 & I_z \end{pmatrix} \begin{pmatrix} \dot{\phi} \\ \dot{\theta} \\ \dot{\psi} \end{pmatrix} + \omega_0 \begin{pmatrix} 0 & 0 & I_y - I_z - I_x \\ 0 & 0 & 0 \\ I_z + I_x - I_y & 0 & 0 \end{pmatrix} \begin{pmatrix} \dot{\phi} \\ \dot{\theta} \\ \dot{\psi} \end{pmatrix} + \omega_0^2 \begin{pmatrix} (I_y - I_z)(4 - 3\omega_0^2) & 0 & 0 \\ 0 & (I_x - I_z)(3 - 3\omega_0^2) & 0 \\ 0 & 0 & (I_y - I_x) \end{pmatrix} \begin{pmatrix} \phi \\ \theta \\ \psi \end{pmatrix} \quad (1)$$

For more details of system dynamics equations please refer to the Appendix section. The above equation can be written in compact form as,

$$M \ddot{q} + G \dot{q} + K q = \hat{B} M \quad (2)$$

Now,  $M$  is positive definite symmetric

$G$  is skew symmetric,

$K$  is positive definite symmetric

Hence for damping the motion we need to add a term like  $C \dot{q}$ . Let us apply magnetic moment according to the formula,

$$M = \alpha B \times \dot{q} = \alpha \hat{B} \dot{q} \text{ and } \hat{B}^T = -\hat{B}, \text{ since } B \text{ is skew-symmetric matrix}$$

$$\therefore B \times M = \hat{B} M = \alpha \hat{B} M = -\alpha \hat{B} \hat{B}^T \dot{q} \quad (3)$$

Substitute (3) in (2),

$$M \ddot{q} + (G + \alpha \hat{B} \hat{B}^T) \dot{q} + K q = 0$$

Now,  $\alpha \hat{B} \hat{B}^T > 0$ , since  $B$  is skew-symmetric and gain  $\alpha > 0$

$$\text{Therefore, } (G + \alpha \hat{B} \hat{B}^T) > 0 \quad (4)$$

Hence, we expect to obtain better damping of the oscillations using the above control law

The stability of the system for above control law can be proved by following Lyapunov analysis,

$$\text{Consider a candidate Lyapunov function, } V = \frac{1}{2} \dot{q}^T M \dot{q} + \frac{1}{2} q^T K q$$

$$\begin{aligned}
\dot{V} &= \dot{q}^T M \ddot{q} + q^T K q \\
&= q^T \{ = q^T [-(G + \alpha \hat{B} \hat{B}^T) q - K q] + q^T K q \\
&= -q^T (G + \alpha \hat{B} \hat{B}^T) q \\
&< 0 \quad \text{for } q \neq 0
\end{aligned}
\tag{from (4)}$$

Thus, the above control law imparts Lypunov stability to the system

### 5.5.2 Other important issues

The other important issues that we need to tackle in good controller design are,

- 1) Control saturation: The power required by the magnetorquer to implement the control required may be large than the power available at certain instants. In other words there is saturation of the control effort. This causes non-linear behaviour of the system and deteriorates the performance from what is required. Hence, this issue needs to be taken care of and proved that the controller works good even under such situation
- 2) Time Delays: The time delay between the reading of a sensor and its implementation by the actuator can be of serious consequences. This can be studied and taken carof by doing hardware in loop simulations.
- 3) Imperfection in modeling and parameter uncertainty: These are two other effects know to deteriorate the performance of the system form the ideal. We need to study the robustness of the system for these parameters.

## **Chapter 6: On Board Computer**

The On Board Computer of the IITB Student Satellite can be divided into the following major categories: Hardware, Software and Data.

### **6.1 Hardware**

The exact hardware to be used on the On Board Computer (OBC) was decided after a detailed analysis of various similar components that go into building a small scale computer. While choosing each specific part many factors were taken into consideration to ensure that it was best suited for our purpose.

#### **6.1.1 Microcontroller**

The microcontroller is like the brain and heart of the satellite. It performs all the operations that are needed for the functioning of a satellite.

While deciding the microprocessor that was going to be used on our satellite, we looked at the various microprocessors which were used in various student satellites or were in very common use. These microprocessors were narrowed down based on information available at that time about their use on board similar satellite systems and their radiation hardness testing.

We analyzed processors of various families, architectures and manufactures having a varied range of properties.

List of microprocessors studied:

iii. Freescale (Motorola) MMC2001

iv. Intel X86:

1. 8051
2. 80C186EC
3. 80188
4. 80386
5. 80960
6. 486

v. Other Intel SA1110

vi. Atmel

1. AT32AP7000
2. AT91M40800

- 3. 80C32E
- vii. Philips P89V51RD2
- viii. MIPS V850,NEC
- ix. Hitachi SH709A
- x. Siemens C167CS
- xi. Microchip
  - 1. PIC16F877
  - 2. PIC16C77

These processors were compared to each other with respect to various characteristics like:

1. Tested for radiation hardness
2. Tolerant to space temperatures
3. Low power consumption
4. Support for ecos OS(we were looking at ecos at that time)
5. Processing Power (MIPS)
6. Number of pins
7. EDAC and watchdog timer
8. Presence of ADC's

After some analysis on the various processors, we short listed the following microprocessors:

Intel 80C186EC

Intel 80386

Atmel AT91M40800

Hitachi SH7709A

Amongst the four microprocessors shortlisted above, the latter three are 32 bit microprocessors while the 80186 is a 16 bit processor. It was preferred to have a 32 bit architecture for our satellite. The reason for this was that eCos has been extensively tested on 32 bit architectures that are supported by gcc.

Hence we ruled out the 80186 processor. Our next logical choice was the i386 processor since we know that it was a very widely used processor and hence would be well-documented.

However, its power consumption was high compared to the alternatives. Also there was unclear documentation as to whether it is suitable for using in space.

That left us with the SH7709A and the AT91M40800. The AT91M40800 chip has already been used by another student satellite. Looking through the table we can see that it has very nice characteristics as required by us. Thus it was an ideal choice.

The SH7709A on the other hand was less documented and was not used in space earlier. Also, it had 204 pins in a Ball Grid Array. This is a number far more than needed and would lead to unnecessary design complications. It provided the same MIPS at a much higher power consumption than the AT91M40800.

So after an analysis of the various processors available we reached a conclusion of using the AT91M40800 microcontroller as the main microcontroller on board our student satellite.

Name of the parameter	Power / Voltage = Current(10)	Temperature Range(8)	Availability(8)	Radiation Tolerance in Krads(8)
Ideal Value	1W/5V	-40 C to 80 C	From Lamington	5 Krads
<b>MicroController Name:-</b>				
<b>Freescale(Motorola)</b>				
MMC2001	40mW			
<b>Ancient Intel</b>				
intel 8051	0.8W / 5v	0 to 70c		
Intel 80C186EC	6.5V	-65 to 100		8 Krads
Intel 80188	3W / 7V	0 to 70C		
Intel 80960	mA)*3.3 / 3.3v	-65 to 110 C		
Intel 486(lowpower)	) / 3.3(4.5)v	-65 to 110 C		
<b>Other Intel</b>				
SA 1110	mW/3.3V	0 to 70C		
<b>Atmel</b>				
AT32AP7000	z / 3.3V	-40 to 85 C		--
AT91M40800	3.6V			
80C32E rad hard	1W / 5.5V	-55 to 125 C		30kRads
<b>Philips</b>				
P89V51RD2		-40 to 85		hence skipped
<b>MIPS</b>				
V850,NEC	50 mW			
<b>Hitachi</b>				
SH7709A	(~200mW)			unknown
<b>Siemens</b>				
C167CS	(0.1 to 0.5 W)	+85(+125)	???	unknown
<b>Microchip</b>				
PIC16F877	4.5-6V(20mW)	+85(+125)	???	>5krad
PIC16C77	4.5-6V(20mW)	+85(+125)	???	>5krad

Name of the parameter	EDAC and Watch-Dog Protection(8)	Internal RAM	Number and Placement of Pins(5)	Ready Availability of C compiler(3)
Ideal Value		300 gm		Free
<b>MicroController Name:-</b>				
<b>Freescale(Motorola)</b>				
MMC2001			144(30)	
<b>Ancient Intel</b>				
intel 8051		addressable RAM 40(4*8)		
Intel 80C186EC	Watchdog		100 QFP	
Intel 80188				68
Intel 80960	no			132
Intel 486(lowpower)	no			176
<b>Other Intel</b>				
SA 1110	Watchdog		256 BGA	
<b>Atmel</b>				
AT32AP7000	Watchdog		100 TQFP(32)	studio)
AT91M40800	Watchdog		100 TQFP(32)	studio)
80C32E rad hard	good		40/44 (32io)	studio)
<b>Philips</b>				
P89V51RD2			44/40(32 I/O)	
<b>MIPS</b>				
V850,NEC				gcc
<b>Hitachi</b>				
SH7709A	watchdog	present	count) QFP	
<b>Siemens</b>				
C167CS	watchdog	ROMLess	144(111 I/O) QFP	15 day trial
<b>Microchip</b>				
PIC16F877	Watchdog	on board RAM	or 28 DIP	ly free)
PIC16C77	Watchdog	K ROM	DIP	ly free)

### 6.1.1.1 AT91M40800 Core

The AT91M40800 contains an ARM7TDMI core. The ARM7TDMI core is a member of the ARM family of general-purpose 32-bit microprocessors. The ARM family offers high performance for very low power consumption, and small size. The ARM architecture is based on *Reduced Instruction Set Computer* (RISC) principles.

The ARM7TDMI core uses a pipeline to increase the speed of the flow of instructions to the processor. This allows several operations to take place simultaneously, and the processing and

memory systems to operate continuously. A three-stage pipeline is used, so instructions are executed in three stages:

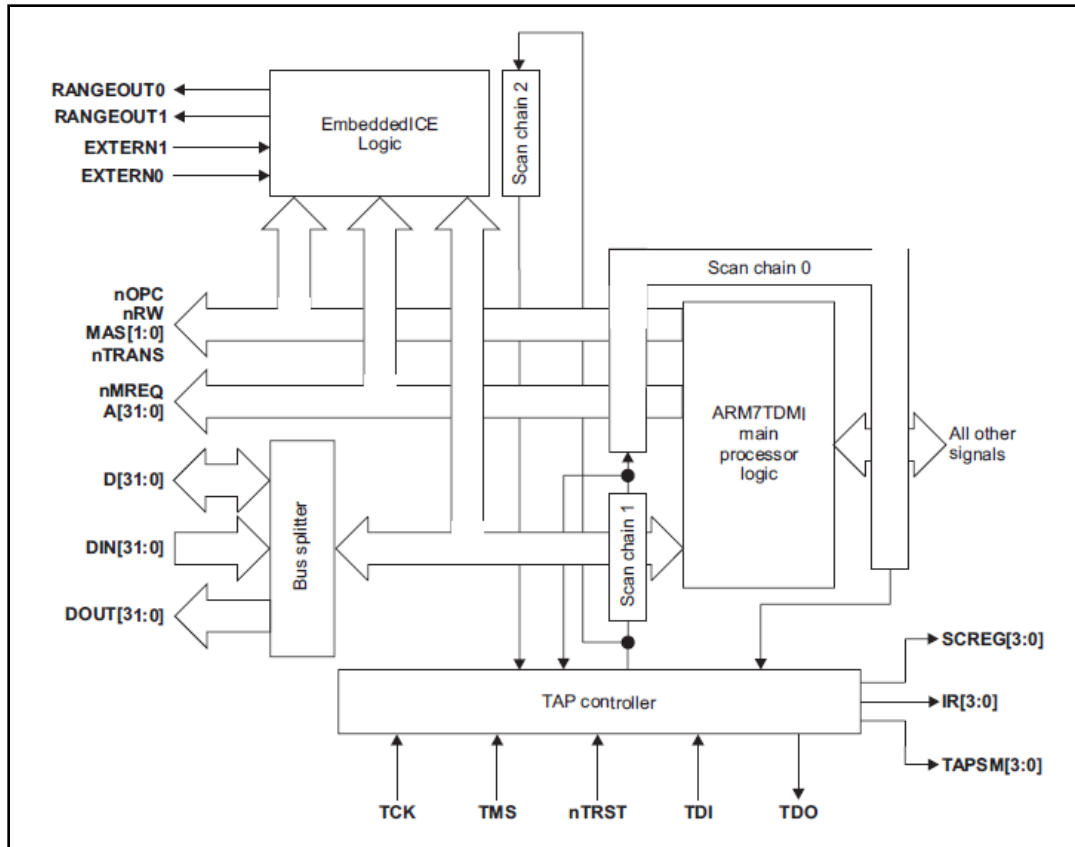


Figure 6. 1: 3 stage pipeline

- Fetch
- Decode
- Execute.

Memory access in the ARM7TDMI core has Von Neumann architecture, with a single 32-bit data bus carrying both instructions and data. Only load, store, and swap instructions can access data from memory.

Data can be:

- 8-bit (bytes)
- 16-bit (halfwords)
- 32-bit (words).

Words must be aligned to 4-byte boundaries. Halfwords must be aligned to 2-byte boundaries

The ARM7TDMI processor memory interface has been designed to allow performance potential to be realized, while minimizing the use of memory

The ARM7TDMI core has four basic types of memory cycle:

- idle cycle
- nonsequential cycle
- sequential cycle
- coprocessor register transfer cycle.

EmbeddedICE Logic is the additional hardware provided by debuggable ARM processors to aid debugging. It allows software tools to debug code running on a target processor. The EmbeddedICE logic is controlled through the *Joint Test Action Group* (JTAG) test access port, using the EmbeddedICE interface.

The ARM7TDMI processor has two instruction sets:

- the 32-bit ARM instruction set
- the 16-bit Thumb instruction set.

#### 6.1.1.2 Radiation Hardening

This particular microprocessor has been tested for radiation hardening. Though it has not been manufactured with the intent of making it space grade, it has been tested by DTUSAT-I for radiation levels upto 10 kRad/s.

This was an important factor in helping us decide this microprocessor for the OBC.

#### 6.1.1.3 ECOS Support

The AT91M40800 has a 32 bit Architecture. We were looking at the ecos operating system at that time and it was ported to this microprocessor (there is an evaluation board available for a very similar(pin identical) microprocessor and ecos has been sucessfully ported to the chip used on the evaluation board namely AT91EB40.)

We preferred eCos because of reasons given in the software section.

#### 6.1.1.4 Low Power

It accepts input voltage levels from 1.8 to 3.6volts. Ideal operating voltage is 3.3v. Its input-output pins are also 5V tolerant.

Compared to other microprocessors the ratio of the computational power to the power consumed for this microprocessor was very high. It consumes power from 1 mW/MHz(idle) to 4.6mW/MHz(writing to memory – maximum power consumed).

This falls well within the total power supplied to the OBC from the power budget(1.5W)

It also has a Power Saving(PS) Mode in which it is in idle state and consumes very little power.

The power-saving (PS) module implements the Idle mode (ARM7TDMI core clock stopped until the next interrupt) and enables the user to adapt the power consumption of the microcontroller to application requirements (independent peripheral clock control).

The clock of each peripheral integrated in the AT91M40800 Series can be individually enabled and disabled by writing to the Peripheral Clock Enable and Peripheral Clock Disable Registers. The status of the peripheral clocks can be read in the Peripheral Clock Status Register. When a peripheral clock is disabled, the clock is immediately stopped. When the clock is reenabled, the peripheral resumes action where it left off. To avoid data corruption or erroneous behavior of the system, the system software only disables the clock after all programmed peripheral operations have finished. The peripheral clocks are automatically enabled after a reset.

#### 6.1.1.5 Computing Power and Speed

It can be operated at internal frequencies up to 40 MHz safely. It has a rich instruction set of the ARM7TDMI core. It has 100 pins with 32 configurable I/O pins.

It functions at approximately one million instructions per second per MHz. Thus its peak performance is 40 mips. This is more than sufficient for our purposes.

Interrupt controller:-

The AT91X40 Series has an 8-level priority, individually maskable, vectored interrupt controller. This feature substantially reduces the software and real-time overhead in handling internal and external interrupts.

### 6.1.1.6 Memory

*Analysis of maximum memory possible and the AT91M40800 multiplexing issue*

The chip select CS4, CS5, CS6 and CS7 pins are multiplexed with pins the address select pins A20, A21, A22, A23.

Data Redundancy is maximum for maximum number of chips. As such only following maximal modes are allowed. Due to low availability of power during start-up we have decided to load our mission critical programs into a flash and due to high density of data move thermopile data into SRAM. Thus remapped memory detail are provided here:

Total number of chips	Memory for Programs and Housekeeping	No of Flash chips	No of SRA chips	State of pins	Max size of chip	Size of SRAM	Total implemented memory	Memory Layout
1	2 MB	1	0	A20 A21 A22 A23	16 MB	0 MB	2 MB	2(F)
2	2 MB	1	1	A20 A21 A22 A23	16 MB	16 MB	18 MB	2(F)+16(S)
3	2 MB	1	2	A20 A21 A22 A23	16 MB	32 MB	34 MB	2(F)+[16+16](S)
4	2 MB	1	3	A20 A21 A22 A23	16 MB	48 MB	50 MB	2(F)+[16+16+16](S)
5	2 MB	1	4	A20 A21 A22 CS4	8 MB	32 MB	34 MB	2(F)+[8+8+8+8](S)

6	2 MB	1	5	A20 A21 CS5 CS4	4 MB	20 MB	22 MB	2(F)+[4+4+4+4+4](S)
7	2 MB	1	6	A20 CS6 CS5 CS4	2 MB	12 MB	14 MB	2(F)+[2+2+2+2+2+2](S)
8	2 MB	2	6	CS7 CS6 CS5 CS4	1 MB	6 MB	8 MB	2(F)+[1+1+1+1+1+1](S)

#### 6.1.1.7 Availability

The AT91M40800 is in current production and be purchased (imported) from various vendors on the internet like:

1. <http://sales.digikey.com/>
2. <https://www.em.avnet.com/>
3. <http://www.onlinecomponents.com/>

There is a company-provided evaluation board for a similar pin-compatible microprocessor namely the AT91M40008. The difference between these two processors is only in terms of the internal memory and power. The 400008 consumes more power and is untested in space.

We have purchased this programmer board and have analyzed its hardware and also tested programs on it.

We are planning to make an engineering board based on the following schematic. This schematic was obtained on the web and was slightly modified for our purposes. All of our software development will take place on this board.

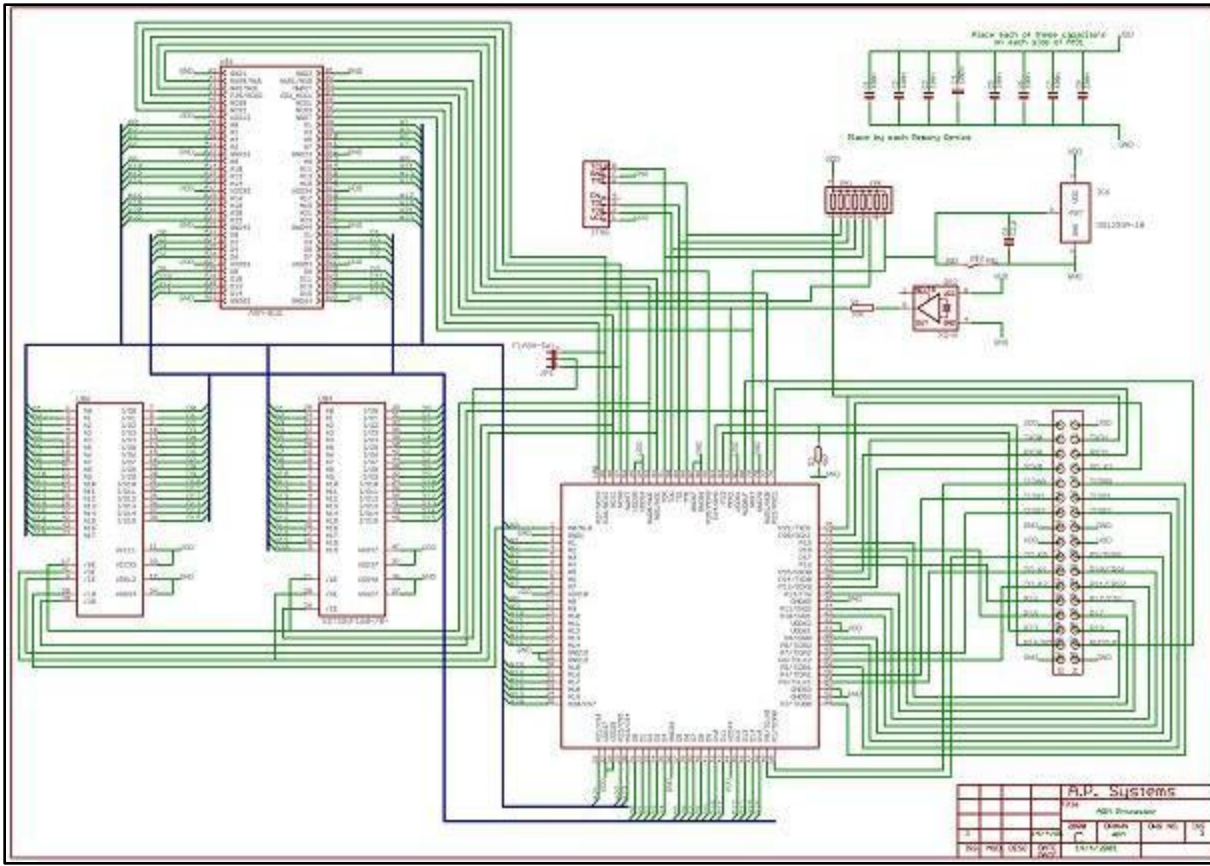


*Figure 6. 2: Microcontroller Board*

Along with this, we have designed the following schematic for the JTAG circuit for the board above, as shown in Fig 6.3.

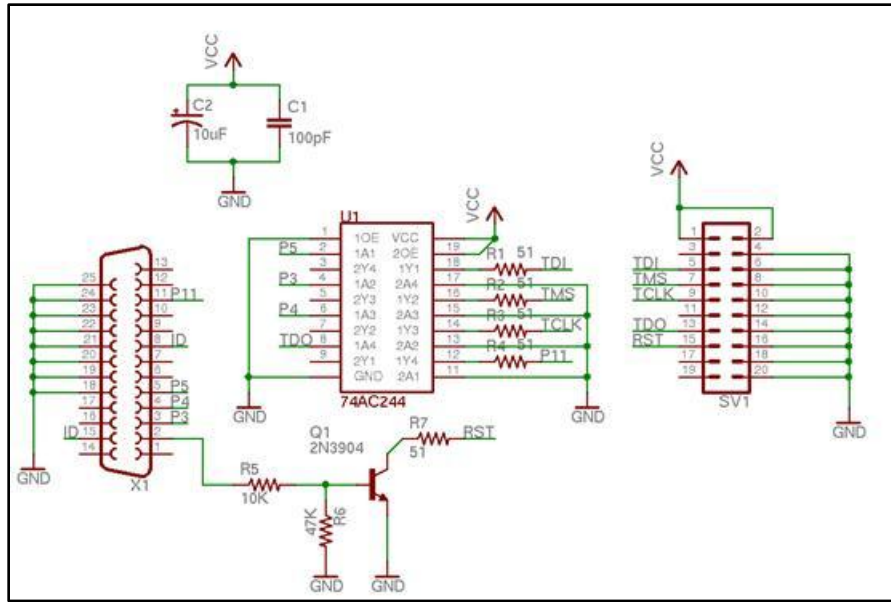


Figure 6. 3: JTAG circuit

#### 6.1.2 SRAM chips

Static Random Access Memory (SRAM) chips will be used to store most of the data on board the satellite. We had done an analysis of many SRAM chip manufacturers including

1. Samsung
2. SuperTalent
3. Glink
4. Alliance
5. AxPRO
6. ISSI
7. IXYS

We compared the chips under consideration with respect to many factors such as

1. Supply voltage (compatibility with uc)
2. Power Consumption
3. Active and Idle currents
4. Temperature Tolerance

We had finally narrowed down to a Samsung SRAM chip of 512 kb size.

However due to recent developments of the payloads team, the data requirements of the satellite have increased greatly. Therefore we require SRAM chips having higher data capacities. They

must be able to store data of upto 8Mb of 116 Mb. So an analysis of SRAM chips available in this data rage is going on and we will soon narrow down on the exact chip to be used in our satellite.

Data requirements are chose to 16MB (without redundancy). So we will be looking for actual data storage capacity in excess of 24 MB.

We may also store data of experiments in Flash chips( not yet finalize))

Although the sizes of the SRAMS below are in Kb , they are representative of the family of chips. Hence, we will eventually go for a chip of the same family but with the size as required by the payloads.

Name of the parameter	Name	Supply Voltage	Size	Availability
Ideal Value		5V	512 KB	From Lamington
<b>RAM Manufacturer</b>				
Samsung	K6F8016V3A	3.0-3.6	1 Mb	--
Samsung sure)	K6T4016V3B	3.0-3.6	512 kb	--
Glink	--	--	--	--
Glink	GLT6400M16	2.2-2.7	128 kb	--
Brilliance	GLT6400M08	2.2-2.7	256 kb	--
Alliance	BS62XV4000	1.2-2.4	512 kb	--
AXPRO	AS6VA25616	2.7-3.3	512 kb	--
ISSI	L	1.65-1.95	512 kb	
IXYS	PDM31096LL	3.0-3.6	512 kb	
IXYS-2	PDM21096LL	2.4-3.0	512 kb	
Alliance 2	7C254096LL	2.3-3.0	512 kb	

Name of the parameter	Temperature Range	Price	Active and Standby Current	Power Dissipation	No of Pins
Ideal Value	Yes			???	
<b>RAM Manufacturer</b>					
Samsung	-40 - 85	\$13	4 mA/.5uA	--	44
Samsung sure)	0 - 70 / -40 - 85		\$13 60 mA/15 uA	--	--
Glink	--	--	--	--	--
Glink	-40 - 85	--	15 mA/5 mA	--	44
Brilliance	-40 - 85	--	15 mA/5mA	--	32
Alliance	-40 - 85	--	15 mA/25 uA	--	
AXPRO	-40 - 85			mW/66mW	44
ISSI	-40 - 85		36mA/9uA		44
IXYS	--			65 mW	32
IXYS-2				65 mW	32
Alliance 2				90 mW	34

### 6.1.3 FLASH chips

This chip will be used to store all the programming data that is used to run the satellite. This will include all the Operating System data and certain other permanent data. We will be using flash chips for this purpose and not SRAM chips as most probably the satellite will be in the OFF state(without power) during the launch and SRAMs require continuous uninterrupted power to store data.

The size required for this chip will around 1 to 2 Mb.

We have narrowed down on a Spansion Flash chip S25FL032A.

Other chips under consideration are from STM Microelectronics, if we decide to store the entire data on flash as they provide higher data density data chips

### 6.1.4 ADC

Data that we get from the thermopiles will be of the analog type. We need to convert this data to the digital format for our microcontroller to analyze it. The AT91M40800 does not have in built ADC's. Therefore, we did a study of various Analog to Digital Convertors (ADCs).

We looked for ADC's that satisfied the following requirements:

1. 10 bit (size of data from thermopile)
2. Multiple channel
3. Radiation hardened(or tested)
4. Right operating voltage
5. Low power consumption

We are currently looking at the following ADC's:

4. ADS 7816
5. MAX 1248
6. MAX 117

The exact choice is MAX 1248 although we may use the other ADC's if need arises due to availability problems.

#### 6.1.5 Location of Hardware Components and the Main Board

Most of the hardware components will be located on a single board

Characteristics of the board

- Size
- Weight
- Number of components

Based on the analysis that we made on the evaluation board that we bought, we are finalizing the details of the actual PCB that will be used on the satellite.

The board should be located somewhat centrally and closer to where the various interfaces- (communication, experiments, controls, power, housekeeping) are.

A separate board will be required for the ADC's which will be located very close to the thermopiles. This board will be then connected to the main board via an interface. The ADC board should be appropriately magnetically shielded to prevent data corruption.

Components to be placed on the Main Board

1. AT91M40800
2. Interface connectors
3. Memory components(Flash And RAM)
4. Many resistors and capacitors.

## 6.2 Software

### 6.2.1 Need for an operating system

The satellite is an embedded system which must function with real time accuracy. As such it is essential for the software implementation to ensure that all tasks be completed within their specified time duration and that they meet their task deadlines. At the same time it is also not necessary that all tasks have the same priority. In such a scenario a complex multi-level multi-tasking system must be implemented.

Thus we will need some form of multi-tasking whether we use an operating system or not. Along with this, we will also need a memory management system. For having both of these functionalities it is better to use a pre-built tested operating system. With this in mind we have chosen to use a well-documented operating system.

#### 6.2.1.1 List of Interfaces connected to the Onboard computer

Consider the entire OBC system as a black box. A list of the interfaces to this black box is given below :-

Inputs:	Outputs:
Control System Inputs	Communication – DataLink
Payload – Datalink	Launch Vehicle Interface
Payload – Housekeeping	Magnetorquer - Control
Power systems – Housekeeping	

Along with this large number of interfaces it must be noted that the type of interface and the protocol used on each interface varies widely from task to task.

#### 6.2.1.2 List of Computational Tasks for the Onboard Computer

The nature of the computational tasks expected from the onboard computer also varies widely. A brief list of tasks follows:

- i. Implementation of an attitude control algorithm maximizing a combination of power generation and data gathering.
- ii. Implementation of a suitable error detection and correction scheme to ensure lossless transmission of data.

- iii. Effective storage of thermopile experiment data.
- iv. Maintaining a record of Current, Voltage and Power consumption housekeeping data from various sub-systems.
- v. Maintaining a record of thermal environment housekeeping data
- vi. Generation of suitable of suitable active control pulse for after processing of attitude control algorithm
- vii. Maintaining the state of the satellite depending upon the power situation
- viii. Implementation of Watch-Dog timer

Most of the house keeping is highly time critical as further decision making is dependent upon it.

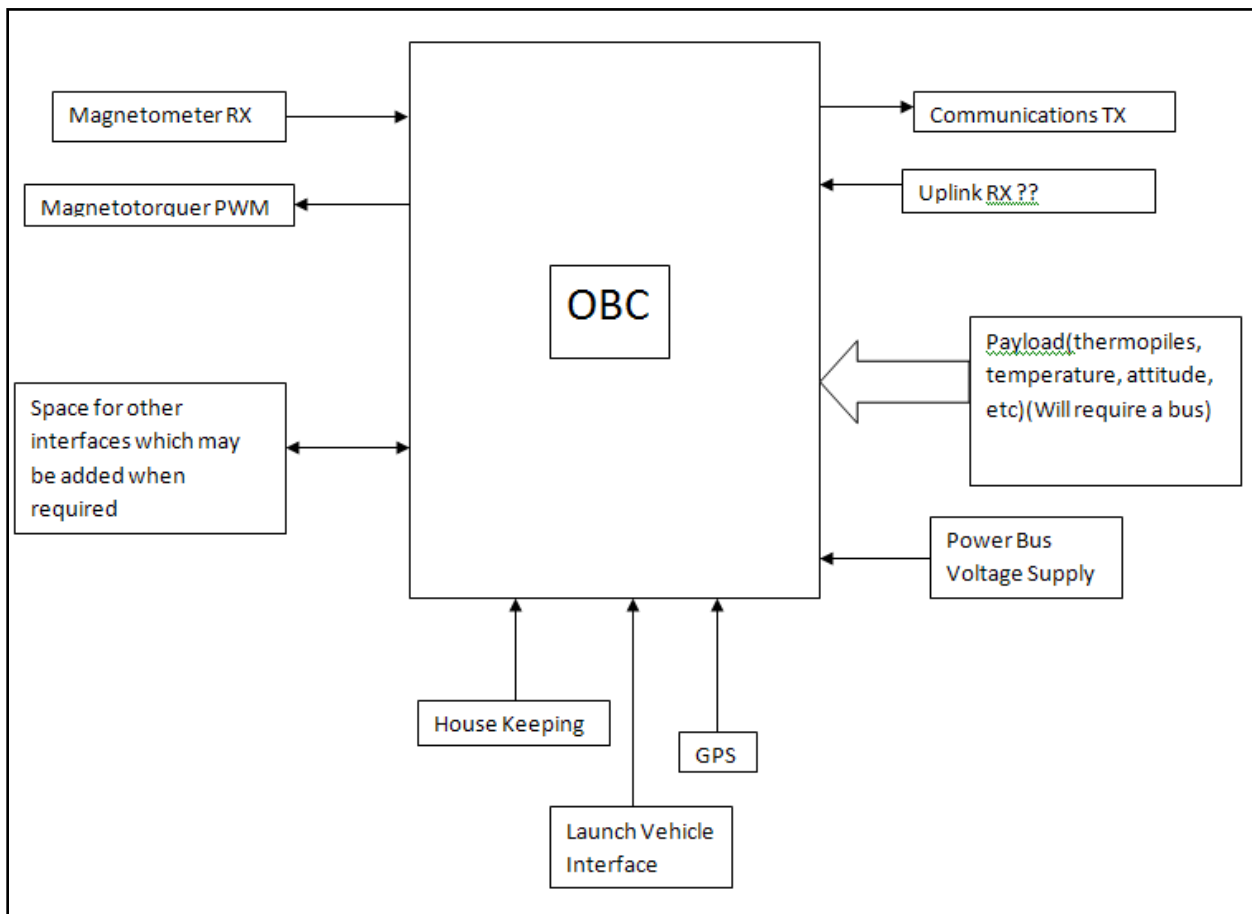


Figure 6. 4: Level 0 Abstraction of the OBC system

#### 6.2.1.3 Other factors

There are two other factors which have led to selection of a pre-built Operating System vis-à-vis developing our own control software:

#### 6.2.1.3.1 Reliability of Software

Development of an operating system is a complicated affair. In this context one must note that the primary reason for implementing an operating system was to reduce point of fault creating amore reliable system. Development of our own operating system seems to nullify this very advantage

#### 6.2.1.3.2 Time Constraint

Also with need for development of such large amount of application software, creating an OS is an unnecessary burden on our resources.

### 6.2.2 Operating Systems

Before we discuss about our method selection of an operating system we consider a few facts about operating systems.

#### 6.2.2.1 Process management

When more than a single process must be executed simultaneously, there must be a specific procedure to implement the sharing net system resources. As such most operating systems implement a process queue and a scheduler. Depending on the how the scheduler implement sharing of these resources operating systems can be classified into Pre-emptive and cooperative.

##### 6.2.2.1.1 Cooperative operating system

In cooperative operating systems every process must give up control of the processor before the scheduler can assign the system resources to another task. Cooperative operating systems are simpler; however it is very difficult to ensure that all processes get an equal time slice. Also in a cooperative set up it interrupt handling becomes very complicated

##### 6.2.2.1.2 Pre-emptive operating systems

In pre-emptive operating systems the scheduler assigns fixed time slices to each process. As such almost all processes get a time slice depending upon their priority. Also in the case that a process must wait for an external input to continue computation, the scheduler can wrest control from the process to increase efficiency. In case of an application failure a co-operative will hang and one must wait till a watch dog timer reset for further operation. In a pre-emptive OS only the portion

time allocated to that specific process remains unfulfilled and hence the entire system continues to remain operational.

#### 6.2.2.2 Memory management

It is essential that the memory space addressed by each application be distinct. Otherwise conflicting addressing can lead to data corruption. It is the task of the OS to implement this context switching. Also paging of available memory and virtual addressing of external memory peripherals can be efficiently done with an operating system.

#### 6.2.2.3 Interrupt handling

In real time operations exception handling is mainly accomplished through a hierarchy of external hardware interrupts. For example, a very basic check of the onboard computer integrity can be ensured through a watchdog timer. It is essential that a correct and timely action with respect to these events be taken. This can be very easily accomplished using an operating system.

### 6.2.3 Selection of Operating System

The following criterions were decided upon while selecting an operating system.

#### 6.2.3.1 Must have multi threading support

The large list of tasks to be accomplished using the OBC makes it essential that the system have the ability to simultaneously execute more than one task. The simplest way to implement this is multi-threading and hence it is desirable for our operating system to support it.

#### 6.2.3.2 Must have low memory and computational requirements

A high memory requirement cited by the payload team as well as significant house-keeping tasks necessitates that resources consumed by the operating system should be very low. In particular our memory requirements from the OS were very stringent not allowing more than 512kB of memory.

#### 6.2.3.3 Must be compatible with our architecture

The processor that has already been finalized on the basis of other considerations is the Atmel AT91M40800 with an ARM7TDMI core with a RISC instruction set. We need our operating system to support the ARM architecture.

#### 6.2.3.4 Pre-emptive

It was decided for safety reasons that the operating system should be pre-emptive so as to reduce points of failure.

#### 6.2.3.5 Very little porting should be required

Even though the architecture may be supported, it was also decided to ensure that the OS was pre-ported to this specific micro-processor or a very close variant. This enables to both use our time resources more efficiently and also makes the system more robust.

#### 6.2.3.6 Free Software

In order to identify any fault in coding it is very convenient to have the source code of the operating system to be available. As such higher preference is given to a free OS as compared to proprietary operating system

#### 6.2.3.7 Documentation

In order to ensure quick and easy identification and correction of bugs, it is essential that the operating system be well documented. This also helps in ensuring that we apply standard solutions and do not end up re-inventing the wheel.

#### 6.2.3.8 Experience

All OBC team members have sufficient experience coding in a gcc environment. As such it was decided that the operating system should be based on a ported gcc toolchain such as the arm-elf toolchain.

### 6.2.4 Comparison of various Operating Systems

Below is a table comparing some of the operating systems that we included in our literature survey.

Operating System	uClinux	eCos	Phoenix RTOS*	Free RTOS	SALVO
Multi Threading	Y	Y	Y	Y	Y
Low Resources	N	Y	Y	Y	Y

ARM compatible	Y	Y	Y	NA	Y
Preemptive	Y	Y	NA	NA	N
Porting (Effort Reqd)	High	Low	High	Medium	Low
Free	Y	Y	Y	Y	N
Documentation	N	Y	N	NA	Y
Experience	N	Little	N	N	Y

Notes: \*Phoenix RTOS was the project of some professor and hence its reliability is doubted

From the above comparison one can see that the two major choices for an operating system are eCos and SALVO.

#### 6.2.4.1 eCos vs. SALVO

The original choice for the operating system was eCos. However during initial implementation stages there were several factors which led us to choose a simpler operating system for testing purposes.

- a) Non availability of the evaluation board for the final processor.
- b) Inability to install eCos on either a Linux or Windows machine.

As such for prototyping some sample application SALVO was chosen. SALVO was found to be very well documented. At the same time it proved to be very easy to implement. In addition to this support for the ARM architecture led us to select SALVO for the final satellite.

However SALVO being a cooperative OS it became necessary to implement external timers or FPGAs for time critical application. This led to a great increase in the system complexity.

#### 6.2.4.2 SALVO

Salvo was an Operating System which was very well documented. Therefore we decided to study it and its implementation.

We successfully managed to compile it and write various programs on it to do various tasks on an ATMEGA16 (a microprocessor which we were very familiar with). This taught a lot of useful implementation about how OS's work and how to program them.

However, due to its cooperative nature, it would not be able to provide the exact timing required to take the data from experiments therefore we were inclined against it.

At the same time two new developments have shifted the focus back eCos.

1. The AT91EB40a application board became finally available.
2. We were able to get eCos running after slightly modifying its install procedure.

As such we have finally decided to implement eCos as our operating system.

### 6.2.5 Implementation of eCos

This is the detailed of the steps involved in the implementation of eCos. We have selected a windows based installation because of the availability of the eCos configuration tool with a GUI. It has been observed from our own observation that the windows configuration tool does not perform well in a debian based graphic environment. The corresponding command line tool requires knowledge of CDL scripting language and conflict resolution in the command line version is notably difficult.

#### 6.2.5.1 Pre-requisites for eCos (Windows based installation)

1. Windows XP or higher
2. Cygwin bash shell with the following components
  - a. gcc
  - b. make
  - c. shareutils
  - d. tcltk
  - e. wget

Additionally d2u, a dos to unix file converter and bzip are also suggested.

#### 6.2.5.2 Step by step procedure to install eCos

The first two steps of this procedure are endorsed by eCosCentric at <http://ecos.sourceforge.org/getstart.html>. The last two steps are mostly my own invention after surveying the build and run time errors and reading some posts at the Redhat mailing lists (<http://sources.redhat.com/ml/ecos-discuss/>). It is possible that much more elegant solutions exist

##### 6.2.5.2.1 Installing the cygwin bash shell

- a. Install the cygwin bash shell with the above components in UNIX line ending mode
- b. Start the cygwin bash shell and navigate to /opt/ecos creating it if necessary

#### 6.2.5.2.2 Downloading the ecos source files

- c. Type the following command at the bash shell:

```
wget --passive-ftp ftp://ecos.sourceforge.net/pub/ecos/ecos-install.tcl
```

- d. Type the following command at the bash shell:

```
sh ecos-install.tcl
```

- e. Configure the proxy if any

- f. Select the /opt/ecos location for install

Note: The above is a POSIX path

- g. Select any of the given mirrors

- h. Select the arm-elf tool chain and press q.

Note: One can also compile the tool chain oneself

#### 6.2.5.2.3 Modifying the default installation for compatibility

- i. After completion of the download run the following commands:

```
d2u ecos-2.0/ecosenv.sh
```

```
./ecos-2.0/ecosenv.sh
```

- j. Go to the <http://www.ecoscentric.com/devzone/configtool.shtml> and download the eCos Configuration Tool version 2 for Windows (2006-07-10) archive to c:\cygwin\opt\ecos

- k. Do not unrar it using WinRAR or any other native windows utility

Go to the cygwin bash shell and type

```
bunzip2 configtool*.bz2
```

- l. Do not access the configtool using a windows file manager. Instead run it using the cygwin command line interface.

- m. Set the eCos source repository as follows c:\cygwin\opt\ecos\ecos-2.0

- n. Run following command at cygwin bash shell

```
mount -tf c:\\ /ecos-c/
```

- o. You may optionally also need to add /opt/ecos/gnutools/arm-elf/bin to the PATH\$ variable if the ecosenv.sh script fails as it did in my case.

#### 6.2.5.2.4 The After Effects of this modified install

- p. You can run the graphic configtool only after invoking it from the bash prompt

- q. You can save .ecc files from the configtool in any location you want.

- r. There is a high probability that the shift+F7 build from the configtool will fail  
In this case follow the following method.
- i. Let the configuration file be foo.ecc and be stored in c:\cygwin\opt\foofolder
- ii. Type the following commands at the bash under /opt  
 cd /foofolder/foo\_build  
 make build

## 6.3 Data

### 6.3.1 Size of Data

No. of Thermopiles = 50

Rate at which Data is Taken = 1 per 4 sec = 0.25 per sec

Data per Thermopile = 10 b

Net data collected per day =  $50 \times 10 \times 86400 / 4 \text{ b}$

$$= 41 \text{ Mb} / 4$$

$$= 10.25 \text{ Mb}$$

$$= 1.28125 \text{ MB}$$

$$= 1.3 \text{ MB}$$

Accounting for EDAC codes = 2.6 MB(roughly)

Temperature sensors = 5

Rate = 1 every 10 sec

Data per temp sensor = 10b

Net Data for temperature =  $5 \times 10 \times 8640$

$$= 0.41$$

$$=.05 \text{ MB}$$

Other upkeep max 1 MB

Net requirement for other tasks = 2 MB

Degradation factor = 2

Net Size =  $(2.6 + 2) \times 2 = 9.2 \text{ MB}$

No. of passes per day = 1/2 (Worst case scenario)

Assumption all data can be down-linked in this one pass

Approximate size of data around 10 MB

Based on the total data the exact storage medium will be decided. That is, flash or SRAM and their exact values. Other factors that need to be taken into consideration while doing this are the limitations of the microprocessor.

### 6.3.2 Error Detection and Correction

There are essentially two tasks where Error Detection and Correction (EDACs) needs to be applied:

- Communication with ground station; and
- Storage and retrieval of data on-board the satellite.

The following EDACs were considered:

1. Parity Checksum(Error Detection only)
2. Hamming Codes
3. CRCs with Reed Solomon
4. CRCs with Reed Muller Codes
5. LDPC Codes(Error Correction)

The major things to look into while selecting the codes to be used for error detection and correction are as follows:

- Channel burst error probabilities, deletion probabilities, erasure probabilities, bit flip probabilities. It is important to find out which of these kinds of error do occur.
- RAM read/storage error probabilities.
- Real time encoding and decoding. For this purpose, we need to choose codes that have low encoding/decoding complexity.

The various options considered along with their advantages and disadvantages are as follows:

### 6.3.2.1 Parity Checksum

This is implemented by concatenating the binary sum of the digits of the word with it. This can be used for error detection only.

Advantages:

- Very easy to implement.

Disadvantages:

- Can detect only odd number of errors and hence useful only for single error detection.
- No way for correcting the errors.
- Useless in case of burst errors.

### 6.3.2.2 Hamming Codes

They are essentially parity-check codes. Used for single error correction and up to 2-bit error detection in a word.

Advantages:

- Self correcting: If a single bit in the word gets flipped, it can be corrected.
- Easy to implement.

Disadvantages:

- Detect only up to two errors, can't correct burst errors.
- Lead to bloating of data by large amounts and hence can't be used in communication due to small bandwidth, time of contact.

### 6.3.2.3 Cyclic Redundancy Check (CRC)

These are very commonly used error detection codes.

Advantages:

- Efficiently detect errors.
- Do not bloat data too much.

Disadvantages:

- Only detect errors, but can be coupled with other error correction codes.

### 6.3.2.4 Reed Solomon Codes

Advantages:

- Very efficient codes and hence do not increase data much.
- Can be used with CRCs.
- Can correct burst errors.

Disadvantages:

- Difficult implementation.
- They take large computation time.

#### 6.3.2.5 Reed Mueller and LDPC codes

Advantages:

- Most efficient data correction methods known, and hence don't bloat the data much.

Disadvantages:

- Implementations are very tough.
- Have high time complexity and hence real time encoding and decoding may not be possible.

#### 6.3.2.6 Conclusion

As a result of this analysis, we decided to go for CRCs with Reed Solomon codes because of the following factors:

- The combination can very well correct burst errors, where hamming codes may fail.
- Even though they may take large computational time, but we have a powerful enough microprocessor for the purpose.
- Better, more space-efficient codes are available, but they are comparatively tough to implement and take longer times.
- Both CRCs and Reed-Solomon codes have been used in satellite communication frequently.

#### 6.3.2.7 Implementation

CRCs:

The CRC algorithm requires division of the message polynomial by the key polynomial. The polynomial is represented by a binary word. Next, to the message, a string of zeros is

concatenated, the number of which is equal to the degree of the code polynomial. Division is implemented by using the bit-wise XOR operation for subtraction (The subtraction operation is the same as XOR over GF(2)). The remainder obtained on division is added (XORed) to the code polynomial. The polynomial hence obtained is divisible by the code word. If the message is altered in transmission, it will not be divisible by the code word and hence error will be detected.

#### REED SOLOMON:

Reed Solomon codes over the field GF(256) will be used. This is convenient because data during communication as well as storage would be stored in 8-bit form. GF(256) would be constructed by choosing a primitive polynomial of degree 8 and using it to extend GF(2). The “k” and “n” for the Reed Solomon code would be chosen based on burst error capabilities required. A sequence of 8-bit data of length k would be encoded to another sequence of 8-bit data of length n. This encoding is done by evaluating a polynomial obtained from the 8-bit words of the input sequence at different elements of GF(256). The evaluation of the polynomial is done by the arithmetic operations of addition and multiplication over GF(256). If necessary, we would puncture the code, that is, we will drop a few elements of the encoded sequence, to satisfy our rate and error correction requirement.

The decoding can be carried out by the BCH decoding technique using the error locator polynomial.

### 6.3.3 Data Compression

In general we cannot hope to compress data without having some prior knowledge of the data that is to be compressed. Using a particular compression algorithm without such information or with wrong information can lead to bloated data instead of compressed one. As a matter of fact all compression algorithms will bloat data on suitable inputs. Presented below is a general overview of the compression algorithms that I have tried to read up and the necessary information that we will need to implement them:-

#### 6.3.3.1 Data compression by fourier transforms

This method relies on a known fact that the fourier transform of a given data waveform will either

1. Have a smaller fourier transformed representation rather than the original one.(e.g, a sine wave can be represented by a simple delta function)
2. We know that we can remove some data beyond a certain frequency band(e.g., jpeg compression of images).

In both these methods the primary thing being compressed is mostly images or sound. I doubt the applicability of such method to our purpose.

#### 6.3.3.2 Data compression by using statistical information

This method relies on the fact that different data values will occur with different probabilities. e.g., in english the letter 'e' is the most frequent one used and hence it is given a shorter bit code than say something like the letter 'x'.

This can be used in two ways by us:-

1. If we know that certain numbers are going to be measured a lot more frequently than other then we may not use the normal binary representation at all and instead have a pre-determined representation that will have shorter codes for the more frequent numbers. e.g., since we have a 10 bit ADC, our values will range from 0 to 1024. Then in that case if we know that the numbers between 100 to 107 are going to be more frequent than others we may represent them with shorter codes like 100<=>000 101<=>001 102<=>010 etc 107<=>111. This will bloat the data greatly if our estimate was wrong and 100-107 happen in reality to be the least frequent values measured.
2. We could use a more dynamic version of the above algorithm wherein we calculate the actual distribution of values for one day and then choose an appropriate encoding. This encoding could then be sent down as a kind of "header" file. This would be reasonably good but the main problem is that if we miss out on the header file at the ground station, then all the readings for that day would essentially be garbage and useless. Also this algorithm would be more difficult to implement.

#### 6.3.3.3 Data compression by advanced techniques using AVL trees

There are more advanced techniques using AVL trees to compress files whose statistical data is not known in advance. These are the most recent developments in the field. However, the question of whether the effort of using it will be worth the improvement over the following method is still to be evaluated.

### 6.3.3.3 Data compression by saving only the differences

Another method is to save only the differences. We have a 10 bit ADC. If we are reasonably assured that there wont be differences of more than say the 4 LSBs of data then we might send an initial value and then send only 4 bit differences. Now if we have an overflow, that would be signified by a value "1111" then followed by another 10 bit value for that instant and then 4-bit differences from that point onwards. thus we would effectively have a near halving of data. Thus , our method of data compression is not finalised yet. Mostly we will be looking at either methods 3 or 4 since the payloads have stated very clearly that they will not be able to provide us with statistical information about the data beforehand.

## 6.3.4 Baseband Data Handling

This section mainly deals with the acquiring of data from the payloads namely the thermopiles. This will be done in the following two stages :-

### 6.3.4.1 Amplification

The voltage levels given by the thermopiles will be ranging in millivolts. We will have a number of voltage amplifiers to increase this voltage to a measurable voltage. (The payloads team is designing the amplifier circuits.)

### 6.3.4.2 Analog to Digital Converter

After the amplification , we will be using 3 16-to-1 analog multi-plexers namely the ADG706/7 mux. This will be give us a total of 48 lines multiplexed into three lines. These will go to the three channels of the ADC to be used namely MAX1248. The fourth channel will be directly connected to the 49<sup>th</sup> thermopile.

## Chapter 7: Power System

### 7.1 Introduction

The Power System of this satellite is a completely autonomous system. Its aim is to provide continuous and regulated power to all the electronic circuits on the satellite. Its major functions are

1. To collect solar power.
2. To supply power to various electronic circuits as required.
3. To store the excess power available.
4. To monitor condition of each load.
5. To switch off a load if it is malfunctioning or not in use.
6. To reset the OBC upon launch

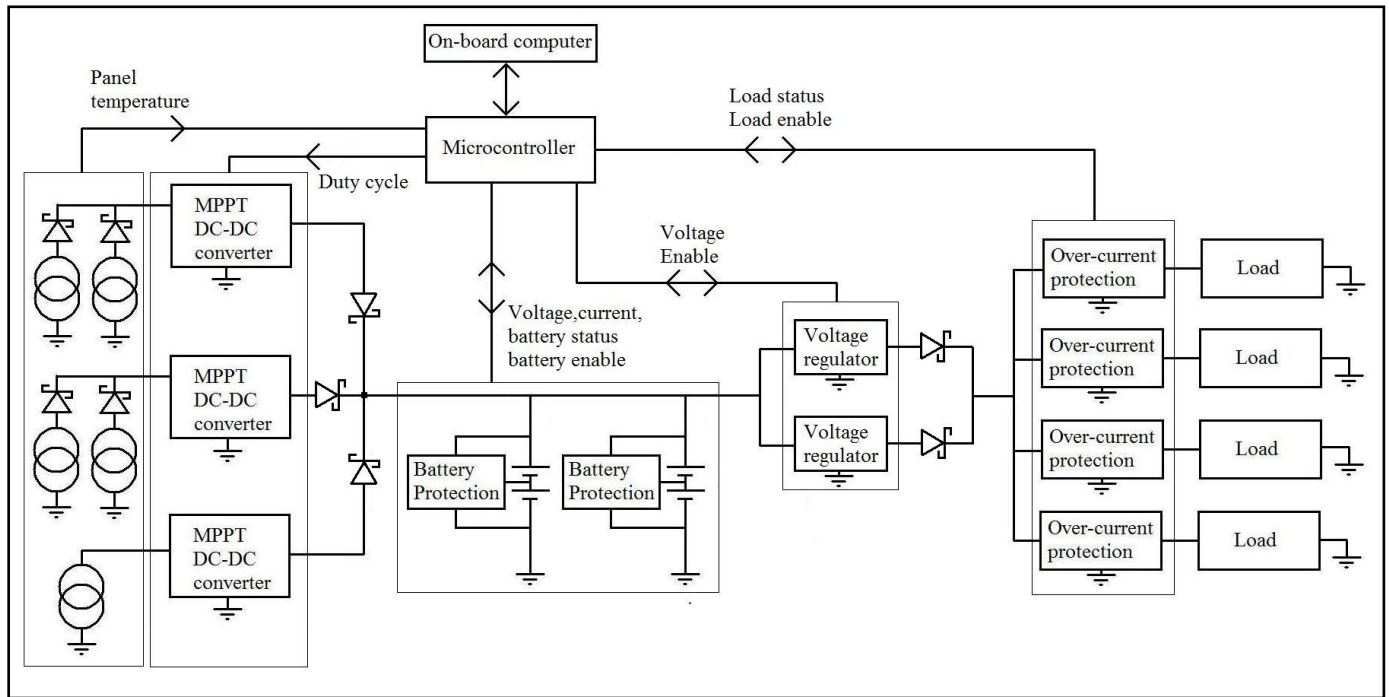


Figure 7. 1: Block diagram of the power system

### 7.2 Solar array

The satellite is powered by solar panels on five faces. The nadir surface is kept open for the experiment and the antenna; so there is no solar panel mounted on that face.

The Ultra Triple Junction (UTJ) cells from Spectrolab and the Advanced Triple Junction (ATJ) cells from Emcore are being considered. However, Spectrolab does not ship to India while

Emcore has a supplier in Bangalore (Mr. Prakash Sundar, Saft India Program Office) who has suggested that we contact Emcore for a discount.

The cells have been chosen considering their flight heritage, high efficiency and resistance to radiation. We will buy the cells in the CIC (covered cell interconnect) form and they will be assembled in a panel at the solar panel lab facility at ISAC. The beginning-of-life specifications of the ATJ cells at air-mass 0 spectrum ( $1353\text{W/m}^2$ ) and  $28^\circ\text{C}$  are:

$$V_{\text{oc}} = 2.60 \text{ V}$$

$$V_{\text{mp}} = 2.30 \text{ V}$$

$$J_{\text{sc}} = 17.1 \text{ mA/cm}^2$$

$$J_{\text{mp}} = 16.20 \text{ mA/cm}^2$$

Efficiency at maximum power point = 28.3%

Fill-factor = 0.84

Courtesy: ATJ high efficiency solar cells for Space Applications, Product brief.

[www.emcore.com](http://www.emcore.com)

The dimension of each cell is 6.89cm x 3.95cm. Each panel will contain a parallel connection of 4 strings of cells. Each string has 7 cells in series. Thus characteristics of each panel are:

$$I_{\text{sc}} = 1.82 \text{ A} \quad V_{\text{oc}} = 18.2 \text{ V}$$

$$I_{\text{mp}} = 1.72 \text{ A} \quad V_{\text{mp}} = 16.1 \text{ V}$$

The power output of the solar panels has been calculated to be between 21.2W to 27.3W at maximum power.

### 7.3 Estimation of solar power incident on the satellite

The satellite is placed in a 9:30am Sun-synchronous orbit at a height of 670km. The following calculations show how much power is incident on the five solar panels of the satellite in this orbit. Assuming that the temperature of the panels does not vary much, we can also estimate the amount of electrical power obtained.

#### 7.3.1 Reference Frame

The co-ordinate axes shown in Fig 7.2 is used throughout. The XY plane is the plane of the Earth's orbit around the Sun. The center of the Earth is taken as the origin.

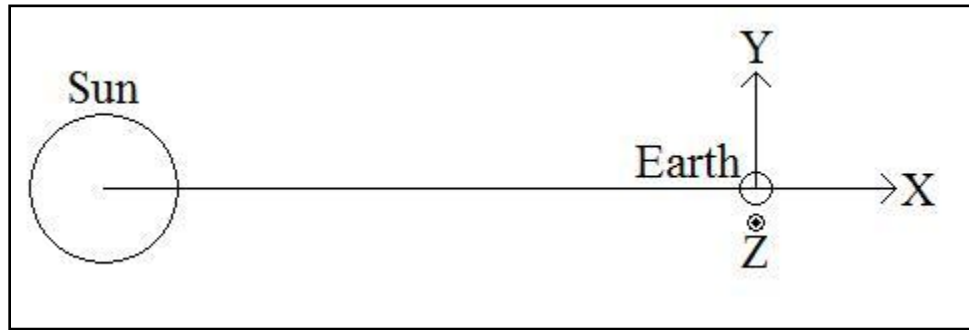


Figure 7.2: Reference Frame

### 7.3.2 Position of the satellite

Let be  $\mathbf{r}(t)$  the position vector of the satellite.

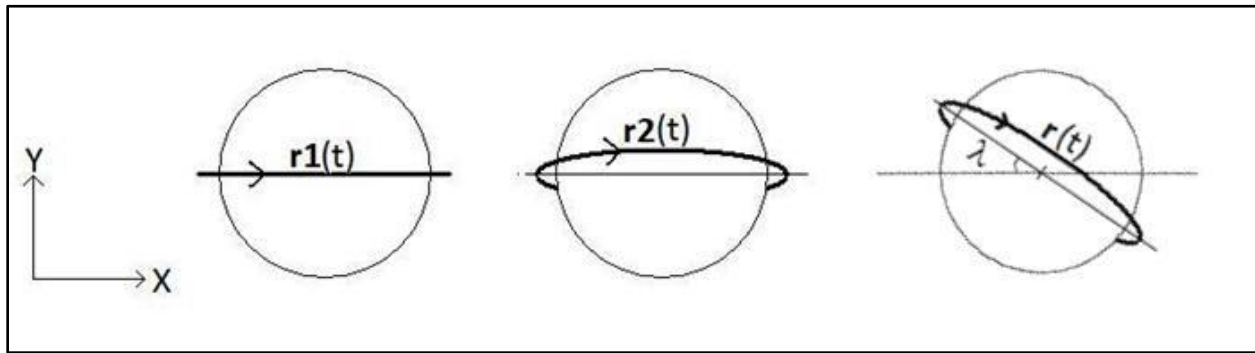


Figure 7.3: Position Vector of Satellite

For the actual orbit,  $\square \square \square \tilde{\square}$  and the radius of orbit  $R = 670 + 6400 \text{ km} = 7070 \text{ km}$

$$\begin{aligned}
 \vec{r}_1(t) &= R \begin{bmatrix} \sin(\omega t) \\ 0 \\ \cos(\omega t) \end{bmatrix} \\
 \therefore \vec{r}_2(t) &= R \begin{bmatrix} 1 & 0 & 0 \\ 0 & \cos 8^\circ & \sin 8^\circ \\ 0 & -\sin 8^\circ & \cos 8^\circ \end{bmatrix} \begin{bmatrix} \sin(\omega t) \\ 0 \\ \cos(\omega t) \end{bmatrix} = R \begin{bmatrix} \sin(\omega t) \\ \cos(\omega t) \sin 8^\circ \\ \cos(\omega t) \cos 8^\circ \end{bmatrix} \\
 \therefore \vec{r}(t) &= R \begin{bmatrix} \cos \lambda & \sin \lambda & 0 \\ -\sin \lambda & \cos \lambda & 0 \\ 0 & 0 & 1 \end{bmatrix} \begin{bmatrix} \sin(\omega t) \\ \cos(\omega t) \sin 8^\circ \\ \cos(\omega t) \cos 8^\circ \end{bmatrix} = R \begin{bmatrix} \cos \lambda \sin(\omega t) + \sin \lambda \cos(\omega t) \sin 8^\circ \\ -\sin \lambda \sin(\omega t) + \cos \lambda \cos(\omega t) \sin 8^\circ \\ \cos(\omega t) \cos 8^\circ \end{bmatrix} \quad ..(1)
 \end{aligned}$$

### 7.3.3 Power incident at a point of time

It can be easily seen that, if the nadir surface always faces the Earth, the power at any point in

space  $\vec{r} = \langle x, y, z \rangle = R \langle \cos \alpha, \cos \beta, \cos \gamma \rangle$  depends only on two angles: the angle of the  $r$  with the direction of the sun-rays which is  $\alpha$  and another local angle (i.e. an angle related to the orientation of the satellite in space and not its position) denoted as  $\phi$ . Hence, to find the power at  $\langle x, y, z \rangle$ , we can simply find the power at  $\vec{r}' = \langle x, \sqrt{y^2 + z^2}, 0 \rangle$ .

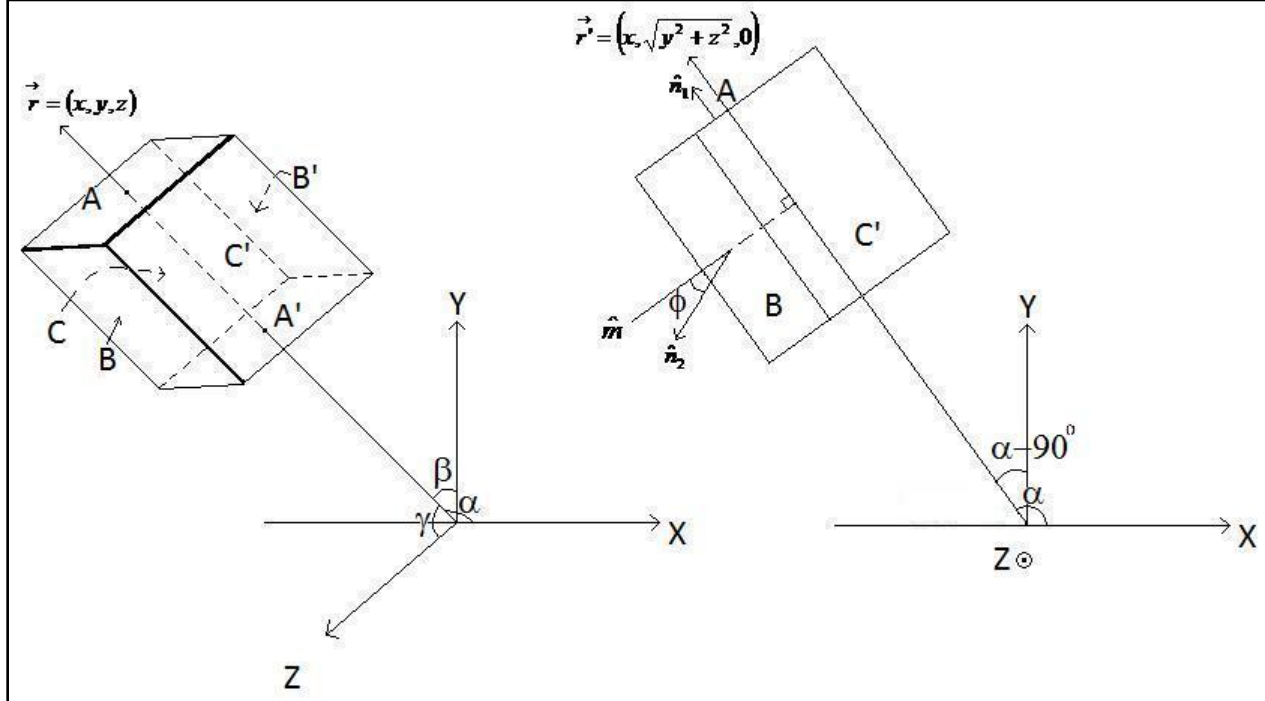


Figure 7.4: Transformation

Let  $\hat{n}_1, \hat{n}_2, \hat{n}_3$  be the normal vectors of the Sun-facing faces A, B and C of the satellite.  $\hat{m}$  is the unit vector in the XY plane and perpendicular to  $\hat{n}_1$ . Thus, if the satellite rotates about the axis defined by its position vector  $\vec{r}'$  by an angle  $\phi$ , the angle between  $\hat{n}_2$  and  $\hat{m}$  is  $\phi$ .

The normal vectors are found to be

$$\begin{aligned}\hat{n}_1 &= \langle \cos \alpha, \sin \alpha, 0 \rangle \\ \hat{n}_2 &= \langle -\sin \alpha \cos \phi, \cos \alpha \cos \phi, -\sin \phi \rangle \\ \hat{n}_3 &= \langle -\sin \alpha \sin \phi, \cos \alpha \sin \phi, -\cos \phi \rangle \quad ..(2)\end{aligned}$$

It can be easily checked that the three vectors are mutually perpendicular and that the angle between  $\hat{n}_2$  and  $\hat{m}$  is  $\phi$  and between  $\hat{n}_3$  and  $\hat{m}$  is  $90-\phi$ .

Therefore, the power incident on the faces A, B and C in the situation shown is

$$P_1 = -SL^2 \cos \alpha$$

$$P_2 = SL^2 |\sin \alpha \cos \phi| \quad \dots(3)$$

$$P_3 = SL^2 |\sin \alpha \sin \phi| \quad \text{where } S = 1366 \text{ W/m}^2 \text{ and } L = 0.3 \text{ m}$$

When the satellite is at a position where A does not face the Sun,  $P_1 = 0$ . However, when not eclipsed by the Earth, either A or A' and B or B' are always illuminated by the Sun.

Now,  $P_2 + P_3 = SL^2 |\sin \alpha| |\cos \phi + |\sin \phi|$  varies from  $SL^2 |\sin \alpha|$  for  $\phi = 0^\circ$  or  $180^\circ$  to

$SL^2 |\sin \alpha| \sqrt{2}$  for  $\phi = 90^\circ$  or  $270^\circ$ . Hence the power contribution of faces B and C depends upon the orientation of satellite which can be controlled to have maximum sunlight falling on them.

$$\begin{aligned} \text{From (1), } \cos \alpha &= \cos \lambda \sin \omega t + \sin \lambda \cos \omega t \sin 8^\circ \\ &= 0.7933 \sin \omega t + 0.0847 \cos \omega t \\ &= 0.798 \sin(\omega t + 6^\circ) \end{aligned}$$

Thus, from this and (3), we know  $P_1(t)$ ,  $P_2(t)$  and  $P_3(t)$ . Therefore, the total incident energy is simply the sum of the individual integrals  $\int P_1 dt$  and  $\int (P_2 + P_3) dt$  with the appropriate limits of integration for both of them. These limits are calculated in the next section.

#### 7.3.4 Calculation of the eclipsed region

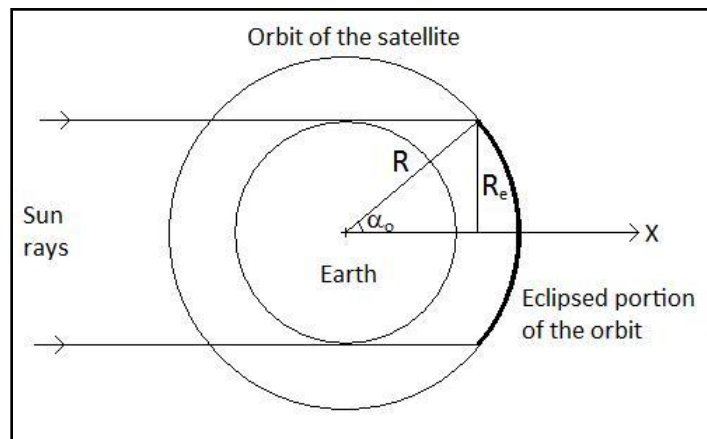


Figure 7. 5: Eclipsed Region

$$\alpha_0 = \sin^{-1}\left(\frac{R_e}{R}\right) = \sin^{-1}\left(\frac{6400}{6400 + 670}\right) = 64.8^\circ$$

Hence, the satellite is in eclipsed region when

$$\alpha < \alpha_0$$

$$\Rightarrow \cos \alpha > \cos \alpha_0$$

$$\Rightarrow 0.798 \sin(\omega t + 6^\circ) > 0.425$$

$$\Rightarrow \sin(\omega t + 6^\circ) > 0.533$$

$$\Rightarrow 32.18^\circ < \omega t + 6^\circ < 147.82^\circ$$

$$\Rightarrow 26.09^\circ < \omega t < 141.73^\circ$$

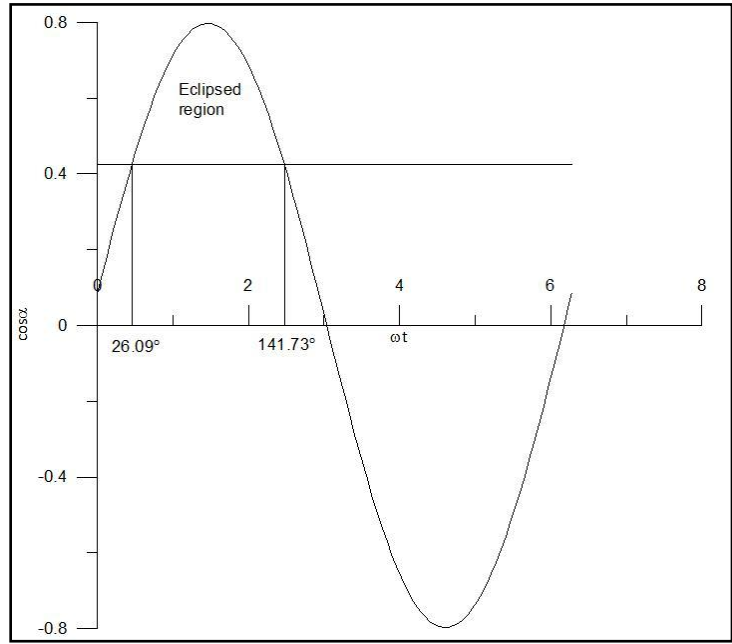


Figure 7. 6: Eclipsed Region

### 7.3.5 Final calculation

$$P_1(t) = -SL^2 \cos \alpha = -0.798 SL^2 \sin(\omega t + 6^\circ) \text{ when } \cos \alpha < 0 \text{ and}$$

$$P_1(t) = 0 \text{ elsewhere}$$

Therefore, the radiation energy falling on face A in one orbit is

$$\begin{aligned} W_1 &= 0.798 \frac{SL^2}{\omega} \int_{174^\circ}^{354^\circ} \sin(\omega t + 6^\circ) d(\omega t) \\ &= 0.798 \frac{SL^2}{\omega} * 2 \\ &= 1.596 \frac{SL^2}{\omega} \end{aligned}$$

If the satellite is kept oriented to receive maximum sunlight, the radiation falling on faces B and C is

$$P_2 + P_3 = \sqrt{2}SL^2|\sin \alpha| \text{ when not eclipsed and}$$

$$P_2 + P_3 = 0 \text{ otherwise.}$$

Therefore, the energy incident on faces B and C during one orbit is

$$\begin{aligned} \Rightarrow W_2 + W_3 &= \sqrt{2} \frac{SL^2}{\omega} \left[ \int_0^{26.09^\circ} |\sin \alpha| d(\omega t) + \int_{141.73}^{360^\circ} |\sin \alpha| d(\omega t) \right] \\ &= \sqrt{2} \frac{SL^2}{\omega} \left[ \int_0^{26.09^\circ} \sqrt{1 - 0.636 \sin^2(\omega t + 6^\circ)} d(\omega t) + \int_{141.73}^{360^\circ} \sqrt{1 - 0.636 \sin^2(\omega t + 6^\circ)} d(\omega t) \right] \\ &= \sqrt{2} \frac{SL^2}{\omega} \left[ \int_0^{32.18^\circ} \sqrt{1 - 0.636 \sin^2(\omega t)} d(\omega t) + \int_{147.82^\circ}^{360^\circ} \sqrt{1 - 0.636 \sin^2(\omega t)} d(\omega t) \right] \\ &= \sqrt{2} \frac{SL^2}{\omega} [0.54348 + 3.1] \\ &= 5.153 \frac{SL^2}{\omega} \end{aligned}$$

Thus, the total energy and the average power during one orbit is calculated to be

$$W_1 + W_2 + W_3 = (1.596 + 5.153) \frac{SL^2}{\omega} = 6.749 \frac{SL^2}{\omega}$$

$$\langle P \rangle = \frac{W_1 + W_2 + W_3}{\text{Orbital-period}} = \frac{W_1 + W_2 + W_3}{2\pi/\omega}$$

$$= \frac{6.749 SL^2}{2\pi}$$

$$= \frac{6.749 * 1366 * 0.09}{2\pi}$$

$$= 132W$$

If the orientation of the satellite is not controlled,  $P_2 + P_3$  will be less. However it may at most reduce by a factor of 0.707. This gives a lower bound to the power to be

$$\langle P \rangle_{\min} = \frac{(0.596 + 0.707 * 5.153) SL^2}{2\pi} = \frac{5.239 * 1366 * 0.09}{2\pi} = 102.5W$$

The following graphs show the variation of the incident power with time for one orbit.

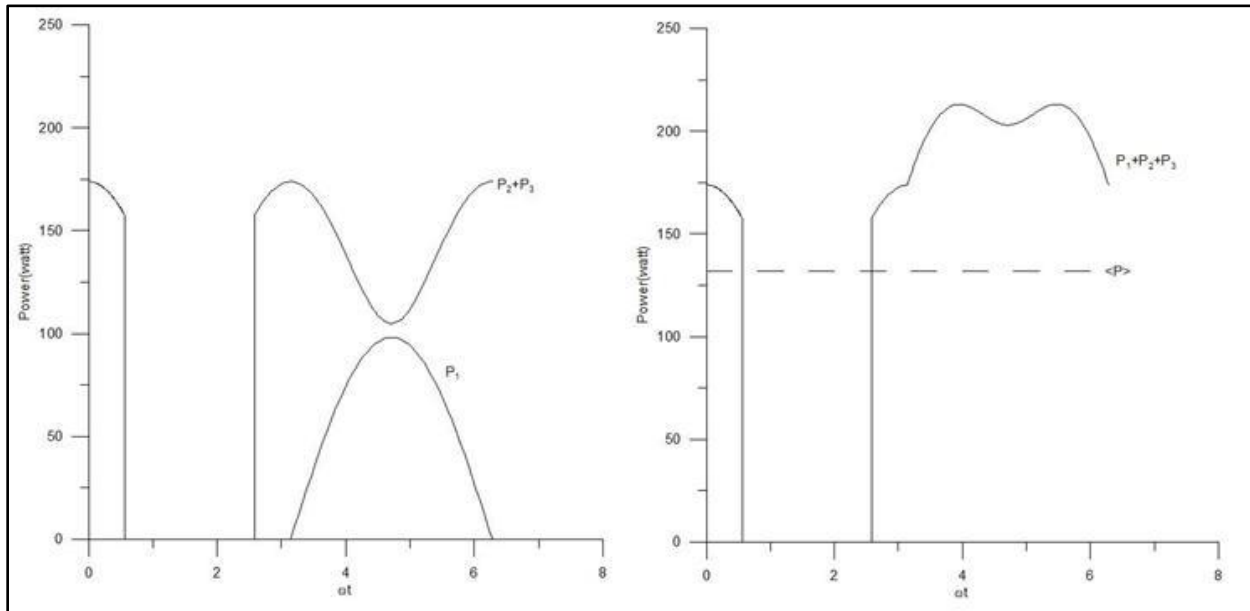


Figure 7. 7: Variation of incident Power in one orbit

### 7.3.6 Estimating the power output of the solar panels

Calculating the power output of the solar panels exactly is not possible as the variation of temperature of the solar panels during orbit is not known. However the efficiency of the cell drops at higher temperatures. So assuming that the temperature of the panels is say,  $70^{\circ}\text{C}$ , we can get an estimate of the power output of the panels.

Consider the 27.5% Advanced Triple Junction (ATJ) Solar Cells from Emcore. The cell has a temperature coefficient of  $J_{mp}$  of  $+11 \mu\text{A}/^{\circ}\text{C} \text{ cm}^2$  and temperature coefficient of  $V_{mp}$  of  $-5.93 \text{ mV}/^{\circ}\text{C}$ .

$$\therefore P(28^{\circ}\text{C}) = 2.30V \times 16.2 \text{ mA/cm}^2 = 37.26 \text{ mW/cm}^2$$

$$V(70^{\circ}\text{C}) = 2.30V - (5.93mV/^{\circ}\text{C} \times 42^{\circ}\text{C}) = 2.05V$$

$$J(70^{\circ}\text{C}) = 16.2 \text{ mA/cm}^2 + (11 \mu\text{A}/^{\circ}\text{C} \text{ cm}^2 \times 42^{\circ}\text{C}) = 16.66 \text{ mA/cm}^2$$

$$\therefore P(70^{\circ}\text{C}) = 2.05V \times 16.66 \text{ mA/cm}^2 = 34.17 \text{ mW/cm}^2$$

So, at  $70^{\circ}\text{C}$ , efficiency of the cell is  $27.5 \times 34.17 / 37.5 = 25\%$ .

The size of each cell is  $3.95\text{cm} \times 6.89\text{cm}$  which means that we can have  $7 \times 4 = 28$  cells on each face. The area of each cell is  $26.6 \text{ cm}^2$ . So, the factor due to unused area is  $28 \times 26.6 / 30 \times 30 = 0.828$

Thus, the maximum power output of the cells will be

$$P_{\max} = 132 \times 0.25 \times 0.828 \text{ W} = 27.3 \text{ W}$$

The minimum power will be

$$P_{\min} = 102.5 \times 0.25 \times 0.828 = 21.2 \text{ W}$$

Note that the value of the beginning-of-life efficiency of the solar cells has been used in the above calculations. At the end of the life of the solar panels i.e. around 4 – 5 years the solar cell degrades by 11%.

So, the end-of-life values are:  $P_{\max} = 24.3 \text{ W}$  and  $P_{\min} = 18.9 \text{ W}$

#### 7.4 Maximum power point tracking and battery charge regulation

Maximum Power Point Tracking (MPPT) is important in solar-powered systems because it makes the solar cells operate at such value of current and voltage so that maximum output power is obtained for given illumination.

Currently, we are exploring two methods for the maximum power point tracking

- 1) A microcontroller based method which implements a standard MPPT algorithm
- 2) An analog method based on step-down voltage regulator with feedback from input voltage.

The analog method is likely to be less efficient but simpler and more reliable than the microcontroller. Which method to use will be taken after testing both the methods.

Selection of the MPPT algorithm to be implemented on microcontroller:

There are various algorithms which can be used for MPPT.

Algorithm	Advantages	Disadvantages
Incremental conductance	Very high efficiency	Complex to implement and requires extra hardware
Constant voltage	Simplest to implement	Least efficiency
Perturb and observe	Easier to implement, higher efficiency than constant voltage	Oscillates around the peak power point

Hence we have decided to use perturb and observe algorithm. This algorithm is based on the “Single sensor MPPT algorithm for multiple solar panels configurations” by Florent Boico,

Northeastern University, Boston. This algorithm requires only one current sensor (to measure output current) and thus a much simpler microcontroller will do as we require only one ADC pin and much simpler calculations. As per the guidance from our OBC team we have decided to use either a PIC or an AVR microcontroller. Various microcontrollers of the PIC family have been used successfully in different student satellite projects.

#### 7.4.1 Description of P&O algorithm

In Perturb & Observe method, the duty ratio in a DC/DC converter is incremented and the output power is measured. If the output power of the array increases, then the duty ratio is incremented in the same direction. If the power decreases, the direction is reversed. The duty ratio then oscillates between positive increments and negative increments as the output voltage of the solar array oscillates around its MPP point.

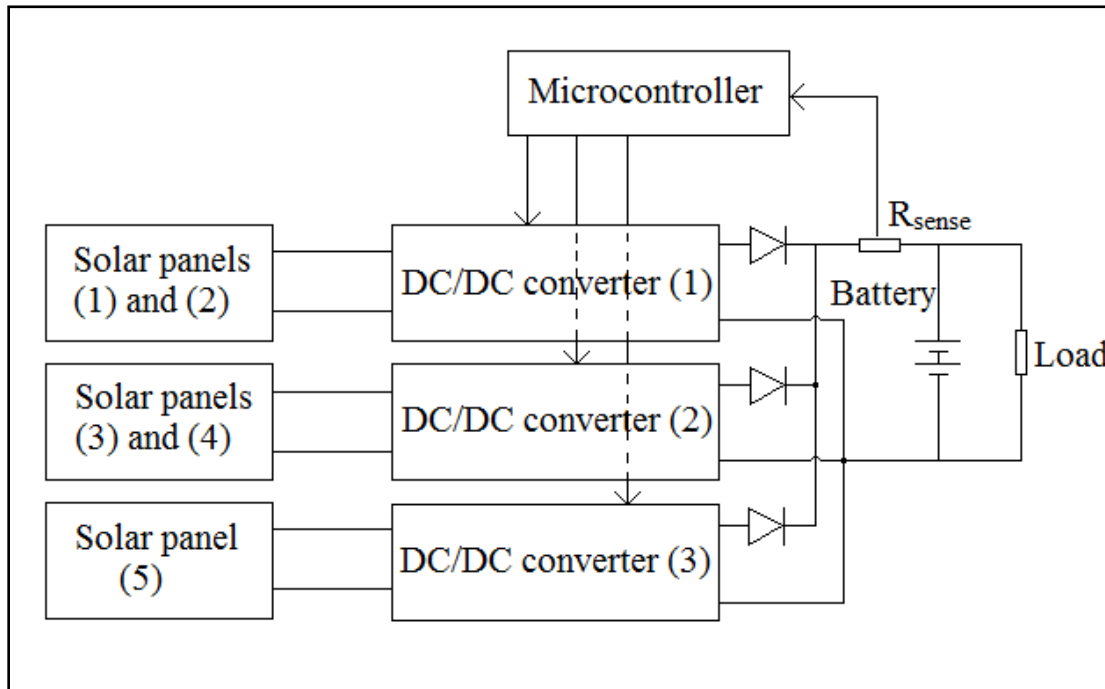


Figure 7. 8: Hardware for MPPT of 5 solar panels

The proposed design is shown in Fig. 7.8 and involves 3 power converters. Buck converter design will be used and only the load current will be sensed. MPPT can be achieved for several solar panels using only the sensed load current.

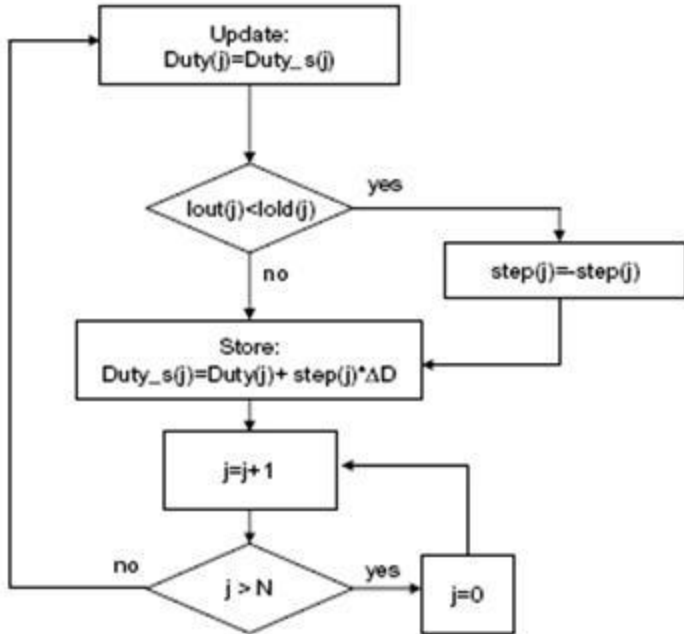


Fig. 2: Interleaved M.P.P.T. algorithm. The duty cycle of each converter is perturbed turn by turn. As a result of a perturbation of one converter the next duty cycle for that converter is calculated and stored. Then, the stored duty cycle of the next converter is applied and the process continues. The algorithm cycles that way through all the converters. (step=1 at initialization, N is the number of PV panels.)

*Figure 7. 9: Interleaved M.P.P.T. algorithm*

(Courtesy: Single Sensor MPPT Algorithm for Multiple Solar Panels Configurations, Florent Boico, Northeastern University)

The basic MPPT algorithm is presented in Fig. 7.9. It consists of an interleaved Perturb & Observe scheme: The duty ratio of one converter is perturbed and the steady state load current sensed and stored. The duty cycle of the next converter is then perturbed; the load current is again sensed, and so on. In this way, it takes three perturbations before a cycle is complete and individual converter's duty ratio is perturbed again. The direction of the duty ratio perturbation depends on whether its previous perturbation (from the last cycle) increased or decreased the load's output current. If it increased the load current, then the perturbation is in the same direction. Otherwise, the duty ratio is adjusted in the opposite direction.

Redundancy: we are planning to set the solar panel's voltage to a certain value in case the microcontroller fails. This will be useful since the MPP voltage does not vary much with the intensity of incident light on it.

#### 7.4.2 The analog method for MPPT

This method uses the current mode step-down voltage regulator IC LTC1625 from Linear along with the amplifier and reference IC LTC 1541. It is based on the design note from Linear Technology. The circuit diagram is shown below.

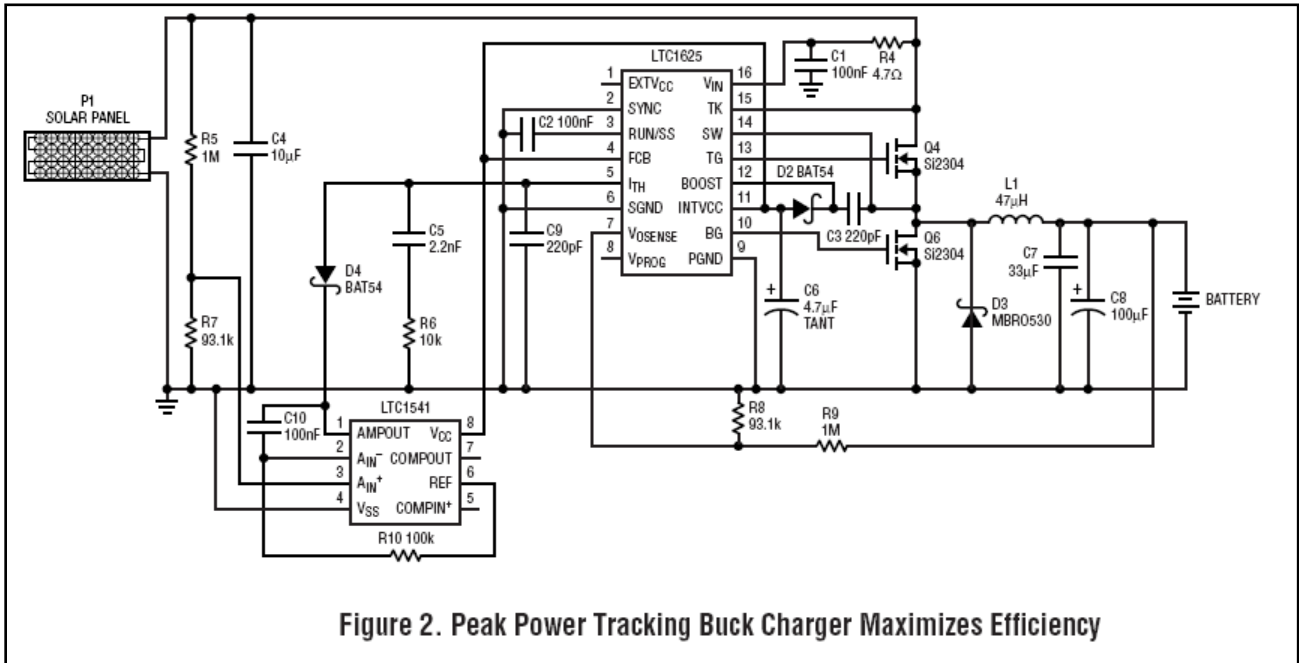


*Figure 7. 10: Analog M.P.P.T. circuit*

(Courtesy: Design Note 1012, “Shrink solar panel size by improving performance”, by John Shannon, Linear Technology.)

The regulator LTC1625 serves to regulate the battery voltage while the LTC1541 based PI control loop forces the charger to operate at the maximum power point of the panel. The benefit of this circuit is that it is simple to make and reduces the load on the microcontroller. Also, these ICs are rated for the industrial temperature range.

#### 7.4.3 Battery charging algorithm

The battery charge current will be limited to a safe value of 1C – 1.5C. The battery charge voltage will be limited to 8.2V according to the battery specifications. The temperature of cells

will be sensed and battery charge will be terminated if the temperature is out of the limits. If the battery is discharged below 8V then a constant charge algorithm will be used, subject to availability of excess power. Battery charging will be handled by the power systems microcontroller.

## 7.5 Battery and battery protection

The battery stores energy and is the only source of energy for the satellite during the eclipse portion of the orbit.

A lithium ion battery is chosen because of its high energy density & absence of memory effect as compared to Ni-Cd or Ni-MH chemistries.

The load requires 3.3 volts; hence two batteries will be connected in series so that it provides an output voltage between 6- 8.4 Volts. For redundancy two such sets are used in parallel & will be controlled independently.

The batteries will be purchased from ‘Saft batteries’. We will be using a battery protection circuit using IC ucc3911-1 from Texas Instruments considering current capacity internal resistance & leakage current drain. This IC takes care of over charge/discharge (by sensing voltages), short circuit or excess load (by sensing current) and gives the battery status (fully charged or fully discharged) for housekeeping purpose and a low power warning signal.

Guaranteed capacity	5.8 Ah
Mean voltage at C/1.5	3.6 V
End of charge voltage	4.1 V
Energy	20 Wh
Specific energy	133 Wh/kg
Dimensions	65mm x 65 mm x 18mm

Weight	0.15kg
Qualified for LEO application	

Thus, the total rating of the battery is

Mean voltage = 7.2V

Guaranteed capacity = 11.6 Ah

Energy = 80Wh

For a power consumption of around 10W, the satellite can run for around 8 hours without solar power on a full battery.

## 7.6 Voltage regulator

The voltage regulator (also known as the power conditioning module) converts the raw battery or solar panel voltage into a regulated voltage for the loads. An industrial grade DC- DC converter will be used considering following factors:

- 1) Output voltage(s) 3.3V
- 2) Input voltage range 5-10 Volts
- 3) Typical and maximum output current 3A (max. continuous)
- 4) Switching frequency
- 5) Efficiency (>85%)
- 6) Output ripple
- 7) Electromagnetic interference(EMI)
- 8) Phase margin (stability)
- 9) Transient response
- 10) Soft start
- 11) Standby mode
- 12) Redundancy

The thermopile payload, on-board-computer and the control system require 3.3V. The PTR08060 step-down switching regulator from Texas Instruments has been selected for this purpose. Two such modules will be paralleled together with cold redundancy. Its electrical specifications are:

- Up to 6A Output Current
- Wide Input Voltage Range (4.5 V to 14 V)
- Wide-Output Voltage Adjust (0.6 V to 5.5 V)
- Efficiencies Up To 96%
- ON/OFF Inhibit
- Undervoltage Lockout (UVLO)
- Output Overcurrent Protection  
(Nonlatching, Auto-Reset)
- Overtemperature Protection
- Ambient Temp. Range:  $-40^{\circ}\text{C}$  to  $85^{\circ}\text{C}$
- Space Saving Vertical SIP Package

The 6A current limit leaves a wide margin with no loss in efficiency. The wide input voltage range covers the entire useful battery voltage range of 6V to 8.4V. The module can be switched on and off by the power systems microcontroller through the ON/OFF inhibit pin. The industrial temperature range makes the module suitable for our application.

The application circuit for the module is shown below.

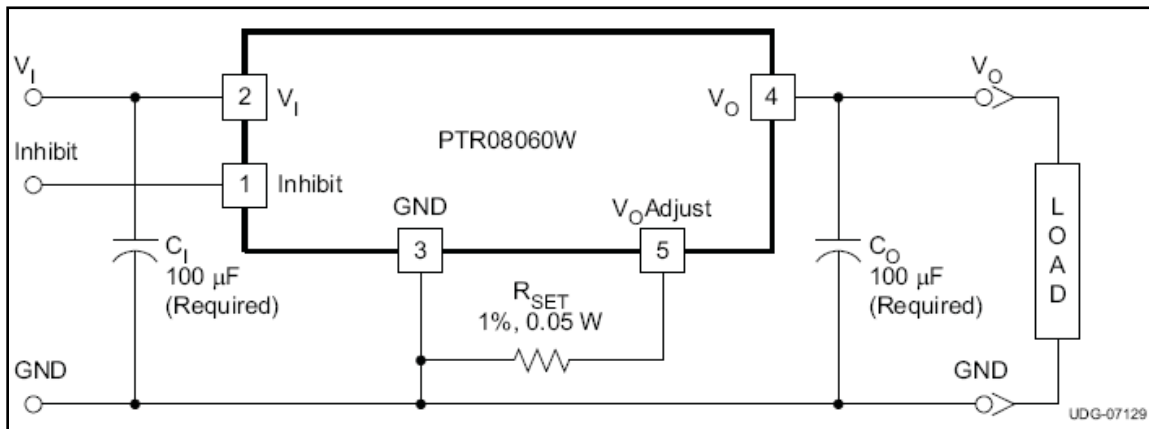


Figure 7. 11: Regulator Circuit

Courtesy: PTR08060 datasheet, Texas Instruments, [www.ti.com](http://www.ti.com)

Aluminum electrolytic capacitors cannot be used at the input and the output as they are not recommended for use below  $0^{\circ}\text{C}$ . Hence, other type of capacitors like OS-CON, poly-aluminum or polymer-tantalum capacitors will be used as recommended in the datasheet. The actual type of capacitor used will depend upon their availability in the market.

The output voltage is set by the Rset resistor. A  $432\Omega$  gives an output voltage of 3.327V.

## 7.7 Power Distribution Switches

MOSFET switches of very low internal resistance will be used for power distribution.

Considering internal resistance, current capacity & flight heritage, IC tps203x from Texas Instruments was chosen.

It has following features

- 33-mΩ internal resistance
- Ambient Temperature Range, -40°C to 85°C
- Short-Circuit and Thermal Protection .
- Overcurrent Logic Output
- Operating Range: 2.7 V to 5.5 V
- Logic-Level Enable Input
- Typical Rise Time: 6.1 ms
- Undervoltage Lockout
- Maximum Standby Supply Current: 10 µA
- No Drain-Source Back-Gate Diode

## 7.8 Power systems microcontroller

The function of the microcontroller would be to regulate the battery charging, to collect housekeeping data such as solar panel and battery temperatures, battery voltage and current. It also keeps track of any faults in loads which will be relayed by the power distribution switches. It will also turn off any load if told to do so by the main on-board computer.

The microcontroller requirements are:

General purpose inputs – 11

General purpose outputs – 9

PWM outputs – 3

ADC inputs – 12

Microcontrollers from the PIC and AVR family of 8-bit microcontrollers are being considered.

## 7.9 Rough power budget

- a) Magneto-torquers: 3W continuous.
- b) Beacon: 2.5W continuous

- c) On-board computer: 1.5W continuous
- d) RF downlink: 2.5W for about 8 minutes every 24 hrs.
- e) Amplifier for the thermopile: few 100mW.

## **Chapter 8: Mechanical and Thermal Configuration**

### **8.1: Introduction**

The Structures, Thermals and Mechanisms Group of the IIT Bombay Student Satellite Project has as its primary aim the design and fabrication of a robust body for the satellite that accommodates all onboard components in their preferred orientations or locations, provides a support for their affixation, protects them from damage during launch or in orbit, thermally and magnetically shields components as requirements dictate, obeys the constraints for moments of inertia as dictated by the Control Algorithm for the satellite, maintains a safe and stable thermal environment within the satellite and helps in the optimal housing of the payload for best possible data acquisition.

The group works under the constraints of size, weight, environment and placement of components as dictated by the other groups. The antennae for communication, the payloads and the gravity-gradient boom all have to be earth-pointing. The batteries and payload require thermal protection and control. The magnetometer and microprocessor require shielding from stray magnetic fields. Stowing and deployment of antennae is also necessitated. Control algorithm dictates that for stability, moments of inertia are greater along roll axis than yaw axis but less along roll axis than sum along yaw and pitch axes. The body of the satellite also has to be such that it can withstand the forces acting upon it during launch, vibrations and thermal fatigue while in orbit.

The group on completion of design by May 2008 will proceed to the fabrication and testing phase in June 2008. Facilities for milling and other machining processes are available within IIT Bombay and also at TIFR, Mumbai. Clean room facilities and a thermovacuum chamber are also available at TIFR. However for further testing it is requested that ISRO extend its facilities to the students for their work.

### **8.2: Structural Aspects of the Satellite**

#### **8.2.1: Introduction**

The Structures Group of the Student Satellite Programme of IIT Bombay has as one of its objectives the design of a mechanical structure for the satellite. This structure must contain all subsystems of the satellite within itself, support the various instruments and components

onboard, provide strength enough to preserve the satellite during launch and in orbit, shield the components within from the outside environment and resist impacts and other causes of damage.

## 8.2.2 Shape of the Satellite

### 8.2.2.1: Factors affecting choice of shape for the satellite

- Volume within the satellite must be sufficient to contain all components but must not exceed the required volume by far as empty spaces render the shell more susceptible to damage by high amplitude vibrations.
- Surface area provided by the shape on the outside must be maximized so as to provide maximum area for affixation of solar panels so that generation of as high an amount of power as possible is facilitated.
- The area facing towards the earth must be sufficient to accommodate all the nadir-pointing components – namely, the two thermopile arrays with collimators, the microstrip antenna, two monopole antennae and the gravity-gradient boom box.
- Body must be robust and not susceptible to failure due to buckling, fatigue or fracture under expected loads during launch or in orbit.
- Shape must be easy to simulate and fabricate.

### 8.2.2.2: Shapes considered for satellite

- Cube
- Sphere
- Dodecahedron
- Other Platonic solids – tetrahedron, octahedron and dodecahedron
- Cuboid

#### 8.2.2.2.1: Satellite with cubical shape

It was initially proposed to have the satellite in the shape of a cube as this shape is most easy to theoretically analyze, perform simulations on and fabricate. However when a cube with enough nadir surface area to accommodate the earth-pointing components was considered, and taking into account the size constraint of 300mmX300mmX300mm, even the minimal sized cube had volume much greater than what would be required by the components, which would remain

empty as the weight constraint does not permit filling up of empty spaces with damper material. Hence, it was decided to reject the cube and look at a more volume-efficient shape.

#### 8.2.2.2.2: Satellite with spherical shape

The sphere is also a shape that is easy to analyze and simulate, and it has the advantage of experiencing minimal aerodynamic drag as the satellite moves through the atmosphere. However, it is extremely difficult to fabricate, deployment becomes tougher, components cannot be easily mounted on the inner walls and surface area is largely reduced thus lowering power generation. Also, not enough area is available for accommodating the payload of fifty thermopiles which must necessarily point radially towards the earth. Hence, the spherical shape was rejected.

#### 8.2.2.2.3: Satellite with dodecahedral shape

The dodecahedral shape provides one face pointing normally to the earth and five other faces having a finite view factor towards the earth. It is also structurally beneficial as loads act largely upon the edges, which are all inclined beam-columns and hence take less compressive load making them less likely to buckle. However the large number of faces makes this shape difficult to fabricate with as few units as possible and having more edges increases the number of joints thus heightening the potential risk of failure along one of them. Also, a dodecahedron with enough surface area to accommodate all components has a height of 500mm which is far in excess of the constraints imposed. Besides, it is difficult to formulate a control algorithm or calculate power generation for a dodecahedron. Hence, the dodecahedral shape, though an attractive option, was rejected as its cons outweigh its pros.

#### 8.2.2.2.4: Satellite with other Platonic solid as shape

- Tetrahedron – Rejected as volume provided is too little
- Octahedron – Rejected as there is no surface pointing directly at Earth
- Icosahedron – Rejected due to difficulty in undertaking theoretical analysis, simulation and fabrication

#### 8.2.2.2.5: Satellite with cuboidal shape

The cuboidal shape was found to be the most advantageous for the satellite. A cuboid of dimensions 300mmX300mmX200mm was found to have the optimal volume and surface area

required for the satellite. The cuboid is also easy to analyze and simulate and can also be fabricated with ease. There is ample area available for accommodating all earth-pointing components. Therefore the shape of the satellite has been settled on as being a cuboid of dimensions 300mmX300mmX200mm, with base being a square of side 300mm and height being 200mm.

### 8.2.3: Method of Fabrication

#### 8.2.3.1: Side panels

The satellite is proposed to be put together from six individual panels. Each panel is fabricated together with all features on its inner and outer surfaces required. The panels will be milled, each from a single block. The supports for the magnetorquers, the slots for the PCBs, the battery case and the nadir surface with collimator assembly will all be milled along with their respective side plates as a single unit, with no fasteners attaching them to the body.

#### 8.2.3.2: Fastening of body panels

The six panels forming the body of the satellite will be joined together to form the final structure. Separate L-sections will be used running along the lengths of the panels to join them. Mechanical fasteners will be used to bolt a side each of two adjacent panels along their common edge to either side of the L-section running between them.

#### 8.2.3.3: Weight reduction methods

In case of those panels which do not carry any PCBs in the middle but only the magnetorquer along the edge, it is proposed to reduce weight by scooping material out in the centre. The proposed methods for weight reduction are

- Cutting large circles out of the panel
- Perforating the panel
- Cutting the pattern shown in Fig 10.1 in the panel

Further decision on which weight reduction method is to be adopted will be taken following simulation of the body and study of stress concentration.

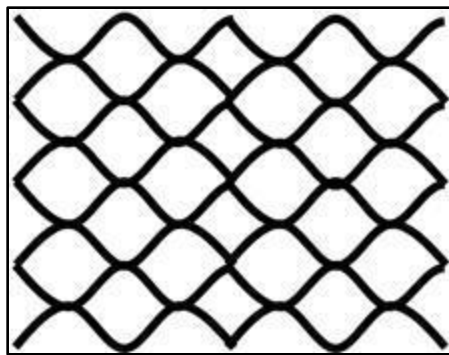


Figure 10. 1 Pattern for panels

#### 8.2.4: Material for Satellite Body

The materials considered for used in the satellite were

- Aluminium honeycomb
- CFRP sheets
- Anodized 6061 aluminium plates

##### 8.2.4.1: Aluminium honeycomb

Aluminium honeycomb was rejected as a structural material as it does not regain its original shape after impact and moreover is more effective as a sandwich material than by itself. Also, it is more difficult and time-consuming to procure.

##### 8.2.4.2: CFRP Sheets

CFRP sheets are lightweight, stiff, have low thermal expansion coefficients and can be easily procured from laboratories at IIT Bombay itself. However it also has very low machinability. All mountings will have to be joined to the body with mechanical fasteners increasing risk of failure. Ductility is very low and the material undergoes brittle failure suddenly, whereas a plastic material undergoing ductile fracture would be preferable. Since a better alternative was available, CFRP was rejected.

##### 8.2.4.3: Anodized aluminium

Anodized aluminium is ductile, lightweight, easily machinable, can have complex structures milled out of whole ingots, easily procurable, cheap, sufficiently stiff, has a coating of oxidized aluminium that imparts the surface high hardness, low electrical and thermal conductivity, and is also characterized for space applications, thus making it a very attractive

alternative. Nibbling of aluminium sheets has been suggested to make them more stiff, and following simulations, it will be decided whether nibbling is required. Due to its favourable properties, anodized aluminium 6061 has been decided upon as the material of choice for the satellite body. In case a better grade of aluminium is required, it is proposed to switch to aluminium 2024.

#### 8.2.5: Conclusion

Thus, the design of the body of the satellite was studied and conclusions reached with regard to the shape, weight reduction method, mounting, fastening, fabrication method and material to be used in the construction of the satellite.

### 8.3: Satellite Subsystems

#### 8.3.1: Payload

##### 8.3.1.1: Mechanical Considerations for Thermopiles

###### 8.3.1.1.1: Introduction

The student satellite being developed by IIT Bombay has as one of its objectives thermal imaging of the Earth, and to achieve this end carries as a payload an array of thermopiles which function as heat flux sensors. The task before the Structures Group was to develop a means of mounting this array of thermopiles onboard the satellite.

###### 8.3.1.1.2: Specifications of Thermopile Array

The thermopile array to be used by the Payload Group is a row of individual thermopile chips. Each chip must have a given field of view and orientation of the same with respect to absolute coordinates.

###### 8.3.1.1.2.1: Thermopile specifications

- Size → 10mm X 10mm X 2mm → Changed to 25mm X 25mm X 2mm
- Method of attachment → Adhesive on rear surface
- Area seen on earth's surface by each thermopile → 688km X 688km
- Number of thermopiles → Assumed to be 20 in a row
- Total swath → 1376km X 688km

### 8.3.1.1.3: Preliminary Calculations

#### 8.3.1.1.3.1: Field of view of each thermopile

Each thermopile views 688km on a side 10mm long. Hence by triangulation, the field of view was found by the payload team to be 36.87 degrees. This has since been altered to 25mm thermopiles now.

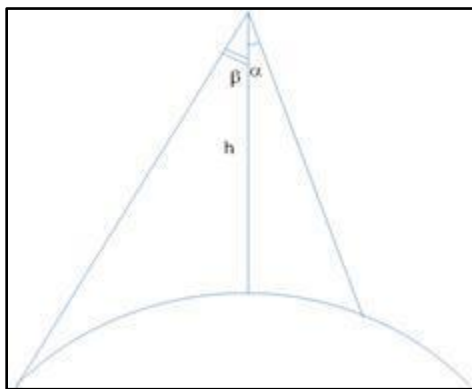


Figure 10. 2 Field of view of each thermopile

Beta – Tangent angle – 63.7 degrees

Alpha – Half of Thermopile field of view –  $0.5 * 31.67$  degrees

#### 8.3.1.1.3.2: Relative orientation of thermopiles

The entire swath of 1376km is viewed by 50 thermopiles each viewing 688 km. Hence, the difference between the areas seen by one thermopile and one of its adjacent neighbours is  $(688 / 24) = 28.6$ km. This corresponds to a difference in the orientation of one thermopile and its adjacent neighbour of 2.2 degrees, by triangulation as above.

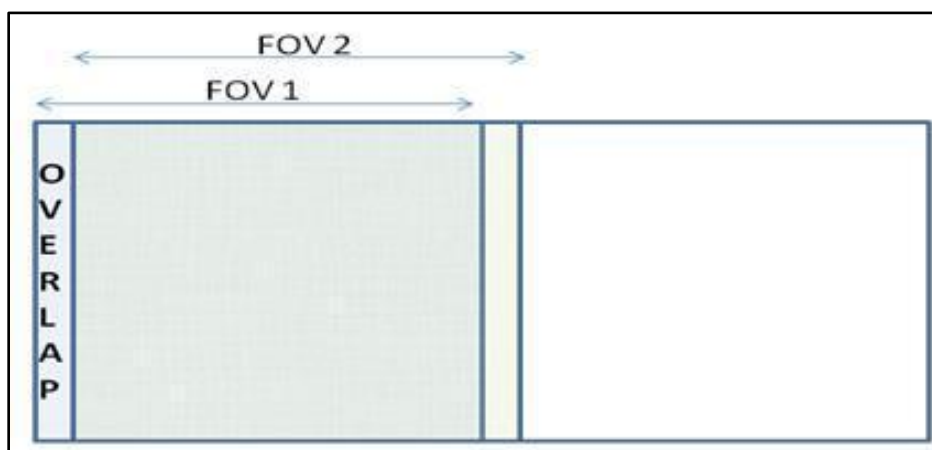


Figure 10. 3 Different field of views of adjacent thermopiles

#### 8.3.1.1.4: Method of Collimation

The possibility of having optics to collimate the thermopile FOVs was considered. However (1) stabilization of the optical system, (2) protection of the equipment during launch and (3) cost and difficulty of grinding lenses were, in order of importance, the reasons for ruling against this option.

It was decided to use mechanical collimators for each thermopile. The collimator would simply consist of a box with open top surrounding the thermopile chip.

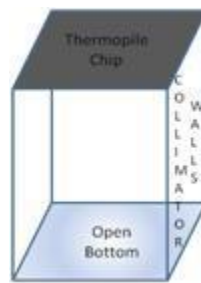


Figure 10. 4 Collimator box

#### 8.3.1.1.5: Arrangement of Thermopile-Collimator Array

##### 8.3.1.1.5.1: Parabolic base

Since each thermopile needs the same angle between itself and its neighbour, and the thermopiles are small enough to be approximated as points, this means the rate of change of slope of the base has to be the same throughout, since slope at a point decides orientation of thermopile. Such a constant curvature curve is the parabola. However, since the number of thermopiles is 20, the angle between the central and the terminal thermopiles is 30 degrees. Hence, considering a parabola with arc length taken as 250mm (to accommodate 20 chips with some accessories) the height was found as being greater than 100mm. This arrangement takes up far too much volume and results in wastage of space and material, hence has been rejected.

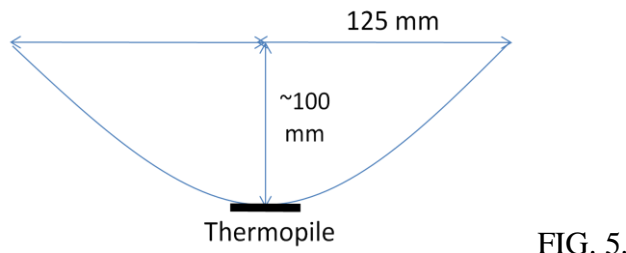


FIG. 5.

### 8.3.1.1.5.2 Alternating arrangement

It was then proposed to have thermopiles at the same angles as required, but not in the same order with respect to each other, and thus mount all thermopiles on a flat base. However this option was rejected as it does not provide space laterally for affixing any collimators and hence FOV is unrestricted.

### 8.3.1.1.5.3 Collimators with variable lengths

The next idea proposed was to have collimators with variable lengths. The lengths would be calculated in such a way that each collimator not only had the required field of view, but the field of view was also angled according to the desired orientation.

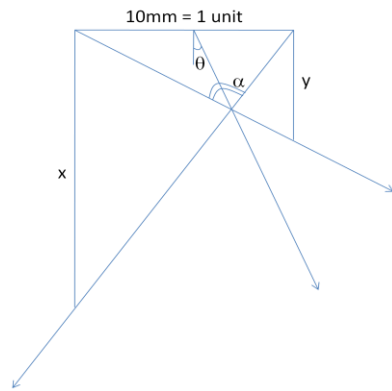


FIG. 6.

The simultaneous equations resulting in this case are as follows →

$$\alpha = \pi - \tan^{-1} x - \tan^{-1} y$$

$$\theta = \tan^{-1} \frac{x - y}{2xy}$$

For given values of alpha and theta, x and y were tabulated using the goal seek function in a spreadsheet package. The results were as follows →

alpha(dg)	alpha(rd)	tan alpha	theta(dg)	theta(rd)	tan theta	y	x
36.87	0.643502	0.750002	0	0	0	2.997006	3.00296
36.87	0.643502	0.750002	3	0.05236	0.052408	2.586446	3.549983
36.87	0.643502	0.750002	6	0.10472	0.105104	2.261118	4.327247
36.87	0.643502	0.750002	9	0.15708	0.158384	2.002801	5.482448
36.87	0.643502	0.750002	12	0.209439	0.212556	1.786186	7.467071
36.87	0.643502	0.750002	15	0.261799	0.267949	1.605702	11.53139

36.87	0.643502	0.750002	18	0.314159	0.324919	1.448599	25.42976
36.87	0.643502	0.750002	21	0.366519	0.383864	1.250542	32.21935
36.87	0.643502	0.750002	24	0.418879	0.445228	0.938549	5.702903
36.87	0.643502	0.750002	27	0.471239	0.509525	0.77189	3.614246
36.87	0.643502	0.750002	30	0.523598	0.57735	0.66186	2.803518

Clearly, from the tabulated lengths of X and Y, such a solution is not viable. However since the baseline was later modified to 25 mm, this option is being reconsidered as the lengths have reduced, as also the inclinations required.

#### 8.3.1.1.5.4 Flat base Cut-and-shift arrangement

This was the final solution reached by the Structures Group. It was decided to have each thermopile and collimator as a section to itself, with all collimators being of same length and mount each of these sections on a flat base such that they made a given angle with the flat base each time, as shown in the crude schematic below.

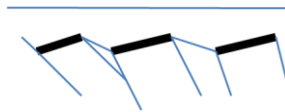


FIG. 7.

This option allows us to leave a gap between each thermopile thus providing for structural strength by filling in the base material in between, and also to provide a flat base taking up approximately 250mm for 20 thermopiles lengthwise and about 50mm in height for the entire assembly. Thus, it is the most efficient and optimal solution arrived at by the Structures Group.

#### 8.3.1.1.6 Specifics of Affixation

The thermopiles are proposed to be pasted onto an epoxy resin board which will in turn be pasted or fastened with small screws onto the base material. Details of the adhesive to be used are still being explored by the material selection subgroup.

#### 8.3.1.1.7 Other Significant Details

##### 8.3.1.1.7.1 Lengths of each collimator

By trigonometry, the length of each collimator was found to be 41.37mm. However this has since been revised under the new plan for having 25mm X 25mm thermopiles.

#### 8.3.1.1.7.2 Material for base

This is under study by the material selection subgroup.

#### 8.3.1.1.7.3 Placement of thermopile array on satellite body

The thermopile array will be placed on the nadir surface of the satellite. Further specifics will be studied along with the overall design and placement details of the satellite as a whole, in conjunction with placement of the gravity gradient boom, two monopole antennae and patch antenna also on the nadir surface.

### 8.3.1.2 Thermal Environment Control and Maintenance for thermopiles

#### 8.3.1.2.1 Introduction

The student satellite being developed by IIT Bombay has as one of its goals thermal imaging of the earth, to which effect it carries as a payload an array of thermopiles as heat flux sensors. The task before the Structures, Thermals & Mechanisms Group was to provide a controlled thermal environment onboard the satellite having minimum interference with thermal data collected.

#### 8.3.1.2.2 Heat Sensory Details of Thermopile Arrays

The thermopiles are required to detect only heat flux coming from the Earth within two wavelength bands. One such band to measure thermal radiation is between 10.5 micron and 12.5 micron. The other band to measure radiation in the carbondioxide absorption spectral region is between 13.5 and 18.5 micron. Such selectivity in detecting infra-red thermal radiation is achieved by coating the thermopiles with an optical filter. The amount of thermal flux received in these bands was estimated with the help of calibration charts as shown here, to be a maximum of  $50 \text{ W/m}^2$ .

#### 8.3.1.2.3 Thermal Environment Requisites for Thermopile Array

The thermopiles have their fields of view collimated using a mechanical collimator shaped like a box around the thermopile of height approximately 30mm.

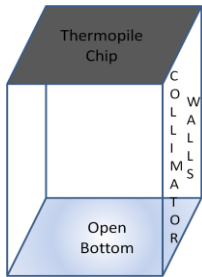


FIG. 4.

It is required that infra-red rays arriving from outside the prescribed field of view be prevented from reaching the thermopile chip through reflection or otherwise, else instead of reading radiation values for its FOV alone the thermopile receives a lot of radiation from outside its FOV as well thus contaminating the data.

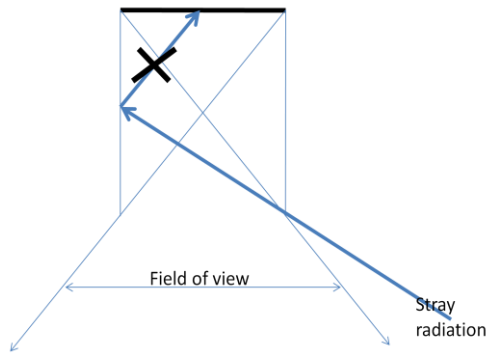


FIG. 8.

The filter, collimator and the substrate on which the thermopile is mounted all receive thermal radiation as well and hence re-radiate thermal noise by emission, thus reducing the signal to noise ratio and creating unsteadiness in the thermal noise levels. From these constraints, we conclude that the scientific requirements of the experiment dictate that either (1) the onboard components do not radiate (or emit minimal radiative noise) in the wavelength range being detected by the sensor or (2) the onboard components reach a thermal steady state so that thermal noise can be eliminated from the readings by pre-calibration on earth in similar experimental conditions.

#### 8.3.1.2.4 Qualitative Description of Design for Thermal Control of Associated Onboard Components

In the absence of definitive data about characteristics of the filter coating, only a qualitative picture of the proposed method of thermal control has been outlined, which will be further refined with precise calculations once the Payload Group chooses a filter and characterizes it for its thermal properties.

#### 8.3.1.2.4.1 Assumed filter characteristics

The STM Group recommends the use of an antireflectivity coating as an optical filter. This filter works on the principle of wavelength sensitive values of reflectivity and transmissivity. The absorptivity of such a filter is generally low, of the order of 0.1 and below. At wavelengths outside the prescribed range, the filter has reflectivity close to 0.9 and transmissivity close to zero, whereas within the prescribed range the filter has transmissivity close to 0.9 and reflectivity close to zero. Thus the filter transmits radiation in its characteristic range and reflects all other radiation, absorbing a small fraction of it. The above thermal characteristics as obtained from a product survey by the STM group have been assumed for the filter in the absence of definitive data provided by the Payload group, which will be obtained at a later stage.

#### 8.3.1.2.4.2 Design for passive thermal control system

The requirements of constrained FOV demand that stray radiation from outside the field of view be prevented from reflecting onto the thermopile chip. Hence it is proposed to coat the inside of the collimator with a highly conducting black absorptive film so that incident radiations are all absorbed and passed on to the substrate material. However the radiation outside the wavelength range of the optical filter will not cause any interference with the data, hence to reduce the amount of radiation absorbed by the collimator, we also propose to coat the collimator with the same antireflectivity coating as the thermopile chip itself, so that stray radiation outside the regions of sensitivity is harmlessly reflected back to space. From the mechanical design of the 4-sided collimator, it is evident that though two sides are in contact with adjacent collimators, two other sides are open to space and hence can be used as radiative surfaces.



FIG. 7.

It is proposed to facilitate radiation from the two exposed surfaces by providing fins to increase the surface area and coating them with a black high-emissivity layer. The following diagram shows a schematic of this idea, however all fins on the facing side have not been shown and no fins have been shown on the obverse side.

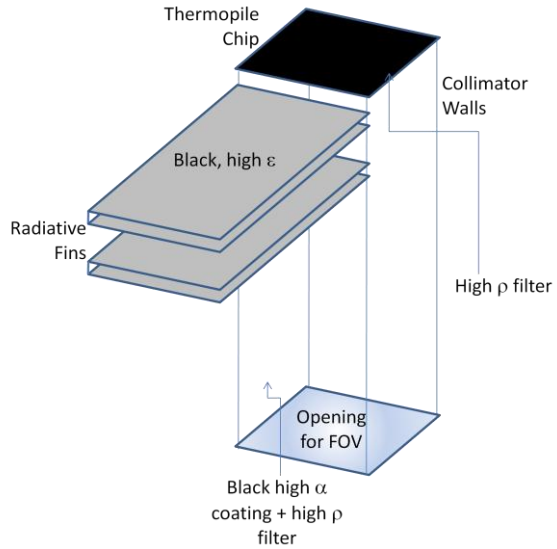


FIG. 9.

#### 8.3.1.2.4.3 Design for active thermal control system

- In case the passive thermal control system does not suffice, it is planned to include an active thermal control system also. The method planned is to achieve simultaneous heating and cooling in two different areas by means of thermoelectric circuits based on the Peltier Effect.
- From the bandwidths of the optical filters, applying Wien's Displacement Law, we find the following temperatures at which a black body has peaks in the defined bandwidth -
  - 10.5um to 12.5um → 232K to 276K
  - 13.5um to 17.5um → 166K to 215K
- Since radiation profiles generally fall off sharply on the side of higher energy but slowly on the side of lower energy, it is proposed to maintain the environment around each thermopile array about 30K less than the lower limit of temperature to whose radiation it is sensitive to. Hence the thermal profile array is proposed to be maintained at around 200K and the carbondioxide spectral absorption array maintained at around 130K, using thermocouples.
- The fixed hot junction of both thermocouples is proposed as being at the tip mass of the gravity gradient boom, which extends for about 10m radially towards the earth and hence sees a constant ambient environment of thermosphere temperature around 230K. The two cold junctions are to be at either thermopile array.

- Voltage is applied appropriately to create the requisite differences in temperature in accordance with the Peltier Effect and the thermoelectric characteristics of the metals used for making the junctions. Since the boom tether is likely to be of copper, it is proposed to use constantan onboard the satellite as calibration data for the copper-constantan thermocouple are readily available.

### 8.3.1.2.5 Conclusion

The above are all qualitative descriptions of ideas for active and passive thermal control of the thermopile environment. Further details will be looked into on receiving more data. The biggest question to be addressed at the moment is that of the conductivity of the substrate. It is also to be decided which type of thermal control mechanism, active, passive or both, will be used, and whether these ideas are feasible or shall have to be revised. In time, with proper calculations and simulations, we hope to arrive at a more precise and concrete design with all parameters specified.

### 8.3.1.3 Specifics of Monopole Antennae

Discussed under communications subsystem.

## 8.3.2 Controls

### 8.3.2.1 Considerations Regarding Moments of Inertia

The coordinate axes of the satellite are defined as follows – along the direction of orbital motion is the X axis, along the gravity-gradient boom is the Y axis and transverse to the direction of orbital motion as being the Z axis. The constraints imposed by the Controls Group to assure boom capture are as follows – (1)  $I_y > I_x > I_z$  and (2)  $I_y < I_x + I_z$

To meet these constraints the structure is such that All components are placed around the boom axis at some distance away from it. The inside of the satellite is more or less symmetric but in order to have moment of inertia greater along one horizontal axis than another, the patch antenna is deployed along one side to make the structure asymmetric.

### 8.3.2.2 Magnetorquers

The magnetorquers consist of metal frames attached to three sides of the satellite on the interior, each corresponding to a particular axis, which have laminated copper wire wound around them. These frames will be as large as the interior if the side plates permit, nominally 280mm X 180 mm, and will be milled out together with the plates, or fastened to them by bolting or riveting. The coils have a U-shape of length 3mm perpendicular to the side and height 2mm along the side.

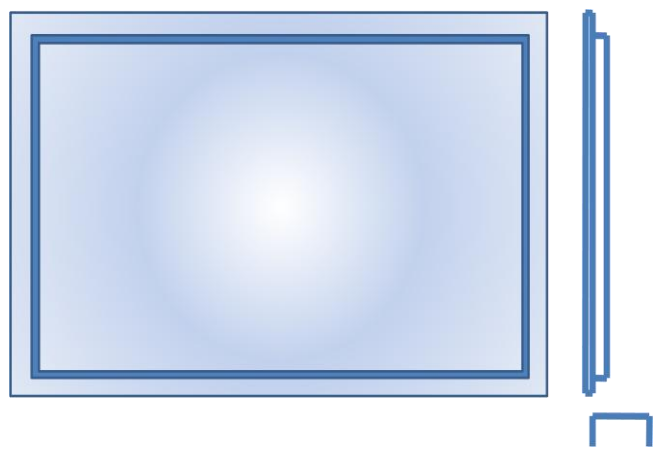


FIG. 10.

### 8.3.2.3 Sun Sensors

The sun sensors are conceived as being small photodiodes protruding from the body of the satellite. Thus, perforations to admit the head of a photodiode will be made on all faces except the nadir surface. These perforations will or will not be countersunk according to the field of view desired for each sensor by the Controls Group.

### 8.3.2.4 Specifics of Placement of Other Components

All other components, namely magnetometer, GPS and controller are placed on PCBs, which are discussed in section 10.4 that follows.

### 8.3.3 Onboard Computer

The Onboard Computer Group has all its components mounted on two PCBs, one of which houses the microprocessor and will be mounted on the side panel, and the other housing ADCs which will sit on the nadir surface on the opposite side as the payload.

The specifics of mounting PCBs are discussed in section 10.4 that follows.

Data buses will be routed to and from each component through passages provided in the housing, which will be finalised upon in detail at a later stage.

### 8.3.4 Power Systems

#### 8.3.4.1 Mounting of Battery

##### 8.3.4.1.1 Issues to be considered

- Thermal
- Structural (Due to Vacuum)
- Inertial (Due to very high mass)
- Electrical Insulation

##### 8.3.4.1.2 Data Required from Other Teams

- Spatial Constraints of other components
- Temperature Distribution

##### 8.3.4.1.3 Structural Issues

Due to Physical Expansion of batteries causes a rapid loss in performance of the battery. A solution to this is to have a dedicated battery pressure box which will not only provide housing to the batteries but also stiffness to prevent them from expanding. Another advantage of such a box is that it makes mounting of batteries much easier. The box can be mounted using mechanical joints. Material to be used is 6061 Aluminium.

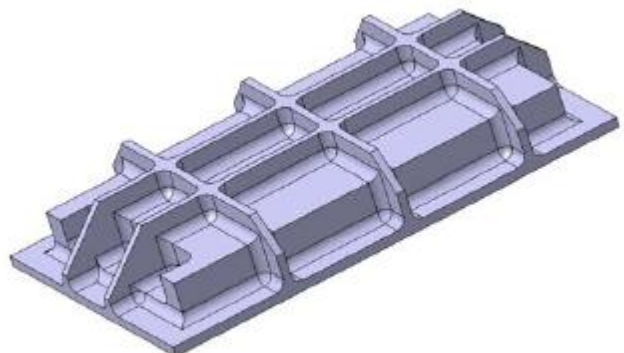


FIG. 11.

#### 8.3.4.1.4 Electrical Insulation

That can be taken care of by anodizing the aluminum box that is being used.

#### 8.3.4.1.5 Inertial Constraints

Since the mass of the total battery stack is high, the spatial arrangement of the battery will be of utmost importance since the controls team has provided moment of inertia constraints. The battery box as such does not have any spatial constraints, but other components do and hence the battery box will be needed to be placed appropriately depending on the positioning of other components. Thus it is proposed to break up the battery housing into two segments of two batteries each and mount each of these segments in between the panels containing the magnetorquers on two sides, excluding the top surface magnetorquer.

#### 8.3.4.1.6 Thermal Issues

The batteries have a very limited temperature operating range. Hence thermal control of the environment in which the batteries are mounted is necessary. If the battery is placed appropriately, only passive thermal control is enough to maintain a suitable environment as was done in HAMSAT using Multi Layer insulation, white and black paint, Low emittance tape and Kapton tape. By using a proper combination of these passive components a suitable thermal environment can be created. If required active thermal control can also be used, in the form of heat pipes.

#### 8.3.4.2 Solar Panels

The Power Systems Group proposes to have externally mounted solar panels on five faces (excluding the nadir surface) for generation of power. The specifics of mounting and fastening of these panels are decided by the Power Systems Group.

#### 8.3.4.3 Power Distribution and Controller Circuits

The Power Systems Group has all its circuit components mounted on 3 PCBs. The specifics of their attachment is dealt with in Section 10.4 that follows.

### 8.3.5 Communication

#### 8.3.5.1 Deployment of Monopole Antennae

##### 8.3.5.1.1 Various Deployment Mechanisms

###### 8.3.5.1.1.1. Antenna deployment using nylon wire

In this mechanism the antenna is a flexible tape(same as measuring tapes)which is coiled and tied using nylon wire.when deployment is to be done a current is passed through resistor (which is very close to nylon wire ) causing nylon wire to burn which in turn causes the antenna to deploy.

Disadvantages:

- iv. sometimes nylon wire breaks due to mechanical shocks and vibration causing deployment during launch.
- v. space (or cavity ) is needed to keep the coiled antenna inside the satellite .

###### 8.3.5.1.1.2 Keeping antenna along one edge

Again antenna is made up of measuring tape. At one end it is permanently attached to the edge using nuts and bolts such that its natural position is normal to the edge, now it is folded along the edge and at the other end it is fastened using nylon wire. At the time of deployment wire is burnt so that antenna becomes normal to the edge.

###### 8.3.5.1.1.3. Using spool

Again antenna is made using measuring tape . It is rolled over the spool which rotates over a axle connected to spring it is coiled in such a way that the spring forces the tape out to the full length.

Disadvantage:

- 1. the high friction between spool axis causes failure of deployment
- 2.spring with high k is required.

###### 8.3.5.1.1.4. Placement on deployed surface

Since we are already deploying our patch antenna there is no need to deploy monopoles separately but just place them on the deployed surface. This is feasible only if it doesn't interfere with thermopiles or patch antenna

Reference : [www.dlr.de/iaa.symp/Portaldatal/49/Resources/dokumente/archiv4/IAA-B4-0907P.pdf](http://www.dlr.de/iaa.symp/Portaldatal/49/Resources/dokumente/archiv4/IAA-B4-0907P.pdf)

### 8.3.5.2 Deployment of Patch Antenna

#### 8.3.5.2.1 Necessity of deployment

Constraints over patch antenna and GG boom are such that deployment is necessary. For example, Patch antennae can't have anything exactly in front of its face and also GG boom tip mass should deploy to the lowest position in the same axis of GG boom .

This constraint eliminates the possibility of having GG boom and patch antennae in the same axis ( in fact, they can't overlap each other ).

Since the patch antennae size is very large (260 mm X 260mm) it occupies almost the whole nadir surface(300 mm X300 mm).

So the only way out is to deploy patch antenna.

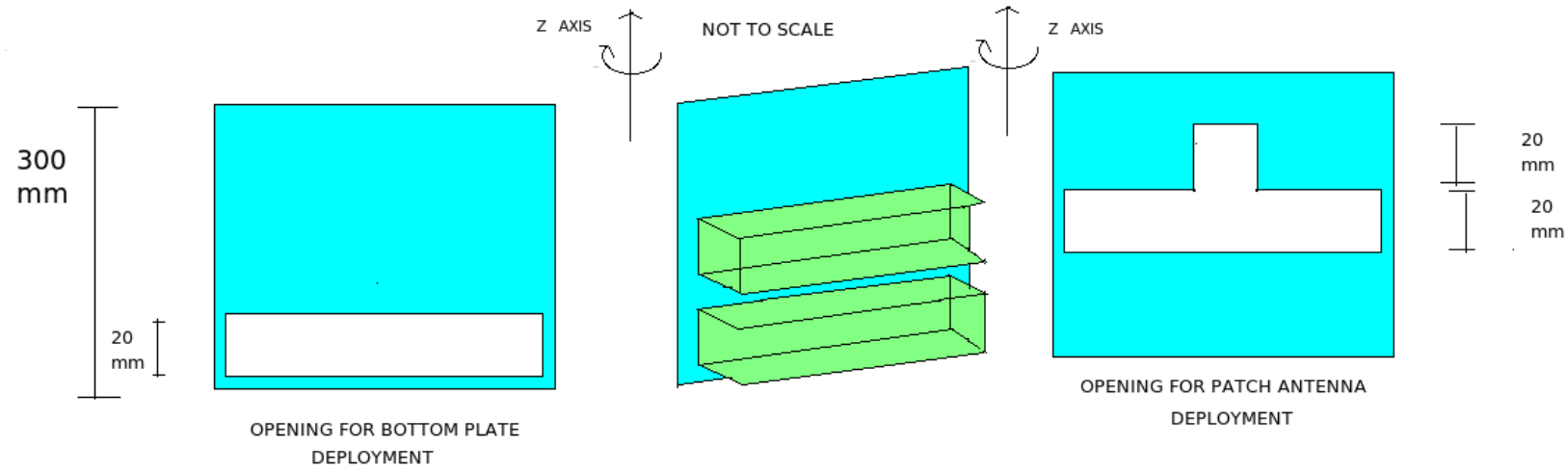
Deployed patch antenna will also expose the thermopile array.

A good deployment mechanism : is to slide the patch antenna parallel to nadir surface from one of the sides like CD drive.

#### 8.3.5.2.2 Description of mechanism

In the lowest part of one side, a rectangular opening will be there. On the two adjacent sides there will be two holders in the plane of the opening such that aluminium sheet can be easily slide on the holders through the opening.

FIG. 12.

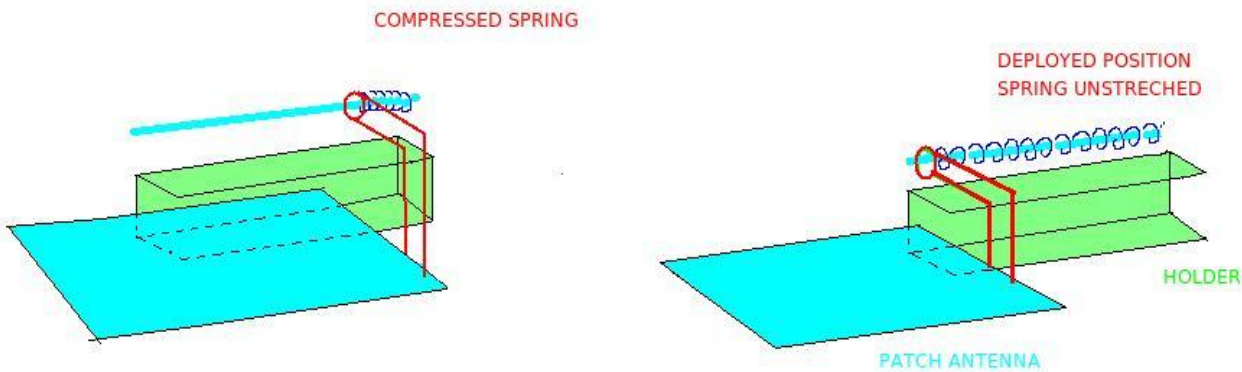


Just above the holder there will be one rod parallel to the holder having a cylindrical spring over it.

- Now one edge of the sheet will be connected to the spring in such a way that in the unstretched position of the spring the sheet is in outer side(that is deployed position). Now the sheet can be pushed in compressing the spring and can be held there using a motor driven latch, which when released causes deployment.

#### 8.3.5.2.3 Alternative mechanism

Rotating the patch antenna about an edge of the nadir side requires high torque motors which



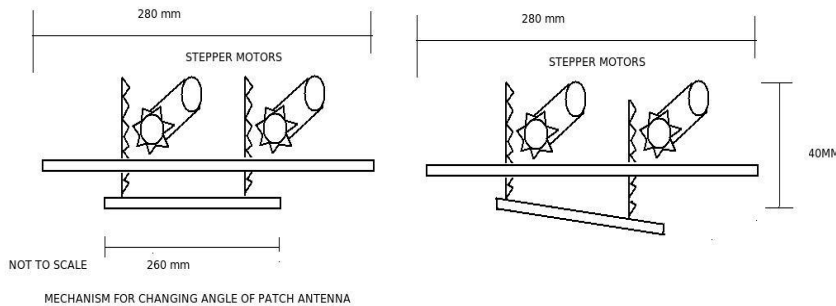
require high power and also add to the weight of the satellite.

Also deploying patch antenna from one of the sides can't be done because in order to have patch antenna on nadir side(after deployment), it has to be exposed to outer surface before deployment. But we can't leave it exposed during launch.

FIG. 13.

#### 8.3.5.2.4 Patch antenna control

Since our satellite is not having an overhead pass everyday. In order to have good communication. we need to have some control over the angle which patch antenna makes with



nadir surface to achieve this. Patch antenna will be connected to a base plate using two rack and pinion arrangement .rotating one motor will allow us to change the angle of patch antenna with the nadir surface

FIG. 14.

Advantage of this mechanism:

1. It requires less power (sliding requires minimum work compared to rotating)
2. Also sliding gives minimum jerk and vibrations.
3. The upper part of deployed plates can have solar panels , which will increase the total power

#### 8.3.5.3 Communication Circuits

The Communications Group has placed its components on a PCB, the specifics of whose mounting are discussed in Section 10.4 that follows.

## 8.4 Satellite Subsystem Layout

### 8.4.1 Mounting of Circuit Boards

#### 8.4.1.1 Introduction

The Student Satellite of IITB has among its onboard components 7 PCBs, thermopile arrays, magnetorquers, microstrip antenna and GPS which need to be mounted on the main body of the satellite. It is the task of the Structures Group to provide a method whereby each components can be firmly held in place onboard the satellite with minimization of damage due to vibrations.

#### 8.4.1.2 Flexural Vibrations of Simply Supported Rectangular Plates

(Courtesy – *Thin Plates and Shells*, Ventsel and Krauthammer, CRC Press, accessed as an e-book using Google Books)

Natural vibrations are functions of the properties of the material of a plate and the geometry of the plate. The fundamental modes of vibration are solutions (eigenfunctions) of the differential equation relating the biharmonic of the displacement function to its second derivative in time, with dependences on plate density, thickness and elastic modulus. For a simply supported rectangular plate of sides ‘a’ and ‘b’, modulus of elasticity ‘E’, density ‘ $\rho$ ’ and thickness ‘t’, fundamental mode is given by

$$\omega = \pi^2 \left( \frac{1}{a^2} + \frac{1}{b^2} \right) \sqrt{\frac{E}{\rho t}}$$

It is proposed to have as high a fundamental mode as possible to prevent damage from acoustic vibrations and minimize damage from random vibrations, as the displacement associated with vibration is inversely related to the frequency.

Since ‘E’ and ‘ $\rho$ ’ are fixed properties, the values of ‘a’, ‘b’ and ‘t’ are chosen such that frequency is raised. Thickness must thus be less, however due to conformal coatings on the PCBs thickness is increased though the coating helps in damping. To prevent high amplitude of vibration and increase natural frequency both, the values of ‘a’ and ‘b’ can be reduced. Hence each team is restricted to having a PCB of dimensions not more than 100mmX70mm, which is just a ballpark estimate.

#### 8.4.1.3 Placement of PCBs

The PCBs are placed against the frame of the satellite and supported at each corner by a threaded fastener. The frame contains sockets made for each PCB within which the board is placed. The three surfaces containing the magnetorquers and the nadir surface are free of boards whereas all free areas on two surfaces of the satellite can be utilised for this purpose. These two faces have each an area of 600 sqcm. Each PCB requires 70 sqcm, which implies that three PCBs can be conveniently stacked on one face, thus accommodating 6 PCBs in all onboard the satellite. The STM group have already urged the reduction in the number of PCBs from 7 due to weight constraints and this is an additional factor motivating this reduction. The middle of the satellite contains the GPS and the batteries which shall be described in another section.

#### 8.4.1.4 Layout of PCBs on Satellite Faces

The diagrammatic representation of slots milled into the satellite face on the inside to accommodate the PCBs is as follows. (*To scale*) The area at the centre is left empty to accommodate a support structure for the battery.

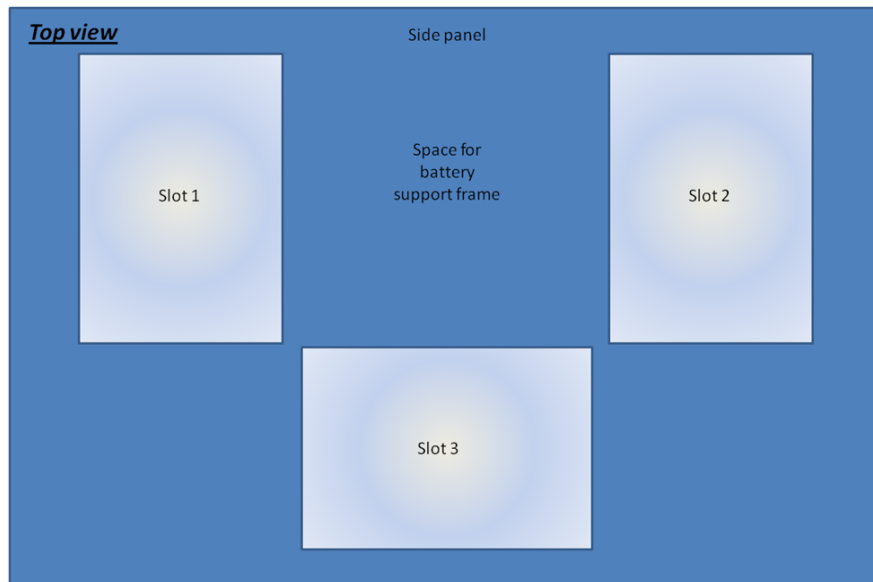


FIG. 15.

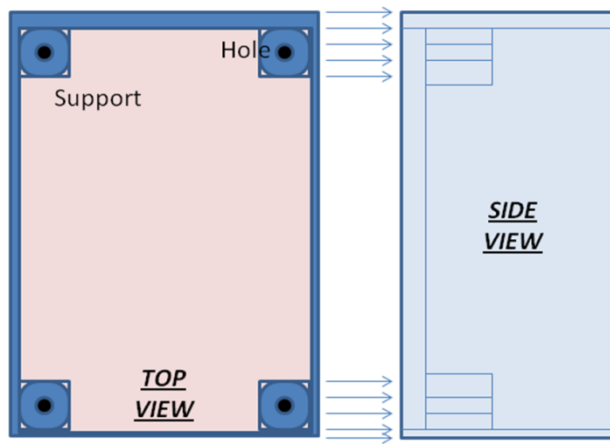


FIG. 16.

#### 8.4.1.5 Conclusion

Using these ideas, a satisfactory and effective way to utilise space and mount the PCBs onboard the satellite such that possibility of damage is minimised has been outlined for implementation in the final design. Further calculations will be subsequently performed to refine the values and dimensions to be used in the detailed design.

#### 8.4.2 Selection of Fasteners

##### 8.4.2.1 Things to consider

1. Type of structure and application
2. Material of joining parts
3. Joint strength
4. Fatigue life
5. Alignment
6. Access
7. Need for disassembly
8. Cost
9. Schedule
10. Quality assurance and reliability

#### 8.4.2.2 Types of attachment

1. Mechanical fasteners
2. Welds
3. Adhesive bonds

#### 8.4.2.3 Comparison of attachment options

Method of attachment	Advantages	Disadvantages	Applications		
Mechanical fasteners	Varsatile (many types)	weight	Suitable for most structures and mechanisms made of ductile materials		
Readily available		Hard to avoid loss of stiffness			
Inexpensive standard sizes and thread geometry		potential joint shift requires end fittings to transfer loads from structure to fastener			
installed without expensive tools and process control		Introduces stress concentration that can cause premature failure			
good for dissimilar materials					
Adds structural damping					
Welds	less expensive than fastening	Cant dissemble	Attaching similar,weldable metals		
Maintains stiffness	residual stresses cause warping	Stiffness critical aluminum truss or frame structures			
reduces strength of aluminum and some other materials		Ground support equipment			
quality varies with processes and workmanship					
Adhesive Bonds	Lightweight	cant dissemble	Assembly of brittle materials that could crack from stress concentrations caused by fasteners		

can add structural damping	quality varies extreamly with process, materials, and workmanship	Joining laminated composite member to metallic part
easiest and most economical	Low tensile strength	shear joints
spreads loads relatively economically	Limited shelf life for adhesive	
results in smooth surfaces	some are brittle	
Effective for dissimilar materials	some adhesives are toxic	
temperature limitations		

#### 8.4.2.4 Mechanical Fasteners

Considerations in designing joints with fasteners:

Design characteristics	Affected decisions	Comments
Application	fastener type	Threaded fasteners are choice for tension joints
design of fittings		
strength	Fastener type	
Size		keep shear joints critical for bearing rather than shear to ensure all fasteners in pattern will be effective
material		
quantity and patterns of joints		
design of fittings		
Stiffness	Fastener quantity	Preload should be enough so that joints wont gap at limit loads
pattern and preload	tuck tension fasteners close to fitting walls	
design of fittings	design tension fittings to have thick end pads	
Joints with many small fasteners are ussually stiffer than those with few bigger ones		
Fatigue life	application	preload to reduce fatigue damage
installation preload	not concern for shear fasteners	
Alignment	fastener type	avoid oversized holes

application		avoid shims and single shear applications (tend to cause local yielding)
Access and available space	Fastener type	rivets and bolts = access from both sides
size and pattern		fastener patterns and fitting provide access for necessary tools
design of fittings		
Need for disassembly	fastener type	rivets can be removed only by drills
Contamination, corrosion and galling	material of mating parts	Cd, Zn, and Sn coatings = contamination
fastening hardware		outgassing due to some coatings
silver can damage Ti		
Cost	Fastener type and size	Installation becomes expensive as size increases
Material		

#### 8.4.2.5 Welding

- Causes residual stresses, structure can distort on cooling and keep on distorting over its life
- Common types of welds:

Butt weld (groove weld)

Fillet weld

- Weld should be as strong as mating parts

Test for checking the weld: when loaded to failure, joint fails in material outside the joint.

#### 8.4.2.6 Adhesive Bonding

Selection of adhesive is based on:

1. Required joint strength:

Joint can fail by

- Failure of adherends
- Failure within adhesive (cohesive failure)

-Failure at bondline (adhesive failure)

Adhesive strength in shear >> adhesive strength in peel hence bonded joints to be primarily in shear but sometimes peel might be important

## 2. Operating Environment:

Needed strength at all temperatures

Acceptable levels of out gassing

## 3. Adherends:

Adhesive must properly wet the adherend surfaces

Adhesive must be strain compatible with the adherends

According to need, adhesive must not be electrically conductive

## 4. Cure Temperature:

Available adhesives cure at room temperature

Adhesive that cures at high temperature – Residual stresses may develop during cooling resulting in distortions

### 8.4.2.7 Choice of Fasteners for Various Applications

#### *Payload*

Thermopile : Adhesive

Beacon : Mechanical fasteners

#### *Controls*

Magnetorquer : Mechanical

Sunsensor : Adhesive or Mechanical

GG boom : Mechanical

Controller circuit : Mechanical

#### *Onboard Computer*

All circuit boards : Mechanical

#### *Power systems*

Battery : Mechanical

Solar panels : Adhesive

Controller circuit : Mechanical

*Communication*

Patch : Mechanical

FSK circuit : Mechanical

Monopole : Mechanical

## 8.5 Handling and Transportation

### 8.5.1 Handling and Storage

#### 8.5.1.1 Issues to be addressed

- Instruments used are extremely sensitive to contamination
- They should not be subjected to excess shock and vibration
- Safe handling required for components sensitive to ESD (Electrostatic Discharge)
- Instruments should not be exposed to contaminating ambient conditions
- Temperature constraints for various instruments
- Storage environment
- Adhesives usage

#### 8.5.1.2 Contamination

Firstly, one should not touch the instruments with bare skin. Approved non-powdered Latex gloves should be used. ESD safe shrouds and Black Kapton Shower cap shall be used to provide a barrier against molecular contamination. While storage Llumalloy bag should be used.

#### 8.5.1.3 Shock & vibration

Do not subject the instruments to excessive Shock and Vibration. It has been noticed that maximum shock and vibration is experienced by the instruments during Transportation. This shall be discussed in detail in the Transportation and Packaging Section.

#### 8.5.1.4 Electrostatic discharge

Most of the semiconductor instruments are sensitive to ESD. ESD safe shrouds also play the role of shielding the sensitive instruments from ESD. Apart from that the instruments should be properly grounded during storage. Ensure that proper grounds are affixed to the instrument prior

to any movement or lifting. Operator must also be properly grounded during handling the instrument. Wrist straps should be used by the operator and they should be in contact with the operator's skin. Avoid handling operations if relative humidity falls below 30%

#### 8.5.1.5 Ambient Conditions

The covers and ESD safe shrouds shall provide the necessary shield against contaminating ambient conditions.

#### 8.5.1.6 Temperature constraints

All instruments have their own temperature constraints, while storing these instruments ensure that they are not subjected to extreme temperatures.

#### 8.5.1.7 Storage Environment

Storing the instruments in clean vacuum (< 100 mtorr) will be preferred.

#### 8.5.1.8 Adhesives

When adhesives must be used, extra precautions must be taken to prevent or minimize exposure of the sensitive parts of the instrument to cross contamination from fumes or uncured resins.

### 8.5.2 Packaging

All issues mentioned in handling and storage should be observed. If the instruments have to be transported in an environment which is not clean upto a certain standard fixed value, then double baggage will be required during transportation. For smaller instruments, zip lock bags can also be used. If it is to leave a building then a third moisture bag is also required. All this is used to prevent contamination. This baggage also provides resistance to shock and vibration. Complete sealing of the bag is required.

Tapes & Adhesives are observed to be a major source of contamination. Approved tapes should be used, but to the minimum in terms of both quantity and time. Use tape with caution as some surfaces are impossible to clean. Do not use tapes to temporarily hold nuts, bolts, screws or other such small parts. Clean all residues thoroughly and test using black light. Preferable to pull

at an angle of 145 degrees or greater. Do not use sharp instruments in any case to remove the contamination particles.

### 8.5.3 Transportation

Specially designed container shall be made to provide shock resistance, protection from external environment, isolation and protection from contaminating environment and handles and wheels shall be employed for easier handling. But all this can be done after finalizing the assembly, as the load sensitive points can only be identified after the assembly is complete. These load sensitive points are required for designing of the container as well as placement of handles and wheels.

## 8.6 Thermal Requirements

Right now whatever thermal control points we have indexed is based purely on prior experiences of various satellites, and the tolerance levels of various components. The final lay outing of the thermal components will only be decided after extensive steady state and transient thermal analysis using ANSYS.

### 8.6.1 Thermal Control Elements

#### 8.6.1.1 Coatings

Black Paint ( Absorptivity .98 Emissivity .87)

Epoxy Paint ( Absorptivity .25 Emissivity .85)

Aluminized Teflon ( Absorptivity .16 Emissivity .8)

#### 8.6.1.2 Other materials

Heat Pipes ( for channelling of heat)

Heat Sinks ( direct contact)

MLI ( number of layers to be decided after simulation )

More coatings are being explored with cost and availability in mind.

## 8.6.2 Thermally Sensitive Points

### 8.6.2.1 Battery Box

It is the most important and sensitive part of the satellite. The problem mainly arises on the eclipse side since it cannot withstand temperatures below 0 degrees. So if we cannot manage to control its temperature via passive means we might have to look into using a heater with a temperature sensor running in a closed loop.

### 8.6.2.2 Surfaces

Since all of our surfaces have either solar panels or thermopiles we need a technique to radiate the heat out of the system. It's not a simple problem and will be considered in greater detail in the next stage of design.

### 8.6.2.3 Internal Circuits that will generate heat

Since we are using board stack the PCBs will be quite close. Hence we need a thermally effective potting and decide on whether we should apply coatings on the stacks.

## 8.7 Specifics of Satellite Design and Layout

### 8.7.1 Allocation of Resources

#### 8.7.1.1. Payload

- Components considered – *48 thermopiles of 30X30 with substrate and collimators, 2 monopoles with stowing containers, one PCB carrying ADCs*
- Maximum volume – *4750 cu cm*  
*9.5X3.1X3.1 cu cm per thermopile, 18X2X2 cu cm per monopole, 7X5X3 cu cm for PCB*
- Maximum surface area – *500 sq cm*  
*450 sq cm for thermopiles, 50 sq cm for monopole attachment and grounding*
- Maximum weight – *1000 gm*  
*250 gm for thermopiles, 300 gm for collimators, 200 gm for monopoles, 250 gm for PCB with ADCs*

#### 8.7.1.2. Controls

- Components considered – *Boom box, magnetorquer, magnetometer, sun sensor, GPS*

- Maximum volume – *1650 cu cm*  
*Boom box, magnetometer, magnetorquer, GPS as specified in documentation of Controls Group, perforations for sun sensors*
- Maximum surface area – *2850 sq cm*  
*5 sq cm for boom deployment, 2700 sq cm for magnetorquers but on interior side, 50 sq cm for sun sensors*
- Maximum weight – *800 gm*

#### 8.7.1.3. Onboard Computer

- Components considered – *1 PCB of 100X70X30*
- Maximum volume – *250 cu cm for one PCB*
- Maximum surface area – *Nil*  
*Components do not require any area on the surface panels*
- Maximum weight – *300 gm for one PCB*

#### 8.7.1.4. Power Systems

- Components considered – *Solar panels, 4 PCBs of 100X70X30, 4 batteries*
- Maximum volume – *1500 cu cm*  
*7X7X2 cu cm per battery, 10X7X3 cu cm per PCB*
- Maximum surface area – *All remaining area except for 10mm grounding strips at edges. All area for solar panels, none for PCBs or batteries*  
*Area approximately 4000 sq cm.*
- Maximum weight – *2700 gm*  
*1000 gm for solar panels, 700 gm for batteries, 1000 gm for PCBs*

#### 8.7.1.5. Communication

- Components considered – *Patch antenna, PCB*
- Maximum volume – *1000 cu cm*  
*750 cu cm for patch antenna as 260X260X10, 250 cu cm for 100X70X30 PCB*
- Maximum surface area – *700 sq cm*  
*700 sq cm for patch antenna*

- Maximum weight – 700 gm  
*400 gm for patch, 300 gm for PCB*

#### 8.7.1.6 Total Allocation

Volume – 9100 cu cm

Surface area – 5400 sq cm

Weight – 5500 gm

#### 8.7.2 List of Mechanics

- Gravity-gradient boom deployer
- Microstrip antenna deployer
- Primary monopole antenna deployer
- Secondary monopole antenna deployer

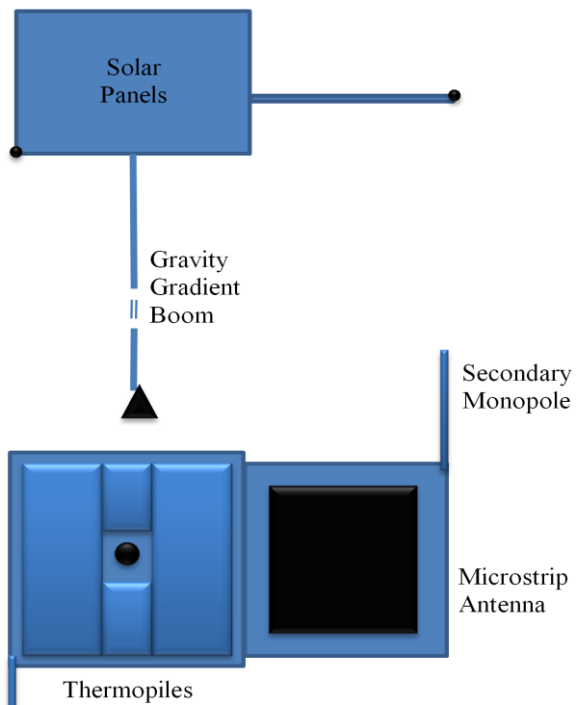
#### 8.7.3 List of thermals

- Fins for passive cooling of thermopile array
- Thermoelectric circuit for active cooling of thermopile array
- Multilayer insulation
- Reflective and emissive paints
- Heat pipes

#### 8.7.4 Satellite in Orbit

The scale model of satellite is shown in FIG. 17.

## ELEVATION



## PLAN

Primary  
Monopole

## **Chapter 9: Review meetings**

The review meetings of 3 subsystems and system integration have been held till now. In this chapter we list down all the review comments and the conclusions from the meeting.

### **9.1 System Engineer's Review**

Here are the minutes of the system engineer's review meeting held on 5<sup>th</sup> April 2008. It was attended by Prof Sudhakar, Prof Arya and Prof Majumdar.

#### **9.1.1 Overall**

- Professors were happy with the amount of work that we had done
- It was strongly commented that we should do a realistic assessment of our deadlines
- It was recommended that we delay the sending of the proposal until we had answers to all the questions that were raised in this review meeting.
- We were also asked to conduct individual reviews.
- The problem of authenticity/validity of our data was pointed and it was commented that there was no way to validate a lot of our claims since we did not cite any literature.
- The problem with conducting the review meetings was discussed and its solution was recommended.
- We were also asked not to worry about the budget.
- The problem of a proper working space was also solved and we were given the activity room, We were also permitted to have a few comps from the department in the activity room.
- Room retention perms were also given.
- It was commented that we did not have a proper place where all the documents that we have generated could be seen.
- It was commented that all the team leaders were not present for the meeting.

Saptarshi explained about the 3 aims of the satellite.

#### **9.1.2 Payload**

- Professors asked- who will benefit from the TEC values. Who will be the end users of the TEC data. Talking to SAMEER ppl was also recommended.
- The idea of social goal was appreciated and we were also asked to think about possibility of

setting up more than one ground stations to downlink the main data.

- There were a lot of queries regarding the thermopiles.
  - Deviation of thermopiles from first order behaviour
  - The resolution of thermopiles at the fringes
  - Variation of thermopiles with latitude of earth
  - How much will the resolution suffer due to jitter
- To solve all these problems the payload team was asked to make a simple simulation which will do two things-
  - Given a temperature profile on the surface values, the position of the satellite it should find out how much is the intensity of light received by each thermopile cell. This should take in to account all the things described above.
  - Given the readings at each thermopile array. The simulation should do the deconvolution and find out the temperature at each gridpoint on earth. Since payload people said that they had already done such simulation, therefore they were asked to present the simulation results to the review team.

### **9.1.3 Controls**

- Need for using sun sensor was challenged considering the payload requirements were already met by the magnetometer itself. It was argued that given the time constraints that we have it would not be advisable to work on sun sensor integration since payload requirements were already being met.
- It was asked if the torquers would be kept on continuously or they would operate in pulses. Simulation results for both orbit and attitude were asked.
- The problem of GPS was asked and we were asked to contact a company called ACCORD in Bangalore if they could supply us with customized gps.

### **9.1.4 OBC**

- Questions about type of clock, and the variation of its characteristics were asked.
- Characteristics of ADC were also enquired and problem of quantization error was discussed.
- We were also told that software part was being underestimated.
- Data compression was also enquired.

### **9.1.5 Communication**

- Why can we not uplink-various advantages of uplink were cited and we were asked to find out good reasons why we did not have uplink.
- It was commented that we did not have any provision to reset the data transmission if there was some problem with transmission
- It was recommended to prioritize the data transmission using FFT or wavelet analysis so that we can send the overall photograph first and then send the details.
- The idea of setting up multiple ground stations was discussed.

### **9.1.6 Power**

- It was asked to plot a Power vs weight and Power vs Volume chart for various microsatellites so that we can know where we stand.
- We were also asked to present the simulations for power generated as a function of orbit and the attitude of the satellite.

### **9.1.7 Structures**

- The weight and power budget were briefly discussed and a detailed review meeting was fixed for 12th April. Shashank was asked to organize the meeting.

## **9.2 Structures and Thermals Review**

The Structures and Thermals Review meeting was held on 12<sup>th</sup> April, 2008. It was attended by Prof Sudhakar, Prof Majamdar, Prof Shimpi and Prof Iyyer.

- A lot of time will be required for milling of components. This has to be factored while planning.
- Proper ideas for thermal balance have to be thought out. Prof. Iyyer will help in that.
- A proper 3d visualization of the satellite has to be built.
- Connectors will play a crucial role when we are dealing with vibrations.
- Load and vibration g's in lateral and transverse directions have to be obtained from the launch people.
- Values of temp range in space has to be fixed

- How much of atomic oxygen is there in space at 700km is it significant enough to oxidize the metallic structure.
- Simulations have to be done of all the structures.
- Heating of battery has to be taken care of.
- Structures team should not deal with design of thermopiles. That is the work of payload group.
- Deployment of antenna is a big problem it has to be figured out with communication and payload people.
- How the thermopiles fit on the nadir surface was not clear.
- How will the satellite be attached to the launch vehicle?
- Divide the structures team into two grp. One should approach Prof . Mujumdar and other Prof. Iyyer. for thermal.

### **9.3 Controls Review**

The Attitude Determination and Control Subsystem Review was held on 14<sup>th</sup> April, 2008. It was attended by Prof Sudhakar, Prof Joshi, Prof Banawar and Prof Kurien.

- What is wobbling accuracy allowed by the payload. A mathematical analysis must be presented.
- It is not possible to do orbit propagation with just uplink, because the first time the satellite must know the position of the ground station.
- Which reference frame do the accelerometers use?
- It was recommended to check the usability of the compass module. The same problem of reference frame was posed. Also the exact value of the readings from the module and what they represented was questioned.
- The insight to the physics of Gravity Gradient Boom was not satisfactory. More detailed mathematical analysis along with simulations was desired.
- Simulation for 2 body with tether were requested to be done. The 2 body problem with rigid boom was found to be grossly inappropriate by the panel. Some basic questions about the sudden jump in the response curve were unanswered.
- Simulations for the stabilization of the satellite with magnetorquer and tether were requested.

- To check for robustness of the control algorithm, more overlap and simulation time were requested.
- Simulations were deemed essential for the success of the project, especially from controls point of view.

#### **9.4 Power System Review**

The review meeting of Power System was held on 26<sup>th</sup> April, 2008. It was attended by Prof Sudhakar, Prof K. Chatterjee and Prof B.G.Fernandes.

- Special care in handling solar panels: Protection, backing, shock absorption
- Power incident on the solar panels graphs should be shown for each P1,P2 and P3 over 1 orbit
- Redundancy issue of OBC and power control by main microcontroller.
- Without too much compromise on power loss you want to do analog MPPT. Both types are being studied.
- 98% efficiency of MPPT circuit is higher than expected. It should be around 90% to 92%.
- Decide on the time for which satellite should be operational in case of failure of the circuit on the charging side. This time should be driven by some good reason.
- Toroidal inductors can be got in EE dept. They will help reduce leakage of magnetic flux.
- Management of available power: OBC needed.
- Switching off faulty circuit: Power uC should take decision. It is good idea to keep the power control local.
- Check efficiency of beacons: Efficiency value used (80%) is too high
- Back pressure created by beacon transmission. Can it produce Torque on satellite?
- List possible failures and suggest method to stop them
- PIC compiler with Arya sir
- Testing guidelines: As results are to be used in the future as well, document properly: objectives, procedure, day conditions while doing experiment, readings and results
- PCB layout: TCS does PCB layout with EMI reduction, Emerson, Mechatronics kits from Pune

## **9.5 Timeline and Budget Review**

The review meeting of Timeline and Budget was held on 1<sup>st</sup> May, 2008. It was attended by Attended by Prof. Kurien (Dean R and D), Prof. Sudhakar, Prof Muzumdar and Prof. Arya.

- 1) TEC - Who needs it? Is its data better than that of GPS receivers?
- 2) Thermopile: Get in touch with nano group. Go for it in the next satellite.
- 3) Success more important than complexity. Other teams haven't understood implications of thermal imaging on their work.
- 4) Present the options of 2 payloads and one payload to ISRO. Take their feedback.
- 5) Social Goal assumes greater importance as other colleges are now our ground stations. We can probably claim to be the TEC measuring satellite with maximum number of ground stations
- 6) Is it so easy for everyone to start analysing our signal. The profs had their own doubts.
- 7) Need simulations for TEC to see how much it would depend on control accuracy
- 8) Manufacturability of mounting for thermopiles has to be looked into. How much does the image quality depend on the manufacturing accuracy
- 9) I don't know for whom, but probably for the controls team: Put more number of sensors
- 10) Look at uplink instead of thermopile. Is it a good idea
- 11) UBLOX and SGR (I guess these are companies that design ckts taking EMI into account)
- 12) What exactly do you mean by 9g forces acting on the satellite. When exactly does this happen? What happens when the boosters are shut off?
- 13) Can we re-use tested model? Can we use some of its parts if not all? This is important because this will decide how many we buy.
- 14) Check the compatibility of ISRO solar panels lab with the solar cells we plan to use before ordering
- 15) Duty 10% and shipping 10% while importing
- 16) Write to Honeywell asking for discount

## **Acknowledgements**

First of all we want to thank Prof Sudhakar for his immense enthusiasm and faith in us. We really want to taste success with this project and we are extremely happy with the opportunities given to us by him. We also wish to thank all the professors who have made this project a reality. From first review till date, many meetings in various departments with various faculties have been held and we are thankful for all their support. Finally we thanks the IIT Bombay Student Satellite team for approximately 40 member, without whom the project would be nothing but a dream.